Ministry of Higher Education
and Scientific Research
University of Babylon
College of Science
Department of Applied Geology

Petroleum Geology of The South Zagros Fold Belt Basin, Maysan Governorate, Iraq

A Thesis Submitted to the College of Science at the University of Babylon
As Partial Fulfillment of the Requirements for the Science Master's Degree in Geology

By
Mahdi Alwan Aziz Hameedi
B.Sc. Geology, University of Baghdad, 1993

Supervised by
Prof. Dr. Amer J. Al-Khafaji **Dr. Qusay Abeed**

2022

شَهِدَ اللّهُ أَنَّهُ لاَ إِلَهَ إِلاَّ هُوَ وَالْمَلاَئِكَةُ وَأُوْلُواْ الْعِلْمِ قَآئِمَاً بِالْقِسْطِ لاَ إِلَهَ إِلاَّ هُوَ الْعَزِيزُ الْحَكِيمُ

آل عمران، الآية ١٨

Dedication

To the soul of my beloved mother,

To the good heart, my dear father,

To my dear brothers, sisters and beloved family,

To all the large family, loved ones and friends,

I dedicate the product of my humble work.

Acknowledgement

Praise God for his grace, kindness, and prayers, and peace will be upon Prophet Muhammad and his family, And after:

The researcher extends his thanks and gratitude to the Department of Applied Geology at University of Babylon for this opportunity, and for facilitating it. All thanks are due to my supported supervisors Dr. Amer J. Alkhafaji, and Dr. Qusay Abeed for their support and guidance.

Thanks, are extended to the Oil Exploration, and Reservoirs directorate in the Ministry of Oil, Maysan Oil Company, and GeoMark Oil research/ Huston, in the USA for conducting the required data to complete this study.

Mahdi

Summary

This study focuses on the petroleum system of the selected region located in a complex region of a series of folds and faults that were formed during the formation of the Zagros Mountains in Maysan Governorate, southeast of Iraq. The Fauqi oilfield is the targeted area, which contains two oil reservoirs, the Mishrif Formation and the Asmari Group. The reservoir properties were calculated, the age and the depositional environment of the potential source rocks were estimated, and the oil system model was made. The obtained data were limited to Mishrif formation, so all petrophysical interpretations are due to the Mishrif formation (Cenomanian-Late Maastrichtian) across five well data based on logs data, logs images, seismic section, and crude oils samples. Four wells were located in the southern fold of Jabal Fauqi, namely FQ-4, FQ-6, FQ-19 and FQ-20, with only one well in the northern fold, the well FQ-14. Input data for las files, image logs, and contour map of the five wells were collected from the National Oil Company (NOC).

The results showed that the main reservoir is the Mishrif Formation, which is composed of seven reservoir units, which were distinguished in the formation through the sharp variation in the Shale Volume, water saturation and porosity. These units are MA, MB11, MB12, MB21, MB22, MC1, and MC2. The main unit in the reservoir is MB21, which is characterized by good effective porosity due to the high value of secondary porosity due to cracking and dissolving processes that affected in the formation, low water content of less than 20%, and high hydrocarbon saturation. Analyzes of the crude oil samples indicate that the age of the source rocks is Upper Jurassic-Lower Cretaceous and the expected sources are the Sulay and Yamama Formations of Early Cretaceous and the Sargelu and Najma formations of Middle and Upper Jurassic. The study of the organic matter also showed the beginning of the thermal maturation of the source rocks and that the organic matter is a Type IIs kerogen. The heat flow model

shows a constant value ranging between 45-50 MW/m2 from the middle Cretaceous to the end of the Triassic period, showing a noticeable increase in the Neogene period reaching about 73 MW/m2 reflecting the influence of the Zagros Orogeny. The one-dimensional model determined the effect of burial date on increased maturity and oil window accessed during the Triassic based on the heat flow history. Oil generation began in the early Cretaceous period, peak expulsion began in the late Miocene, while the peak of maturation for oil formation was in the Holocene. The migration of oil began from the late Cretaceous period and continued until the present, taking its way through the fissures that affected the region, and accumulated in the oil reservoirs and traps that were formed before oil was generated as a result of the distortions accompanying the Zagros Synorogenic.

Table of Contents

List of Tables

Chapter One

Chapter One

Introduction

1.1. Preface

To cover most of the fields that deal with petroleum geology in seeking of best understanding of the study area as it takes high importance from the economic site, the study attempts to estimate and appraisal the reservoirs characteristics for chosen wells in it and studying the important petrophysical properties such as Shale Volume, porosity, water saturation, and permeability. The geochemical analysis is the next step to estimate the source rock depositional environment, the thermal maturity of it and the age of deposition throughout collecting and analyzing crude oil samples from number of wells within the study field. At the final step, building 1D petroleum system modeling to realize the burial and thermal history of the basin in the study area.

The exhaustion of its pre-existing supplies during the early phase suggests a potentially robust petroleum system at the time. The late stage, on the other hand, extracted the high taper and destroyed most of the early petroleum system. The introduction of synthetic sources caused them to mature through both local and dynamic subsidence, resulting in the formation of a later set of petroleum systems (Kendall et al., 2020).

1.2. The studying area

The study area is located in the southern part of the Zagros Belt Basin in Maysan Governorate, near the Iraqi-Iranian border which compromises three promising oilfields, these are: Fauqi, Abu Ghirab, and Buzurgan oilfields (Fig. 1.1).

Giant hydrocarbon accumulations in the Zagros Basin were the result of a preferable tectonic and geologic history. Since the Paleozoic, multiple sources, reservoirs, seals and overburdened sedimentary rocks were deposited in the

Zagros basin creating one of the most prolific hydrocarbons petroleum systems in the world (Sharland et al., 2004).

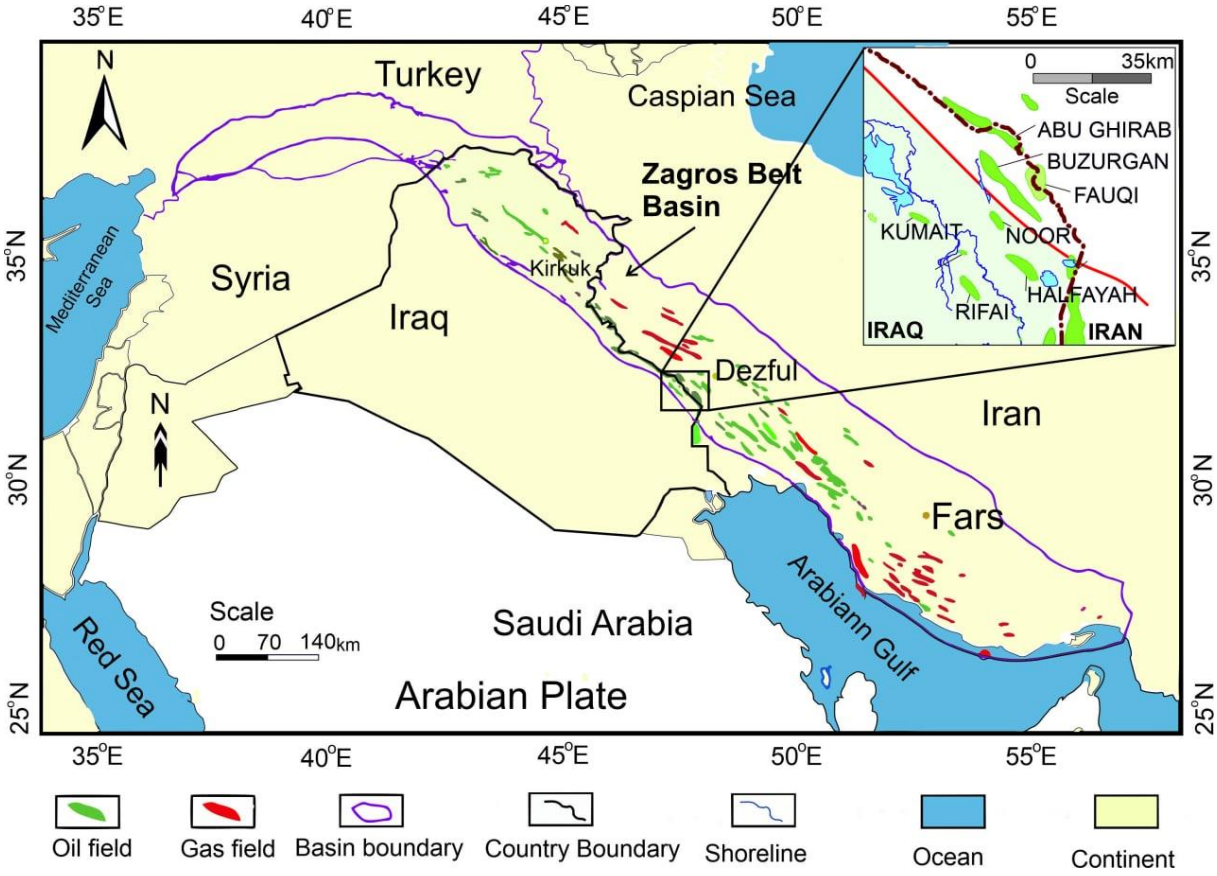

Fig. 1.1. A regional map of the Northern Arabian & Iranian plates showing the Zagros Belt Basin, zooming on the study area, modified after, (Le Garzic et al., 2019).

For a better understanding of the oil geology of the study area, a detailed study of the Fauqi oilfield was adopted. This oilfield was discovered as a result of seismic surveys carried out by the French company (CGG) for the national oil company in 1968, 1974, and 1977 (Maysan Oil Company) MOC.

In the Maysan Governorate southern Iraq, a significant oil reserve was discovered in the southern Zagros Basin, near the Iraq-Iran border. This includes Abu Ghirab, Buzurgan, and Fauqi oilfields. The Fauqi oilfield was selected in this study as an example of the petroleum geology of the southernmost part of the Zagros Basin within Iraq and studied from reservoir and source perspectives. The geochemistry of a few oil samples collected from the main reservoirs was analyzed to study their origin, migration pathways, and accumulation.

The Fauqi oilfield was located in Maysan Governorate, about 50 km northeast of capital Amara City, between the 737E-743E and 3565N-3554N. Fauqi oilfield is divided into south and north domes based on structure and OWC (Sharland et al., 2004). Its structure is one of many structural traps on the northern Arabian Plate that were inherited from the Paleozoic and Mesozoic, as well as later activation that had added more implications for the Zagros sedimentary basin (Misra et al., 2015).

The structure area is approximately 30 kilometers long and 6 kilometers wide, with north and south domes and a long-axis anticline running northwest to southeast (Sharland et al., 2004). The northern part of the field is extended within the Iranian territory as a shared oilfield, and in general, it is consisted of two significant reservoirs; Mishrif Formation as the main Cretaceous reservoir, and Asmari reservoir as the Tertiary sub-reservoir (Misra et al., 2015; Al-Baldawi, 2015)

Fauqi field figured as two anticlines extended to the north and south with depression forming between them. Two significant reservoirs are recognized in this field, the Mishrif formation as the main Cretaceous reservoir, and the Asmari reservoir as the Tertiary secondary reservoir (Misra et al., 2015; Al-Baldawi, 2015).

The anticlinal structure is NW-SE oriented, which formed as a result of the horizontal compressional stresses that caused the Zagros mountain uplift. The geology of Fauqi consists of extensive marine sedimentary rocks extending in age between the Cretaceous to Neogene (145-3.6 ma) and consists of prone source rocks, carbonate reservoirs, and mainly mudstone and evaporites cap rocks (Ou et al., 2016).

There are two anticlines with NW-SE orientation developed in the Missan Oilfields, which namely eastern anticlinal belts and western anticlinal belts. Fauqi oilfields rest on the eastern anticlinal belt which dipped southward gradually. The

The studied wells in the field showed varieties of depths and thicknesses particularly in the Injana and Fatha formations, with significant thickness. A comparable units' depth as shown in (Fig. 1.2) and (Table 1.1) that reflects the varieties of depths and thicknesses among the formations in the studied wells. There was a noticeable change in the thickness of the Injana and Fatha formations. Injana (Injana) Formation ranges from 1978m in well FQ-4 reaching maximum thickness in well FQ-14 in the north dome at about 2100m, while the Fatha (Fatha) Formation has the maximum thickness in well FQ-4 with 1003m and the minimum thickness in well FQ-20 with 831m. Also, there was a reduction in the thickness in the well FQ-14 with 878m.

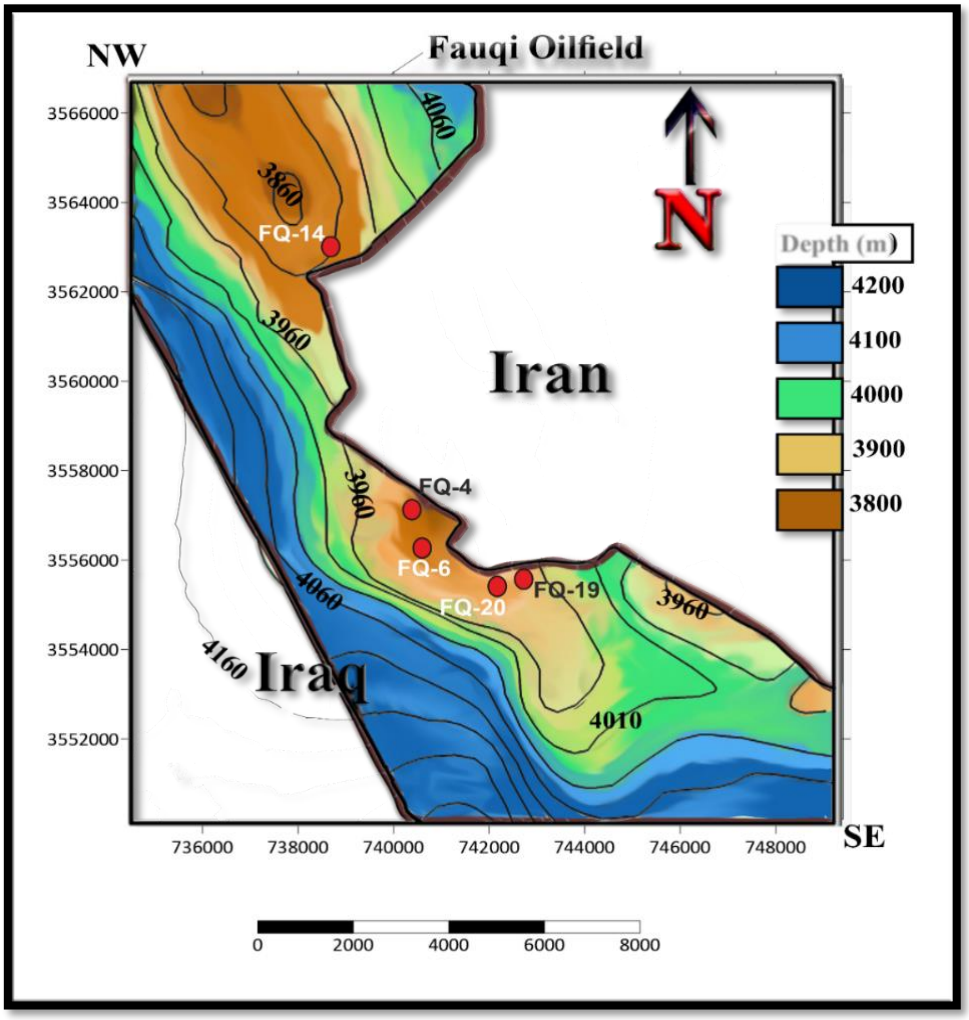

Fig. 1.2: Top of Mishrif isopach map in Fauqi oilfield distributed on it the wells of study area, edited from the Explorations Oil Company (EOC).

Table 1.1: showing the depths and thicknesses of some stratigraphic units present in the studied wells of Fauqi Oilfield, from the Final Geologic Report (FGR), 1978.

Formation	FQ-4 top depth	Bottom depth	thick m	FQ-6 top depth	Bottom depth	thick m	FQ-14 top depth	Bottom depth	thick m	FQ-19 top depth	Bottom depth	thick m	FQ-20 top depth	Bottom depth	thick m
Injana	**0**	**1978**	**1978**	**0**	**2068**	**2068**	**0**	**2201**	**2201**	**0**	**2081**	**2081**	**0**	**2143**	**2143**
Fatha	**1978**	**2981**	**1003**	**2068**	**2994**	**926**	**2201**	**3079**	**878**	**2081**	**3021**	**940**	**2143**	**2974**	**831**
Jeribe	**2981**	**2996**	**15**	**2994**	**3024**	**30**	**3079**	**3108**	**29**	**3021**	**3046.5**	**25.5**	**2974**	**3001**	**27**
Upper K	**2996**	**3210**	**214**	**3024**	**3154**	**130**	**3108**	**3195.5**	**87.5**	**3046.5**	**3172**	**125.5**	**3001**	**3088**	**87**
Middle-lower K	**3210**	**3372.5**	**162.5**	**3154**	**3389.5**	**235.5**	**3195.5**	**3467**	**271.5**	**3172**	**3422.5**	**250.5**	**3088**	**3376**	**288**
Jaddala	**3372.5**	**3531**	**158.5**	**3389.5**	**3545**	**155.5**	**3467**	**3637**	**170**	**3422.5**	**3575**	**152.5**	**3376**	**3527**	**151**
Aaliji	**3531**	**3570.5**	**39.5**	**3545**	**3575**	**30**	**3637**	**3693**	**56**	**3575**	**3616**	**41**	**3527**	**3567**	**40**
Shiranish	**3570.5**	**3605**	**34.5**	**3575**	**3607**	**32**	**3693**	**3733**	**40**	**3616**	**3648.5**	**32.5**	**3567**	**3599**	**32**
Hartha	**3605**	**3667.5**	**62.5**	**3607**	**3675**	**68**	**3733**	**3795.5**	**62.5**	**3648.5**	**3704**	**55.5**	**3599**	**3680**	**81**
Sa'adi	**3667.5**	**3780**	**112.5**	**3675**	**3794**	**119**	**3795.5**	**3895.5**	**100**	**3704**	**3827**	**123**	**3680**	**3779**	**99**
Tanuma	**3780**	**3797**	**17**	**3794**	**3815**	**21**	**3895.5**	**3913**	**17.5**	**3827**	**3847**	**20**	**3779**	**3803**	**24**
Khasib	**3797**	**3868**	**71**	**3815**	**3887.5**	**72.5**	**3913**	**3979.5**	**66.5**	**3847**	**3914.5**	**67.5**	**3803**	**3875**	**72**
Mishrif	**3868**	**4225**	**357**	**3887.5**	**4243**	**355.5**	**3979.5**	**4350**	**370.5**	**3914.5**	**4272**	**357.5**	**3875**	**4236**	**361**

1.3. Aims of Study

The purpose of the current study is to better understand the petroleum system of the southern part of Zagros through:

1) Limit the reservoir characterization and identify the best pay unit, and to achieve this matter need to determine the lithology, Shale Volume, porosity, water saturation and permeability.
2) Throughout the crude oil samples, estimating the conditions of the depositional environment, thermal maturity of the source rocks, and the predicted source rocks age.
3) Make 1D petroleum system modeling to determine the burial history and thermal gradient history to prospect the beginning of the oil window. Furthermore, in order to expect the oil generation, migration and accumulation in the final trap, the reservoirs.

1.4. Geologic setting

The Zagros Fold-and-Thrust Belt extends for more than 2000 kms and initiates from Turkey to SE Iran across E-Iraqi land including the area of study (Fig. 1.3). The Zagros basin was formed as a result of the closure of the Neo-Tethys Ocean between the Arabian and Eurasian Plates (Vergés et al., 2011).

Topographically, the main part of the Zagros fold belt is the lower part and it is characterized by large anticlines trending to the northwest. In the southwestern part of the fold belt, synclinal areas are covered by Neogene sediments. In the northwestern part of the fold belt, Paleogene strata are exposed in synclines. The Zagros fold belt forms a large structural embayment, called the Kirkuk embayment, in the overall Zagros fold belt. Many oil and gas fields that occur within this zone including the super-giant Kirkuk oilfield (Sepehr et al., 2006).

There are two distinct trends in this orogenic belt, NW-SE between the Arabian and the central Iranian Plates (called Zagros trend), and E-W between the Arabian and South-Armenian Plates (called Taurus trend). The Kurdistan Region of Iraq (KRI) Fold-and-Thrust Belt concludes the intervention of the Zagros and Taurus trends (Grosjean et al., 2022).

Zagros Thrust Belt consists of five tectonic regions that trend NW-SE: (1) the Urumieh-Dokhtar Magmatic Arc formed due to the subduction of the Neo-Tethys, (2) the metamorphic and magmatic Sanandaj-Sirjan Zone, (3) Thrust or Nappe Zone in the KRI and the Imbricated Zone in Iran (which frequently called "High Zagros Thrust Belt" or "Crush Zone"), (4) the High Folded Zone (Mountain Foothills) and the Simply Folded Belt in Kurdistan and Iran respectively, and (5) the Low Folded Zone (Buried Foothills or Foothill Zone) in KRI which is adjacent to the Mesopotamian foreland basin in the SE and it is persisting along the Arabian Gulf. The Sanandaj-Sirjan Zone and the Thrust Zone are separated by the Main Zagros Fault (MZF), which is classically interpreted as the Neo-Tethys suture (Blanc et al., 2003).

The Thrust Zone is a highly deformed zone consisting of multiple tectonic parts including the distal part of the Arabian plate margin, fragments of Cretaceous ophiolites and relicts of island arcs and accretionary prisms (Allen, 2013; Vergés et al., 2011). This Zone was pushed out on top of the High Folded Zone (HFZ) over the High Zagros Faults (HZF) (Fig. 1.3). The HFZ is mainly recognized by a fold and thrust system embedding the sedimentary cover of the Arabian Plate subducting Margin. In Iran, folding embedded the whole sedimentary succession over a feeble basal separation level, which is consistent with the Hormuz salt (Lower Cambrian-Ediacaran) or lateral equivalents (e.g. Blanc et al., 2003; Sepehr et al., 2006).

In the Southeastern zone of the KRI and in Lurestan, there are three main tectonic segments that were settled throughout the obduction juvenile, from bottom to top (Vergés et al., 2011). The Cretaceous Qulqula/ Kermanshah radiolarian chert, the Triassic Avroman/ Bisotun carbonates, and the upper Cretaceous ophiolite complexes. In the Central part of the KRI, the Mesozoic

carbonate platform of Avroman- Bisotun is missing proposing it was supported by a continental block and no further extension to the NE.

The earliest deformation events in KRI that related to the obduction of the oceanic residues onto the Arabian plate Margin were only registered in the hinterland (Lawa et al., 2013). The Iranian block collision with the Arabian margin was initiated during the Neogene and it is standing still active nowadays (Aqrawi et al., 2010). The Walash-Naopurdan intra-oceanic island arc in KRI is Eocene-Oligocene volcano-sedimentary rocks which are tantamount to the Gaveh Rud domain in Iran formed throughout the Miocene and were transferred above the Cretaceous ophiolite complexes as well as the early foreland basin (Ali et al., 2014).

Thereafter, the Sanandaj-Sirjan Zone consisting of Mesozoic metamorphic rocks, volcanic and intrusive rocks, which result due to the development of the main Mesopotamian foreland Basin in acquiescence to the crustal thickening in the distal area. Later, this foreland basin was distorted with a general southwest propagation of distortion (Lawa et al, 2013).

Zagros belt is interpreted standardly as a thin-skinned belt sophisticating to a thick-skinned tectonic wedge based on large-scale crustal sections (Vergés et al., 2011) and digital modeling (Saura et al., 2011). A new tectonic division of the Zagros thrust-belt area inside Iraq was proposed by (Fouad, 2015) regarding the intensity of deformation (Fouad, 2015). The current study area is part of the Low Folded Zone (Fig. 1.3).

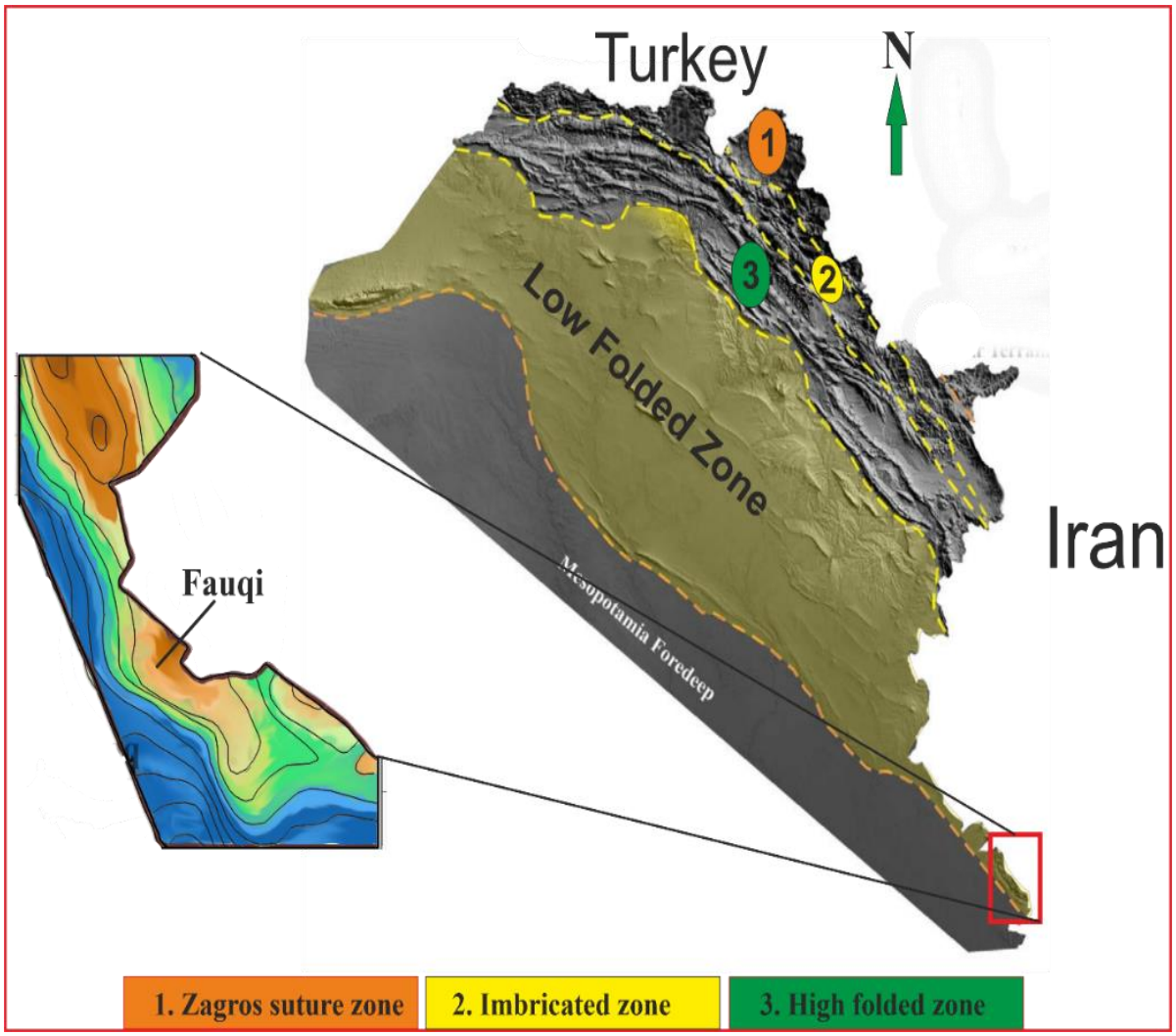

Fig. 1.3: Map of the Zagros zones inside Iraq, shows the Fauqi oilfield in the Low Folded Zone, modified after (Fouad, 2015).

1.4.1. Low Folded Zone (LFZ)

The western part of Zagros extends along the Iraqi borders, with the Low Folded Zone located between the Zagros high-folded zone and the Mesopotamian Basin (Fig. 1.3). Both zone boundaries extend in NW-SE direction. The southeast of LFZ ends with Buzurgan and Fauqi anticlines (Fouad, 2015). The zone's boundaries are well developed morphological and structural and distinguishable even from the high folded zone or from the Mesopotamian foredeep basin (Sepehr et al., 2006). The boundary trends of northeast and southeast along the high folded zone is characterized by number of arcs and embayments. Fars and Lurestan arcs, and Dezful embayment inside the Iranian land, whereas Kirkuk embayment is the

lonely structure in the Iraq territory (Berberian & King, 1981; Sepehr et al., 2006; Fouad, 2015). Along the northwest-southeast trend, the Fatha Formation at the top of the zone can be seen within a high range of thickness from about 150m in the northwest (Mosul), to nearly 900m in the southeast (Maysan). Fatha Formation is overlaid by the Injana Formation which has the highest thickness in the southwest part of about 2000m and thinning to the northwest, then disappears in the Mosul region (Berberian & King, 1981).

Low Folded Zone of Zagros in a structural manner is well-studied on the Iranian side and divided LFZ zone mechanically into five groups (Colman-Sadd, 1978; Callot, 2007):

1.5. Tectonic and Stratigraphic Setting

1.5.1. Tectonic

The Zagros Belt Basin extends from Turkey, Iraq, and Iran, and has a high economic importance due to the availability of multiple promising source rocks and numerous oil reservoirs. The main reservoir of this field is the mid-Cretaceous carbonate Mishrif Formation, and the secondary reservoir is consisting of; Jeribe-Euphrates Formation and Kirkuk group. Asmari and Mishrif reservoirs are among the most important producing reservoirs in the south of the Zagros Basin. The production at the Fauqi oilfield began in 1977 (Aqrawi et al., 2010).

The Zagros suture line represents the Arabian Plate border and the thickness of basement overlying sediments of the flysch wedge is estimated to be about 9000m continuously deposited during the Cretaceous-Paleogene period. The Qamchuqa Ridge and Zagros mountains separate between the basement low of the foothill and the basement low of the Arabian Plate margin (Jassim & Goff, 2006).

The Arabian Plate margin front of the Iranian territories, a trace of volcanic and sedimentary thrusts of the Neo-Tethys opening which are overlying clastic and carbonate sediments of Maastrichtian-Paleogene time which are onlap the

volcanic and carbonates thrusts of Late-Cretaceous. During the Neogene period, these sediments were overridden by the volcanic thrusts of Late-Neogene synorogenic deformations add to the Paleogene sediments (clastic & carbonates). In the highest areas along the Iranian border, an occurrence of igneous and metamorphic rocks as thrust sheets belonging to the Sanandaj-Sirjan zone was intruded on the Iraqi territories due to the collision of the Arabian-Iranian plates (Jassim & Goff, 2006). The evolution of Zagros Belt Basin was through four stages begin from Pre-Cambrian to Recent (Le Garzic et al., 2019) (Fig. 1.4; Fig. 1.5).

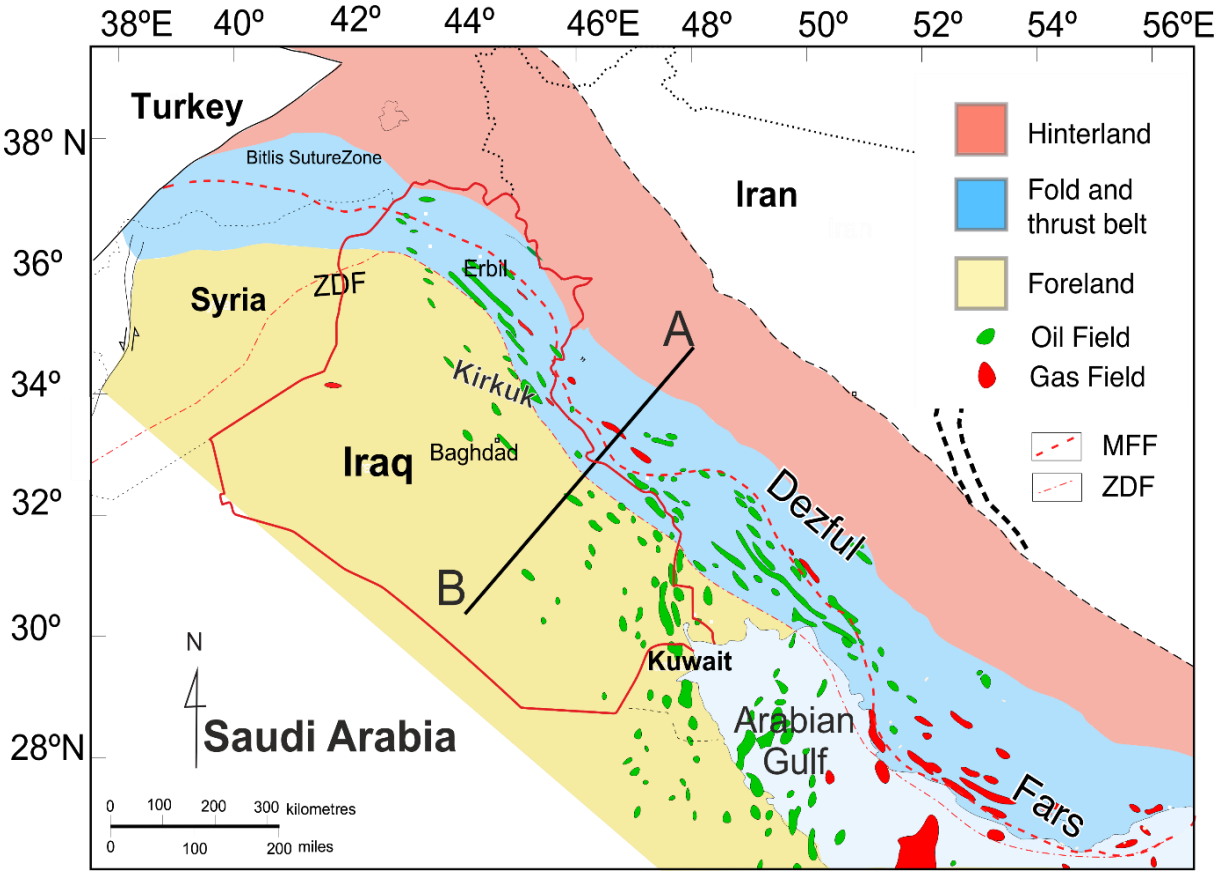

Fig. 1.4: Geologic map showing the Zagros divisions, limit on it the area of study, modified after (Le Garzic et al., 2019).

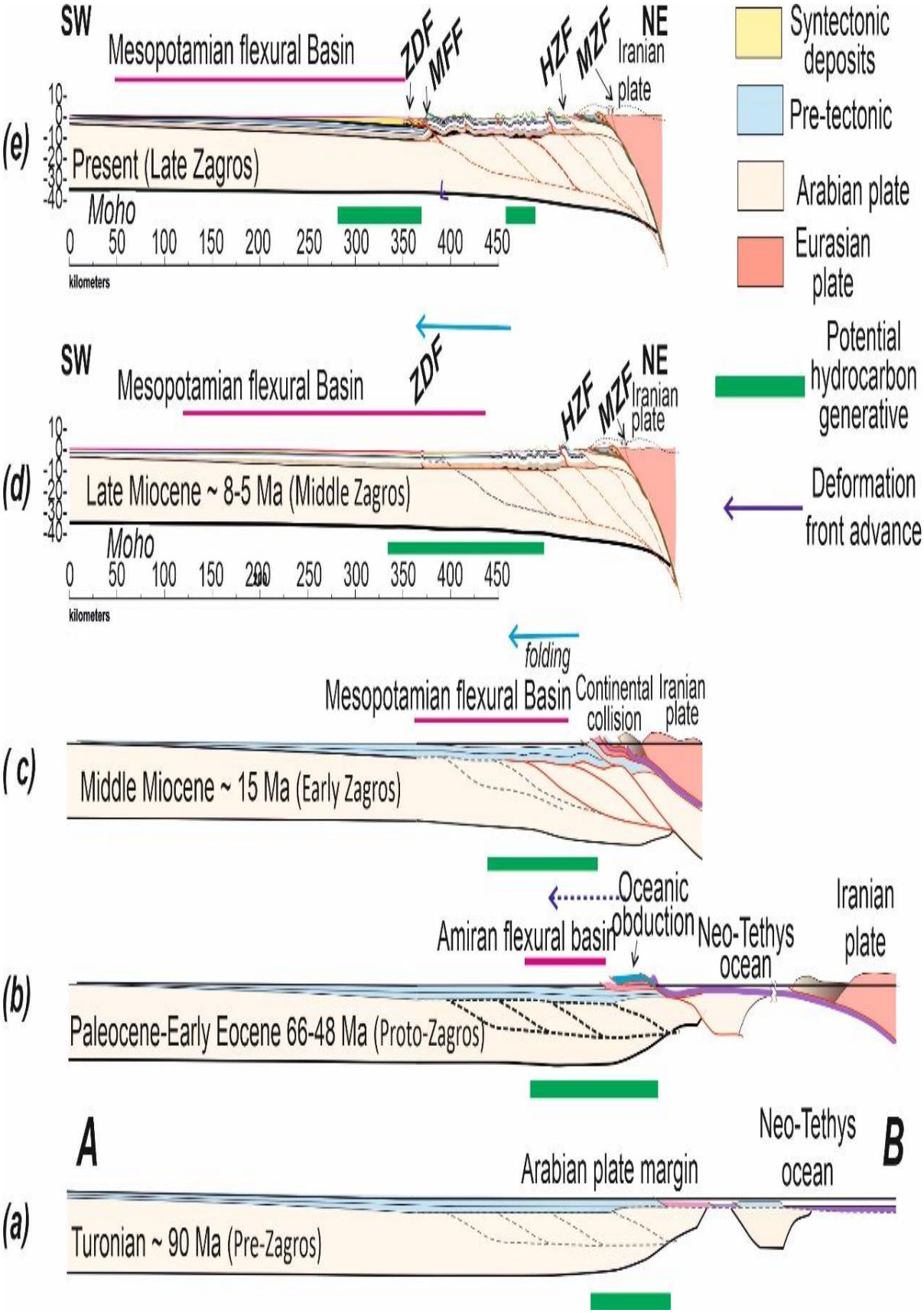

Figure1.5: The A-B cross-section on (Fig. 1.6-A) that trending SW-NE of Zagros thrust belt, illustrates the 4 main stages of Zagros basin evolution. Modified after (Vergés et al., 2011).

The A-B cross-section that trending SW-NE (Fig. 1.5) illustrates the 4 main stages of Zagros basin evolution from pre-Campanian to Recent (Le Garzic et al., 2019), as follow:

(a) Stage A: Proto-Zagros, in the Campanian-Maastrichtian ages, displays the development of the Tanjero flexural basin during the Neo-Tethys oceanic obduction event. After drift separation along the Zagros suture, a significant change of isopach and facies patterns is seen on the lower-middle Jurassic map (Fig. 1.5, a) (Le Garzic et al., 2019). The Fars platform appears as appositive area of thin carbonate deposition. Local domal uplifts on this platform are attributed to an infra-Cambrian salt movement. The deeper water swilled evaporite-carbonate-shale basin of the Basrah-Lurestan area, was initiated during this same interval. The overall pattern of upper Jurassic remained very similar to those of the lower and middle Jurassic (Koop & Stoneley, 1982).

The basin-wide Aptian was abruptly terminated with Albian regression that resulted in some erosion and another major clastic facies pushed the carbonated deposits to the northeast. the middle cretaceous isopach is strongly affected by pre-late cretaceous tectonism and erosion along conspicuous north-south linear trends of the northern Gulf region. This tectonism marked the onset of the collision phenomena along the outer continental shelf margin of the Arabian plate as the neo – Tethys oceanic seaway began to close (Jahani et al., 2007).

(b) Stage B: Early-Zagros, at Paleocene-Eocene ages reproducing the foreland wards propagation of the deformation and concomitant sedimentary depocenter (Fig. 1.5, b). Regional uplift in the late cretaceous resulted in an unconformity that affected most of the elongate basin except in parts of Lurestan where pelagic sedimentation was continuous from late cretaceous to early Miocene. Pre-Oligocene, a minor phase of uplift appears to have rejuvenated the ancestral inner Zagros mountain, shifting the axis of the depocenter to the SW and then confining marine sedimentation to the shallow elongate basin in the Oligocene – early Miocene Fars (upper Paddeh Fm.) with neritic carbonate (Asmari Fm.) (Le Garzic et al., 2019).

(c) Stage C: Middle-Zagros, in the Miocene age during the Fars deposition showing the continental collision dominated by thick-skinned tectonic. Zagros mountain was created during orogeny by the collision of the Arabian Plate with the continental Eurasian margin segments, where the Arabian oceanic plate was subducted northward beneath the Eurasian so as the continent-continent collision that happened locally in the late Eocene and continues today (Fig. 1.5, c) (Beydoun ZR, 1991).

(d) Stage D: Late-Zagros, during the Muqdadiya and younger deposition about 5 ma to Recent, reproduces thrusting beneath the Mountain Front Flexure and the thin-skinned propagation of the deformation in the LFZ (Fig. 1.5, d).

In the petroleum province of Iraq, in general, the oilfields are mainly located in the foredeep zone, while the gas fields are mostly in the simply folded zone and few fields are in the Zagros thrust fault zone (Pitman et al., 2004; Al-Ameri & Zumberge, 2012; Liu et al., 2018), with two main embayments that is Dezful embayment in Iranian region and Kirkuk embayments in Iraqi region that connected over the Lurestan arcs (Allen, 2013).

1.6. Stratigraphy:

The Arabian Plate megasequences were confined to four groups regarding to the geological time scale (Paleozoic, Paleozoic-Mesozoic, Mesozoic and Cenozoic) (Sharland et al., 2003) and these megasequences divided into other secondary sequences depending on unconformities, nonconformities, or hiatus surfaces to 11 AP, initiate with Vendian period to recent, (Fig. 1.6); (Buday, 1980) (Sharland et al., 2004; Aqrawi & Badics, 2015).

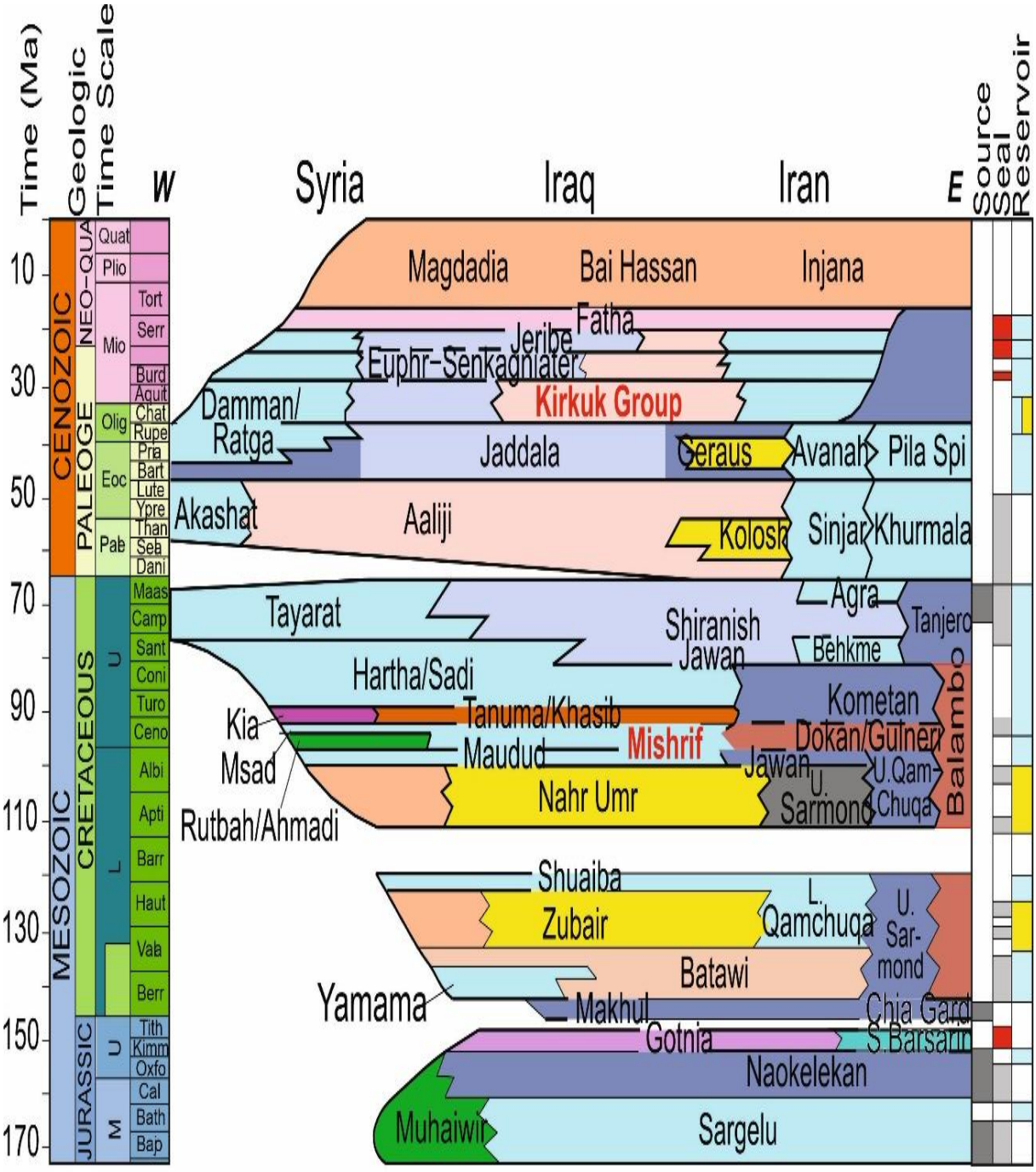

Fig. 1.6: Regional chronostratigraphic of Iraq shows the main reservoirs in the study are, modified from (Buday, 1980).

The tectonic mega-sequences AP1-AP6 from the post-Pan-African orogeny to the Early-Jurassic period were not evaluated in this study.

The AP7 whole Jurassic mega-sequence certified the opening of the Mediterranean basin and the rising of global sea level. This period was enriched with the highest level of organic matter and excellent source rocks were deposited

in an anoxic environment showed in the Sargelu Formation (Jassim & Goff, 2006). The dominance of the Jurassic carbonate platform was observed, this carbonate is mostly bituminous dolomitic limestone which represents the main oil source of the Cretaceous reservoirs (Sharland et al., 2004). During mid-late Jurassic, a regression in sea level happened and restricted basins were formed and controlled by a euxinic environment which deposited the formations of Najma and Naokelekan. In the late Jurassic, the regression continued and the environment of restricted lagoons and Sabkha were dominant forming Gotnia Formation as a regional seal (Jassim & Goff, 2006).

The late Jurassic-late Cretaceous (AP8) was concluded with two cycles of sea level transgression and regression. The first cycle of Tithonian-Hauterivian deposited in inner shelf facies with good organic matter content and reduction conditions. Many formations were deposited during this period, and as appears in the studied area, the Sulay and Yamama formations are considered as the main source rocks. In the second cycle in the Albian-Early Turonian, a varying from the deltaic to carbonate and rudist reef environment was noticed that deposited several formations within the Iraqi territories and the formations found in the stratigraphic column of the studied wells from the bottom are Zubair, Maudud, Shuaiba, Ahmadi, Rumaila, and Mishrif. Most of these formations are considered good reservoirs (Jassim & Goff, 2006). The main reservoir of the studied field is the Mishrif Formation of rudist reef facies was deposited during this stage within a reefal and open marine environment.

The AP9 tectonostratigraphic mega sequence from the late Cretaceous to Early Paleogene was the beginning of Neo-Tethys closing and ophiolite obduction as a result of the rapid opening of the Atlantic Ocean and regarding that, the deposition environments varied from deep inner shelf to lagoon, outer shelf and carbonate. The formation of this time megasequence (TMS) as seen in the studied wells from

the bottom are Khasib, Tanuma, Sa'adi, Hartha, and Shiranish (Sharland et al., 2004; Jassim & Goff, 2006).

The last two TMS are AP10 and AP11, which lasted from Early-Paleogene to the Recent. The AP10 testified the subduction zones renew synchronize with the last stage of Neo-Tethys sea closing and the northeast edge of the Arabian Plate has risen which is considered the reason for the vast erosion of the sediments in this region. A good reservoir was deposited in this period, especially in the Kirkuk group or as known as the Asmari reservoir. At the end of this stage, the Fatha formation was deposited in a restricted basin forming a regional seal of evaporitic rocks. The deposition environment was in the outer shelf, restricted lagoon and carbonate. While the Ap11 is characterized by the weak clastic sediments of the Quaternary period (Fig. 1.7) (Busk & Mayo., 1918; Jassim & Goff, 2006).

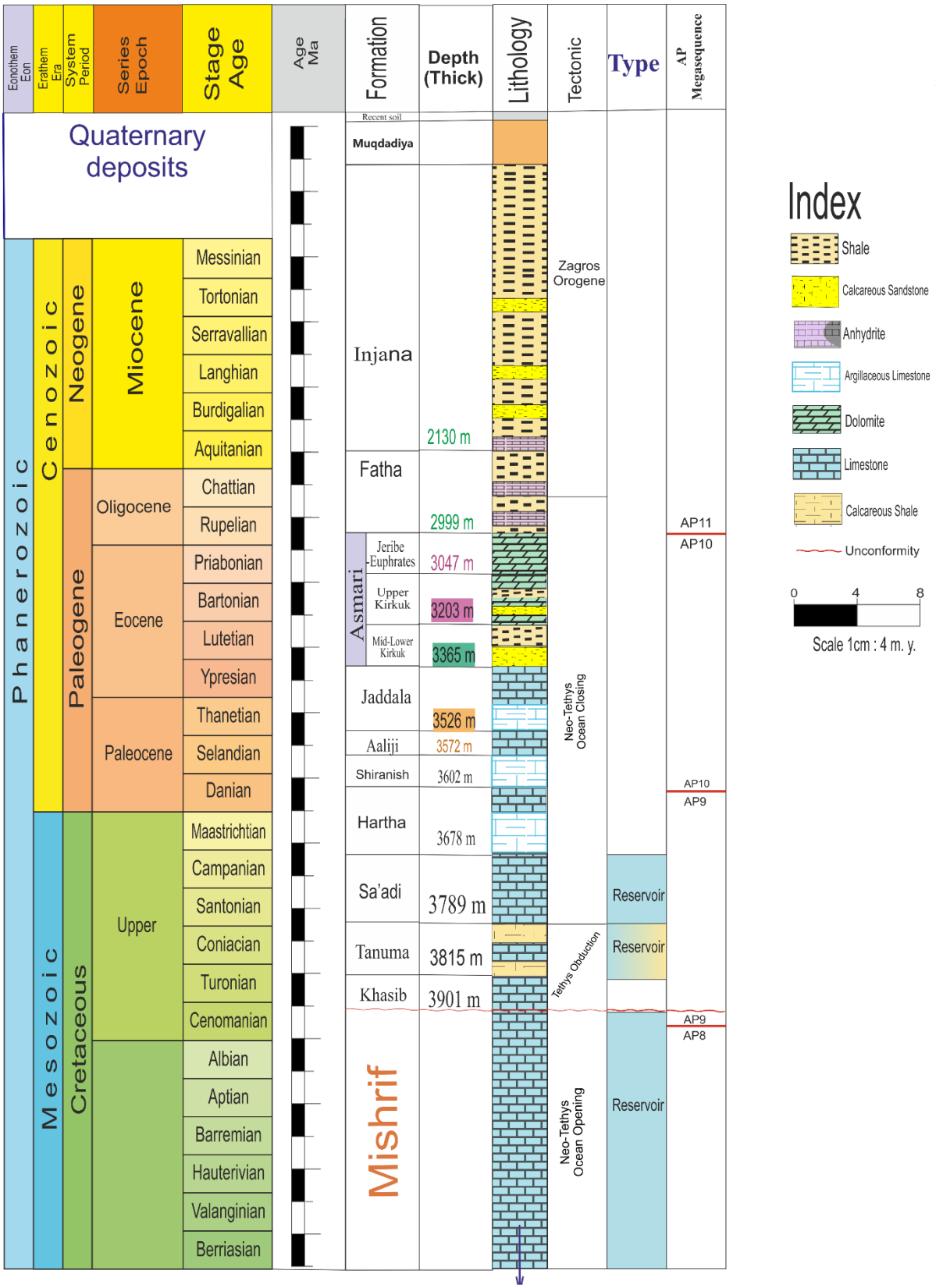

Figure1.7.: the stratigraphic column of zagros thrust fold belt southeastern Iraq depend on the final report of Fauqi oilfield at the top of Mishrif formation in the well FQ-19, depending on the Final Geologic Report (FGR, 1978).

1.7. Methodology

In order to get the best result, and as a classical method for any researcher, there are some procedures should to be done. As well as our study in its nature "field study", so the steps were office and field study listed below.

1.7.1. Data collection

Samples of crude oil and set of well logs were collected to study from wells in the Fauqi oilfield, final reports, image logs, maps, seismic sections and previous studies gathered from the Iraqi oil companies, such as the Oil Explorations Company, Reservoirs Department, and MOC.

1.7.2. Data Processing and Analyzing

Making such procedures, a lot of applications are available by giving an excellent outlet that produce significant information about the subsurface targeted object. Many software packages are used to achieve this study, as follows:

1. Didger5 Software

Is using to solve the problem of combining data files in different file formats and in different coordinate systems, by providing extensive tools to transform your GIS data into one cohesive coordinate system. Principally we use it to digitize and coordinate the contour map and converse it to another file could be deals with Surfer app.

2. Surfer Software

A product of Golden Software, Inc. and finds its use among others in creating representations of terrain surface. With its use, one can for example generate isoline maps, 3D maps, create sections of 3D maps, and calculate volumes and surface areas. We depending on this program to make a processing to the contour maps got from Didger5 app and do conversion to be readable file with Petrel software.

3. Interactive Petrophysics Software

The IP™ helps to determine the amounts of hydrocarbons in a reservoir by calculating porosity and water saturation using well logging data. Also, it is a tool for geologists and Reservoir Engineers who want to take control of their analysis and interpretation. IP™ is easy to learn so that you get going quickly, able to focus on accurate calculations that get the most out of your reservoir.

4. PetroMod Software

Petroleum systems models 1D, 2D, or 3D can cover multiple scales ranging from a single charge area for a prospect to regional studies of entire basins to multi-basin resource assessments. The models are dynamic, which means they provide a complete record of the structural evolution, temperature, and pressure history, as well as the effects on generation, migration, accumulation, and eventual loss of oil and gas by top seal leakage through geologic time. Properties such as gas/oil ratios (GOR) and API gravities can be predicted and analyzed.

5. Corel Draw Software

A vector graphics editor developed and marketed by Corel Corporation. CorelDraw is a program used in the professional space to create brochures, newsletters, business card etc. Some of the common uses of CorelDraw are: Magazine Designing, News Paper Designing, Books Designing, Illustration Making, Logo Making and so on. So, we depend on it to make the geologic maps and the stratigraphic columns.

1.7.3. Logging Tools

Well logs are a record of the changing lithology characteristics with a depth of the penetrated well geologic formations. Interpreters may use these plots to identify lithologies, differentiate between porous and nonporous rock and fast identifies pay zones for the subsurface formations (Liu et al., 2018). The significance of each measurement comes from the ability of how well to interpret a log (Archie, 1950). The tools are used in various methods, and hereunder is a review of such logs:

a. Electricity log (e-log)

Could just give info about the resistivity of the formation that reflects the nature of the liquids filling out the pores of the rock formation and of course its measuring in Ohm. m unit. The resultant data of the logs, if showed good resistivity, the pores may contain either pure water or hydrocarbons, and while getting pure water in subsurface beds is a rare situation regarding the soluble minerals and salts that dissolve in water giving it low resistivity. The reciprocal term for resistivity is conductivity, and the hydrocarbons (oil or/and gas) have high resistance values with no conductivity opposite to saline water (Schlumberger Ltd., 1984). The researcher can estimate the diameter of an invaded zone via mud filtrate and may be able to identify which zones are more permeable than others by appraisal of the differences between these curves (Asquith et al., 2004).

b. Spontaneous potential log (SP log)

It is calculated synchronously with E-log to measure the voltage differentiation between two electrodes in various forms of an array to get the desired results. During the drilling works, sometimes, mud filtrate may invade the pores in the permeable rocks, and if the drilling mud filtrate was less saline then the SP curve will be left deflected depending on permeability, porosity, water formation, and mud filtrate properties. When the permeable formation rock is fulfilled with water fresher than the drilling mud filtrate then the SP curve will be right-deflected (Schlumberger Ltd., 1984).

c. Density log

Its measurement is based on gamma-ray scattering as an index to the bulk density of the irradiated material. The bulk density term is describing the whole density of the matrix and within the pore's fluids (water, oil, gas). The stream of Gamma rays that irradiate into the formation, goes in three directions where some of them are adsorbed, the others passed on through the formation, and some are

scattered. The intensity of scattered Gamma rays reaching two steady spaces from the source identifies the matrix's ability to attenuate the Gamma rays. The bulk density of the matrix is calculated by a correlation between the intensity of detected Gamma rays and the data used for the calibration of the instrument (Darling, 2005).

d. Gamma ray log (GR)

It measures the natural radioactivity of the rock formation and helps geo-researchers to distinguish between reservoir (sands and carbonate) and non-reservoir (shales and clays) formation. As the shale and clay rocks are originated from a source containing radioactive materials like potassium, radium, thorium, …etc., where these elements deflect the GR curve to the shale baseline and for non-radioactive rocks the curve will tend to sand baseline and give the probability of a reservoir presence (Castagna et al., 1985). Formation density is a characteristic and too useful parameter for evaluating formation. For a known matrix lithology, porosity is well-defined and easily computed out of density data. If the density logs are used with other porosity-agile tools, such as Sonic and Neutron logs, then maybe identified both lithology and porosity with good accuracy. Mud-cakes on permeable lithologies and rough walls of the borehole have been, in the same manner, causing miss-reading since the device was banned from contact directly with the formation body. For such conditions, a conation to do corrected measurements is by making a synchronizing caliper log, and estimation tries to make knowledge of the composition of the intrusion materials (Wahl et al, 1964).

e. Sonic log

recording the required time for the sound wave to passage the assured length of a formation. Sonic waves' time of travelling is contra-proportion to the speed of sound in the various formations. This speed is depending on the elastic properties of the rock matrix, porosity and fluid content and its pressure in the formation. At

the low-velocity layer, the velocity ranges from 50 to 100 ft, and may range from about 6,000 ft/sec in shallow shales to nearly about 24,000 ft/sec in dolomites. In the well cemented and/or compacted (hard formations), the sonic log records the quantity of fluid in the formations; hence, it makes a correlation of the wells with their porosity (Tixier et al., 1959).

f. Neutron log

Mainly susceptible to a lot of hydrogen atoms in the formation. Principally, using it to determine the porosity of the formation. The instrument operates by shelling the formation with neutrons having high energy. Neutrons in the formation scattering undergo, so, losing their energy and liberating high-energy Gamma rays. Most scattering reactions efficiently occur within hydrogen atoms. The output low-energy neutrons or Gamma rays can be sensed, and the amount is proportional to the number of hydrogen atoms in the formation (Glover, 2000). In formations within a high rate of hydrogen atoms, the neutrons are absorbed very quickly because their velocity is reduced in a short distance. So, the count rate of idle neutrons (captured Gamma rays) will be low in the tool which is mean that the count rate would be low in a high porosity matrix. On the opposite, for the formations with a small count rate of hydrogen atoms, the neutron velocity is reduced and absorbed more slowly, in the first case, and it will travel furthermore through the rock before being absorbed. Subsequently, the rate of slow neutrons or capture Gamma rays in the tool is higher, so the count rate will be higher in the low porosity matrix (Glover, 2000).

1.7.4. Crude Oil Analyzing tools

a. Gas Chromatography

Gas chromatography (GC) is an analytical technique used to separate and detect the chemical components of a sample mixture to determine their presence or absence and/or quantities. These chemical components are usually organic molecules or gases. For GC to be successful in their analysis, these components

need to be volatile, usually with a molecular weight below 1250 Da, and thermally stable so they don’t degrade in the GC system. GC is a widely used technique across most industries, including for: Quality control in the manufacture of many products from cars to chemicals and petrochemicals, to pharmaceuticals, Research purposes from the analysis of meteorites to natural products, and Safety and monitoring from environmental samples, microplastics and food and wine, to forensics. In the current study GC used to separate the aromatic and saturate oil, asphaltene and NSO compound .

Gas chromatographs are frequently hyphenated to mass spectrometers (GC-MS) to enable the identification of the chemical components (Turner & CONSULTING, 2020).

b. Gas Chromatography Mass Spectrometry GC/MS

Gas chromatography mass spectrometry (GC/MS) is an instrumental technique, comprising a gas chromatograph (GC) coupled to a mass spectrometer (MS), by which complex mixtures of chemicals may be separated, identified and quantified. This makes it ideal for the analysis of the hundreds of relatively low molecular weight compounds found in environmental materials. In order for a compound to be analyzed by GC/MS it must be sufficiently volatile and thermally stable. In addition, functionalized compounds may require chemical modification (derivatization), prior to analysis, to eliminate undesirable adsorption effects that would otherwise affect the quality of the data obtained. Samples are usually analyzed as organic solutions consequently materials of interest (e.g. soils, sediments, tissues etc.) need to be solvent extracted and the extract subjected to various 'wet chemical' techniques before GC/MS analysis is possible (Karasek, 2012).

In the current study the GC/MS tool is used in limit the values of Pristane, Phytanes, and carbon isotopes (saturates and aromatics).

1.8. Previous studies

Beydoun, 1988

Studied the Tertiary sediments and their influence on the petroleum maturity and hydrocarbons habitant in the Zagros basin as well as in the Mesopotamian Basin. Ending with an important concept aims to evaluate the Zagros hydrocarbons potential to estimate the total amount lost from this basin throughout geochemically studying the source rock in the future exploration regarding the vast importance of the Zagros Basin for oil (and gas) production.

Sharland, 2004

He revised the Arabian Plate tectonostratigraphic megasequences and gave attention to the new geological time scale by the International Commission of Stratigraphy in 2004 synchronously with his study also put a re-definition to the unconformity boundaries at the top of AP4 and AP5 as:

Janet K. Pitman, 2004

The study evaluates petroleum generation and migration histories in the Mesopotamian Basin and Zagros fold belt in Iraq by making a 3D petroleum system modeling concluding the litho-facies, structural maps, isopach maps, and thermal maturity to the studied units as input parameters. He studied the oil source for Jurassic, Cretaceous and Tertiary reservoir rocks, and did modeling by using hydrous pyrolysis (Type II-S) Kerogen Kinetic.

Fouad, 2012

He studies the Low Folded Zone part of the Zagros fold belt to interpret the structural styles and geometries of the folds and the associated structures and their variations across and along the zone depending on the field, seismic, and well data. Also, he searched the structural forms and identify the weak line resulting from the folding processes and ended with the conclusion of the differentiation of

the mechanical properties of the folds in southwest Iran from the folds in the Kirkuk group as well as the absence of this geologic form up in Mosul area.

AlBaldawi, 2015

By using the petrel software, the study end with a 3D geological model for the Asmari reservoir using the data collected from five wells in the Fauqi oilfield. The physical properties (good porosity and low water saturation) improved the quality of the reservoir which considers as the secondary reservoir in this field.

Lawa, & Sulaiman, 2015

Analyze super sequences of Early Jurassic-the Late Pliocene in age by using tectonostratigraphic and cross-sectional balancing across several structural domains and a stratigraphic framework. The study put a shortening range to the Zagros rock body where it was about 4-6% during Tertiary, the shortening range reached 20% through Cretaceous period time and the high values were in Iranian Zagros side.

Hakimi, 2016

Studied the origin of crude oils from oilfields in the Zagros Fold Belt, southern Iraq. Crude oil samples from Cretaceous and Tertiary reservoir sections in the Zagros Fold Belt oil fields, southern Iraq were investigated using non-biomarker and biomarker parameters.

Al-Ameri et al., 2012

Made an analytical study to estimate the hydrocarbon potential of the source of oil-prone rock of the Zagros basin in the north of Iraq to the Jurassic-Early Cretaceous period. Used biomarker distributions to accomplish the evaluation of the oil-prone potential of some important source formations such as (Sargelu, Chia Gara, Naokelekan, and Gotnia). The main aim of his study was to confirm the studied sequences' oil generation capability.

Sang, 2017

A sedimentary study of litho-facies and the relationship between facies distribution and reservoir characteristics to construct a predictive geologic model. The target was the Mishrif Formation as the main reservoir in the Fauqi field (study project).

Kendall, et al., 2020

A comparative study aimed to make petroleum tectonic comparing of fold and thrust belts in chosen basin distributed around the world. These basins were; the Zagros of Iraq and Iran, the Pyrenees of Spain, the Sevier of Western USA and the Beni Sub-Andean of Bolivia. The study inferred with a result; that the pre-orogeny rock formation and the structural forms affect the post-orogeny folds and thrusts as well as the reservoir characteristic and petroleum distribution.

Aziz, & Hussein, 2021

Studied the mechanical and petrophysical rock properties and presents a set of empirical correlations that can be used when core samples are missing or incomplete.

Mohajer, 2022

Studied the Zagros fold and thrust belt N–S shortening between the Arabian and Eurasian plates since the Miocene and investigates the growth of fold in the area NE of Erbil (Kurdistan, Iraq). His study focused on the interaction of the transient development of drainage patterns along growing anti-forms, as this directly reflects the kinematics of progressive fold growth. Also made a comparison of natural examples from the Zagros fold and thrust belt in Iraq with published numerically modelled fold growth in Iran.

Chapter Two

Chapter Two

Reservoir Appraisal of Fauqi Oilfield, Mishrif Formation

2.1 Introduction

This chapter focused on the petrophysical properties of the Mishrif Formation the main reservoir in the Fauqi oilfield and one of the most prolific reservoirs in southern Iraq (Owen & Nasr, 1958; Alsharhan & Nairn, 1990). Previously, the Mishrif Formation's petrophysical properties were determined by its content of an organic detrital limestone (wackestone and packstone) accompanied by rudist, algal, and colonial coral limestones (Al-Najm et al., 2022). In the study area, the formation is composed of dense, algal limestones, corals, and detrital, porous, and foraminiferal limestones with rudist debris (Aqrawi, 1998) and it was deposited in an environment of carbonate platform ramp grades from restricted to open marine (Kendall et al., 2020).

Mishrif Formation was divided into three rock units A, B, and C with seven stratigraphic sub-units according to (Reulet, 1970). Many previous studies showed that this formation is one of the main oil carbonate reservoirs in the Mesopotamian and Zagros basins, and it is estimated to be containing about 30% of the ratified oil reserves in Iraq (Al-Ameri et al., 2009; Al-Khafaji et al., 2021; Al-Aradi et al., 2022).

There are some dependent principles to determining reservoir estimation for a known formation could be throughout the core analysis, microfacies and petrography analysis, or by interpretations of logs data. So, our study here depends on reservoir lithology characteristics like primary and secondary porosity, type of fluids as well as their saturation as water saturation, and log interpretation that also aids in limitation of the stratigraphic boundaries.

2.1. Results and Discussion

Well logs from boreholes can help the geologist to understand the nature of targeted area and help better evaluate the reservoir economics (Castagna et al., 1985). The most important parameter can be tested by logs are:

a. Lithology distinction

The lithology was estimated with the interactive petrophysics default function of (M-N) on a cross plot between density and neutron logs which appears main lithologies. In this study, the result revealed that the main lithology of the FQ-4 well was limestone, which is the dominant lithology in the MB21 with the low content of shale dispersion (Fig. 2.1, A). The results showed also a fair abundant of shale and lesser presence of dolomite in the lower units (Fig. 2.1, B).

Software procedures were used to define automatic lithographic prescription for studying well formations by combining wireline measurements with a lithofacies database. The well log responses can be transferred to database lithofacies (Delfiner et al, 1987).

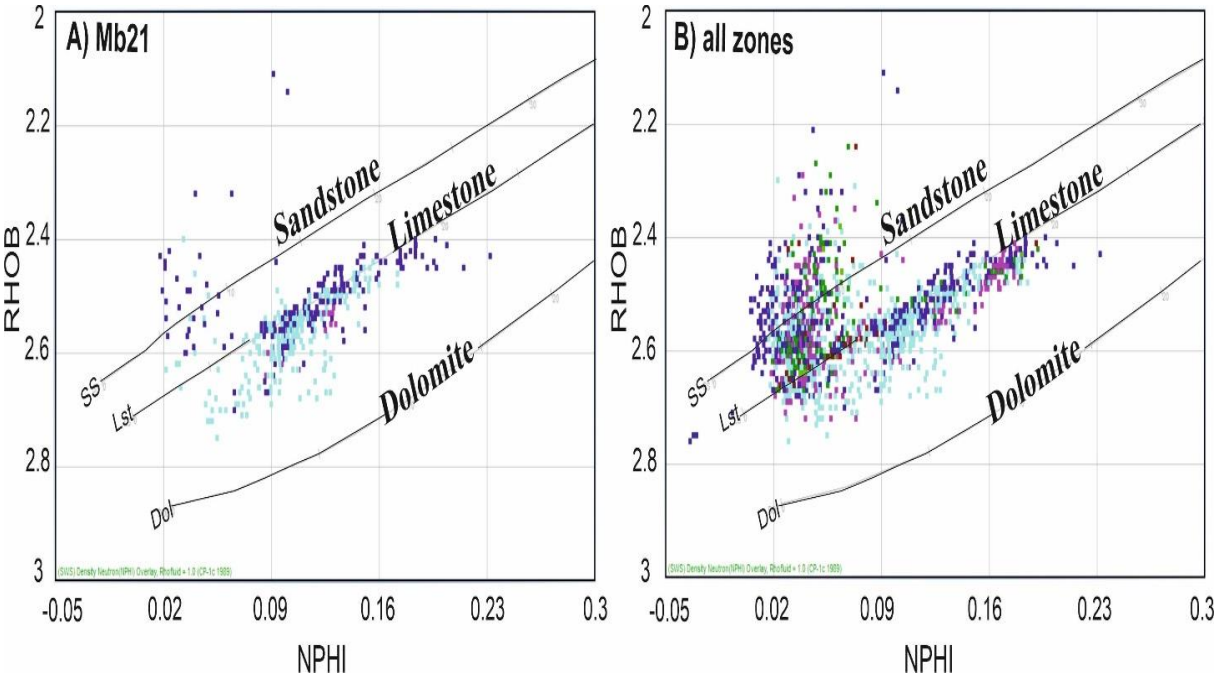

Fig. 2.1: M-N X-plot, A) shows the main lithology of the MB21 unit, limestone with few shale presences. B) shows the whole Mishrif Formation lithology is limestone with some shale and traces of dolomite.

In the other wells the results were matching this result, and the variations across wells were not taken into consideration (Fig. 2.2). from the result could distinguish acute values of porosity and the points gathering as vertical line. This vertical line can be interpreting to be fault or compacted non porous rock (Fig. 2.3).

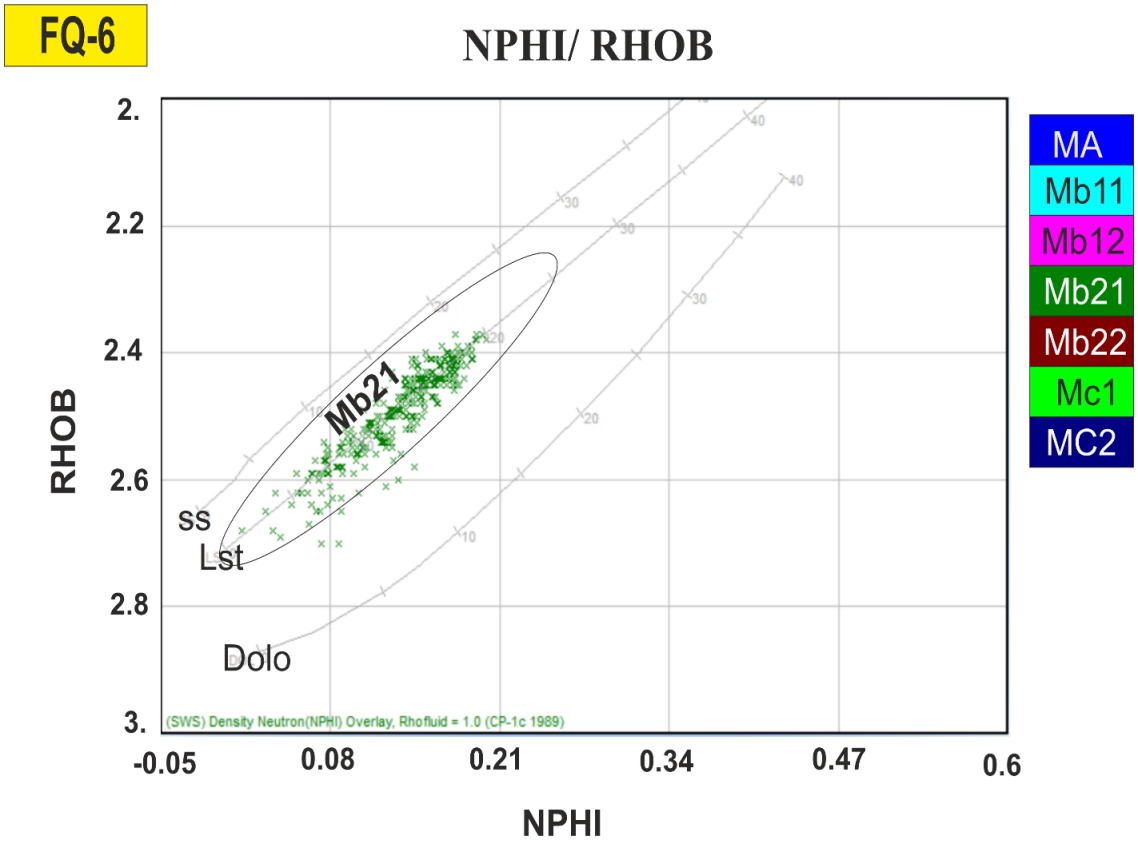

Fig. 2.2: the porosity/density plot shows the min lithology of MB21 reservoir unit in well FQ-6.

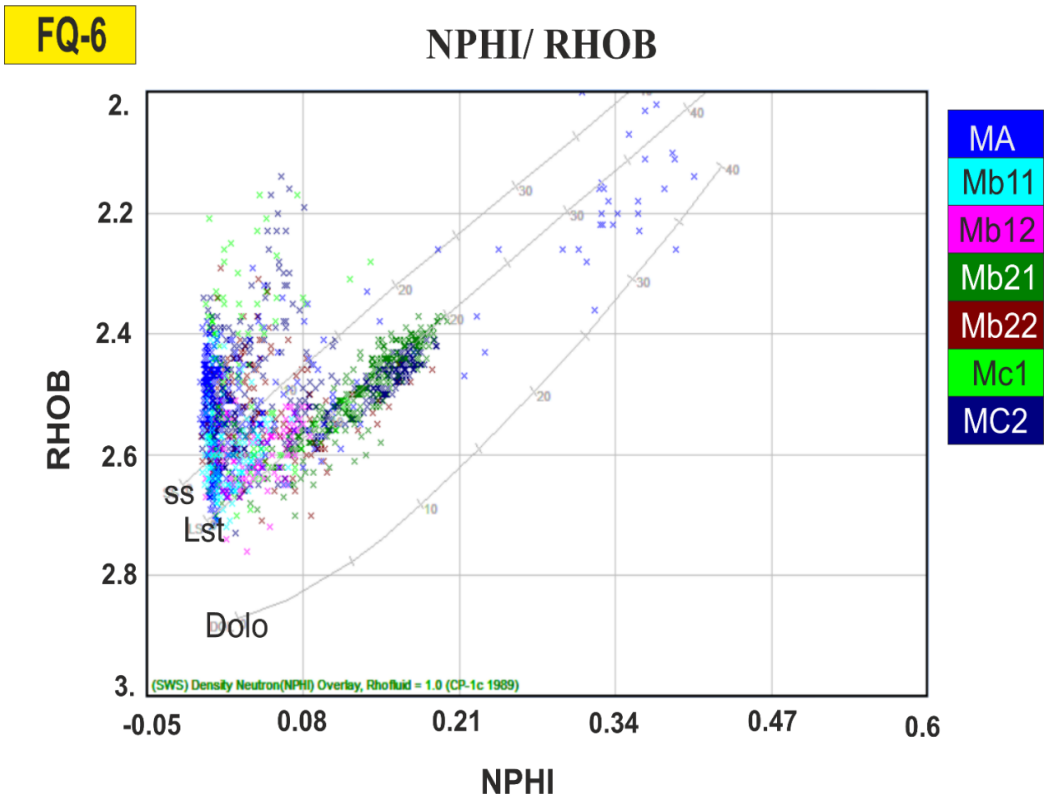

Fig. 2.3: porosity/density plot for whole Mishrif Formation in well FQ-6.

b. Shale Volume (V_{sh})

The Shale Volume in the formation reflects the porosity and water saturation, and for that, it takes an important place in the petrophysical calculations when studying the reservoirs' characteristics to evaluate the hydrocarbons in the targeting layers (Beydoun, 1989).

The presence of shale (or mud) affects the reservoir properties if the rate is 10-15% proportional to the total volume of rock, and the other significant effect is to reduce the resistivity difference between water formation and hydrocarbons (oil & gas) in the log registers. There are a number of logs dealing with shale containing, like R, SP, N, and GR logs, but the Gamma Ray (GR) log is the best one so as to its reading to the radiative elements that are occasionally found in shale, and the way to calculate depending on the sedimentation periods throughout some various equations (Table 2.1) (Kamel & Mabrouk, 2003).

Table 2.1: Shale Volume equations aafter (Kamel & Mabrouk, 2003).

Item	Log	Equation	Index
	Resistivity	$V_{sh} = \left(\frac{R_{sh}}{R_t}\right)^{0.5}$ (2.13)	High V_{sh}= high res.
	Self-Potential	$V_{sh} = 1 - \left[\frac{sp - sp_{sh}}{sp_{cl} - sp_{sh}}\right]$ (2.14)	Hydrocarbon bearing fms., give high dispersed V_{sh}
	Neutron	$V_{sh} = \frac{\emptyset_N}{\emptyset_{N.sh}}$ (2.15)	
	Gamma Ray	$IGR = \frac{GR_{log} - GR_{min}}{GR_{max} - GR_{min}}$ (2.16)	For Jurassic-Cretaceous rocks.
		$V_{sh} = 0.33(2^{2*IGR} - 1)$ (2.17)	For Tertiary rocks.

The Gamma Ray plot is used to estimate the Shale Volume. Calculation of Shale Volume for the depths of interesting has different formulas relatively to the age of deposition, so for the Tertiary reservoir it depends young rock modulus while for cretaceous and earlier ages take an old rock modulus for computing the volume of shale from the GR log.

Considering the values of total and effective porosity, they were taken from Neutron and density logs of the studied wells and regarding the sharp changes in Gamma ray reading, they were used to limit the Mishrif Formation units. The chosen wells were from both north and south domes, and the values of Shale Volume according to this calculation were in range of 9%-28 % of the bulk volume, and the Shale Volume in average for all studied wells in the field was 17.47%.

The low value at all wells is in the MB21 unit that has steady range of the shale dispersion amount through the unit body in value about 12% of its volume, and may increase up and down ward away from this unit (Table 2.2), Figures 2.4, 2.5, and 2.6.

Table 2.2: contains the average of the Shale Volume in the Mishrif Formation 's units for studied wells.

Strtigraphic Units	% Vsh (well FQ-4)	% Vsh (well FQ-6)	% Vsh (well FQ-14)	% Vsh (well FQ-19)	% Vsh (well FQ-20)
MA	9.379	24.16	15.113	7.8325	15.005
MB11	23.434	14.712	13.62	11.453	24.0126
MB12	20.59	16.003	11.18	13.634	19.003
MB21	12.486	12.314	10.4	10.233	14.012
MB22	24.842	19.0023	17.112	23.596	24.027
MC1	28.338	19.817	21.315	28.028	19.121
MC2	15.767	16.839	24.323	25.785	17.633
Overall	19.262	17.549	16.15	15.838	18.554

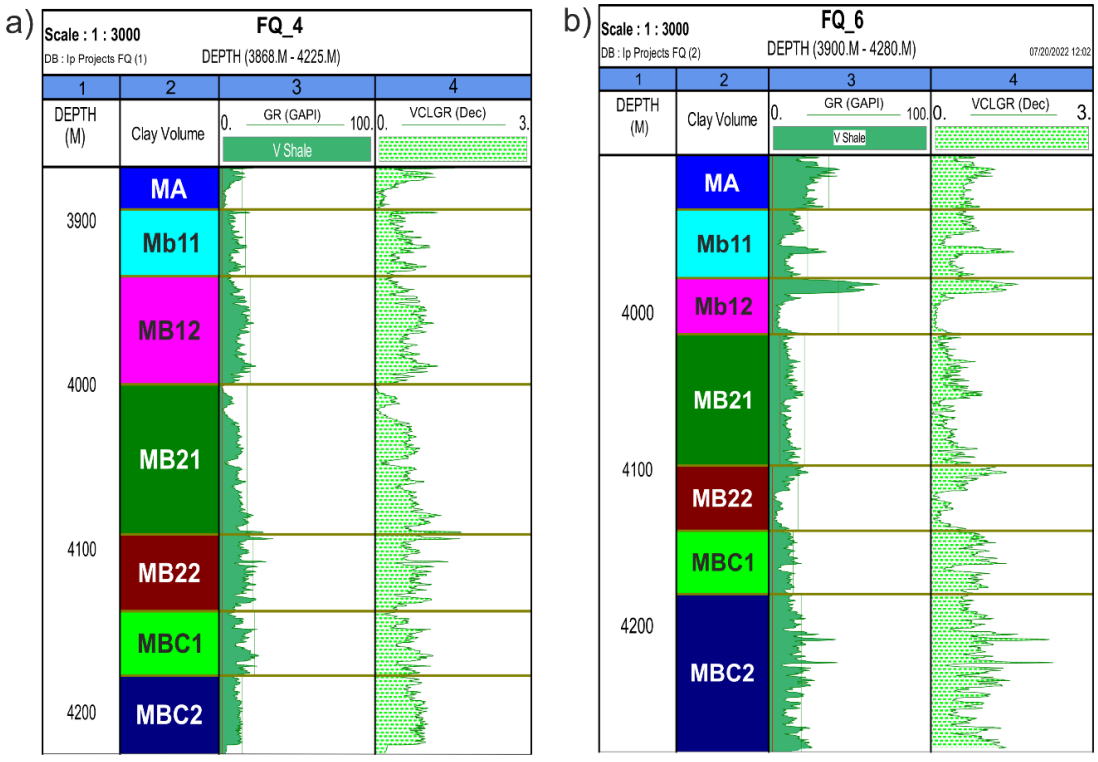

Fig. 2.4: showing the Shale Volume of Mishrif units at well FQ_4 & FQ-6.

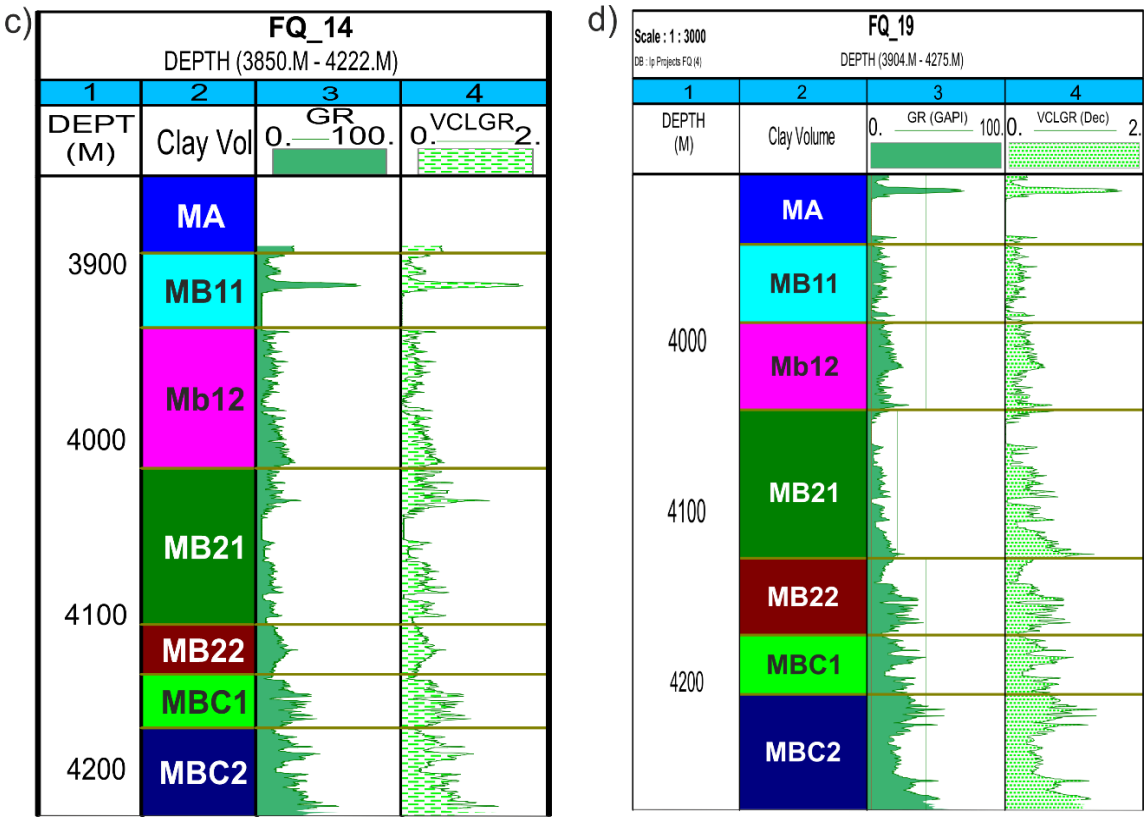

Fig. 2.5: showing the Shale Volume of Mishrif units at well FQ_14 & FQ-19.

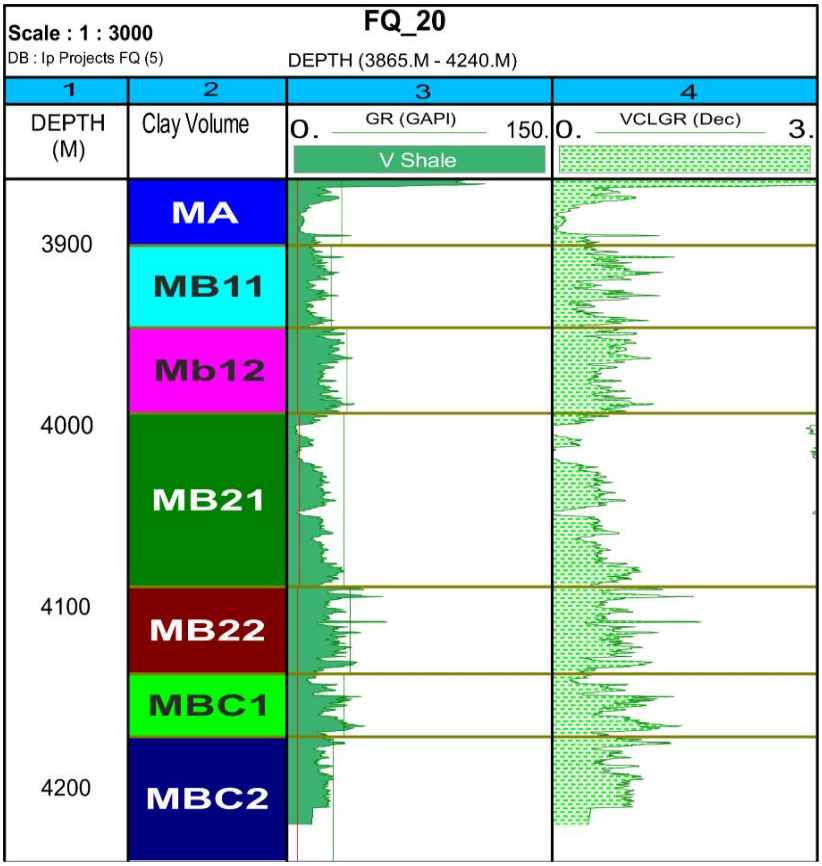

Fig. 2.6: showing the Shale Volume of Mishrif units at well FQ_20.

c. Porosity (Ø)

Porosity represents the percentage of void space in a rock's body. It is defined as the ratio of voids volume to the total volume and written as either a decimal fraction between 0 and 1 or as a percentage ratio (Vomocil, 1965). Description of formation's pore system is too important during investigation works of the storage and movement of water as well as hydrocarbon, and the nature of the pores in the rock, if it was connected (active porosity as in sand) or detached (inactive porosity as in shale) could help to estimate the formation considering reservoir or not. Simply, Soil pore systems are not a band of straight, uniform bore capillary tubes. In spite, if the capillary theory can be assumed valid in the pore system, the calculated radius from the equation will represent the minimum size of the pore neck which allows the air-water interface to move during drainage. And the general equation to calculate porosity is (Vomocil, 1965):

$$\emptyset = \frac{Vv}{Vt} \qquad (2.1)$$

Where: ø = porosity, Vv = voids volume, Vt = total volume of rock body). Fortunately, there are proposal limits for porosity, which could be found in (Table 2.3).

Table 2.3: Types of porosity after (Vomocil, 1965).

No	Ø value	Type of porosity
1	< 5	Negligible
2	5-10	Poor
3	10-15	Fair
4	15-20	Good
5	20-25	Very good
6	> 25	Excellent

The importance of calculating porosity discussed in this study previously, and it can be attained by (Neutron, Density, and Sonic) logs in some different methods (Table 2.4) (Pushnov, 2006).

Table 2.4: porosity equations for various logs data (Wylie, 1958).

No.	Log	Index
1	Density log	For shale-free formations, depend on Wyllie equation (Wylie, 1958): $\emptyset_D = \frac{\rho_{ma}-\rho_b}{\rho_{ma}-\rho_f}$ (2.2)
		For shale-containing formations, correction will be making with Dresser Atlas, 1979 formula: $\emptyset_{D_{corr}} = \frac{\rho_{ma}-\rho_b}{\rho_{ma}-\rho_f} - \left[\frac{\rho_{ma}-\rho_{sh}}{\rho_{ma}-\rho_f}\right] * V_{sh}$ (2.3)
2	Neutron log	The porosity of shale-free formation, reads directly from log, and for the shaly formation make a correction with Donaldson, 1996 formula: $\emptyset_{N_{corr}} = \emptyset_N - (V_{sh} * \emptyset_{N_{sh}})$ (2.4)
3	Sonic log	Form (Wylie, 1958), calculated porosity by the relation between travel time and porosity: $\emptyset_s = \frac{\Delta t_{log}-\Delta t_{ma}}{\Delta t_f-\Delta t_{ma}}$ (2.5)
		For shaly formation, doing correction with (Dresser Atlas, 1979) formula: $\emptyset_s = \frac{\Delta t_{log}-\Delta t_{ma}}{\Delta t_f-\Delta t_{ma}} - \frac{\Delta t_{sh}-\Delta t_{ma}}{\Delta t_f-\Delta t_{ma}} * V_{sh}$ (2.6)
		For hydrocarbon-bearing formation, the correction is with (Hilchie, 1978) formula: $\emptyset = \emptyset_s * B_{hc}$ (2.7)

The porosity is an important part of the interpretations that help limiting and identifying the possibility of the water amounts in the reservoir as it is naturally found in the rock formation (Wylie, 1958). The resultant porosity values can be seen in the correlation plot from the interactive petrophysics software version 3.5 depending on registers of Neutron, density, and sonic logs can be seen in the Fig. (2.7)

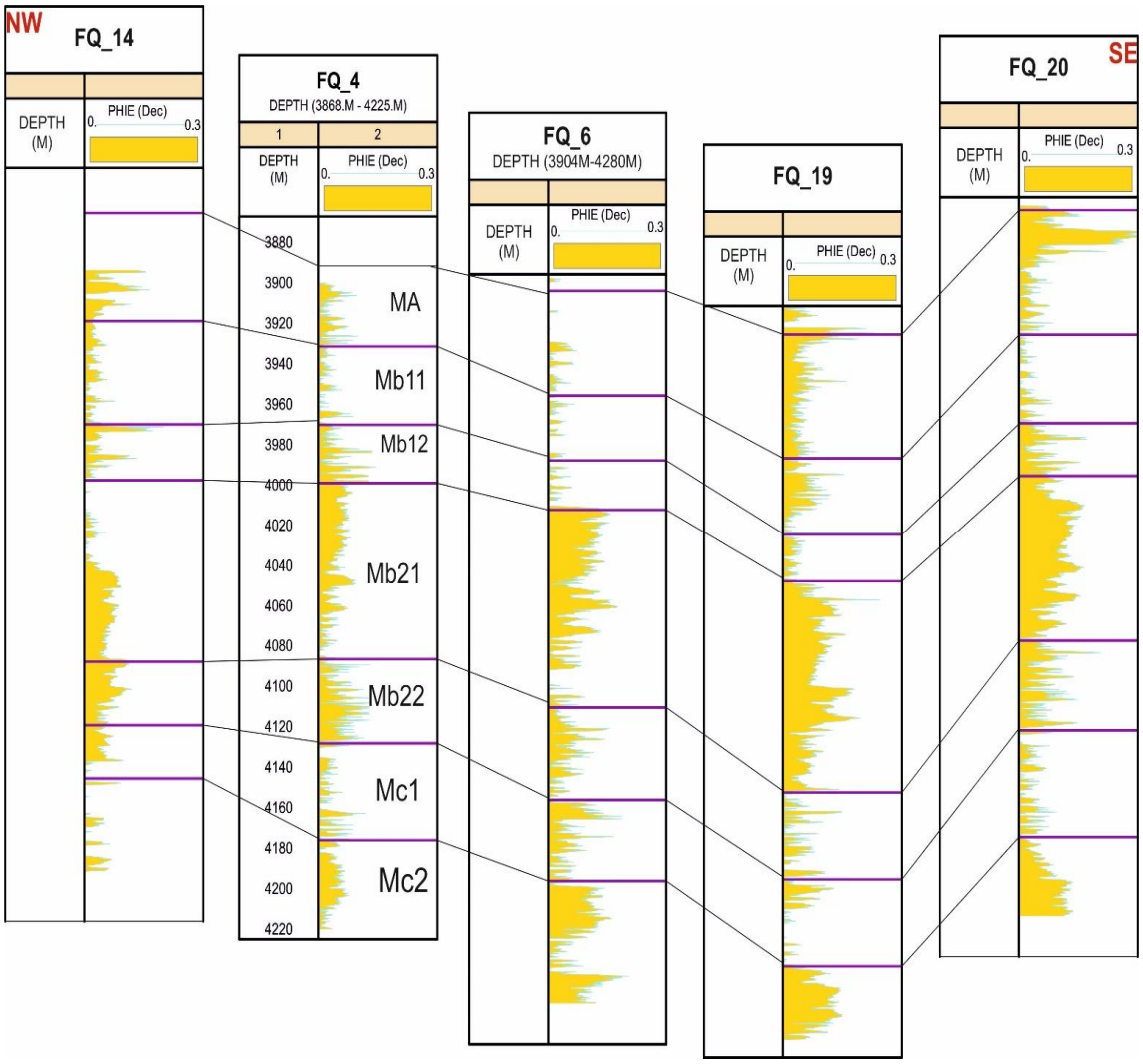

Fig. 2.7: shows the correlation of porosity for the studied wells warding (NW -SE), in all wells appeared the MB21 unit with good value of porosity. The well FQ-14 shows poor data reading in order to the poor log reflectance.

The effective and total porosity, taken from the sonic log, did not represent the total porosity where the sonic log, unfortunately, could not measure the porosity of the fracture. The values of the total porosity (PHIT) and effective porosity (PHIE) for studied wells in the area of study are shown in (Table 2. 5)

Table 2.5: the total and effective porosity calculated for studied wells.

Well No.	FQ_4	FQ_6	FQ_14	FQ_19	FQ_20
PHIT $_{total}$	6.8%	7.8%	8.1%	7.7%	9.7%
PHIE $_{effect}$	6%	6.7%	4.1%	5.2%	6.2%

The secondary porosity came from the fractures even in carbonates rocks or clastic sand stones, but other forms could be found in the carbonates like vugs

due to dissolution processes (van Golf-Racht, 1982). This type of porosity to be calculated from the well logs can be estimated by the difference between the total density porosity and total sonic porosity (Fig. 2.8) (www.Geoloil.com, 2020), where the density porosity log measures the whole porosity spaces in the formation while sonic log does not passing through the vugs or opened fractures (Zerrouki et al., 2014), so:

$$\emptyset_f = \emptyset_d - \emptyset_s \quad (2.12)$$

Where, $ø_f$ is the porosity of fractures and/or vugs, $ø_d$ is the density porosity, and $ø_s$ is the sonic porosity.

The porosity that considers one of the most important properties to the fluid (including hydrocarbons) preserves potential for a good reservoir (Ehrlic et al, 1984). Neutron and Density logs readings depended on porosity estimation values, and the best value recorded was in the zone of MB21 unit which was about 16% with a range of unit's porosity values 4.5%-18% (Fig. 4-b).

The porosity value represents both primary and secondary values, where the primary porosity developed during the period of sedimentation which is calculated from the sonic log interpretation, and the secondary porosity which is post-developing over a tectonic or/and diageneses processes (van Golf-Racht, 1982). The secondary porosity is distinguished character for the carbonate rocks more than in the clastic one, and in this study, the evaluation of the secondary porosity for the Mishrif reservoir formation calculated from the variance between the total and primary porosity as a secondary porosity index SPI (Ghafoori et al., 2009). In the Mishrif Formation, the secondary porosity grades between 1.5%-5.5 %, and the values showed that the best developing secondary porosity overall was recorded in the MB21 unit.

For all registered porosity values, an effective porosity considers the more important one because it is representing the interconnection of pores that permit the fluid to be moved through. The modifying porosity with the values recorded

in the core samples endorsed the estimation of effective porosity and it was in the averages in the MB21 with a grade of 16%.

More precise porosity values of rock formations usually recorded from the core sample with some difficulties, but the symbiosis between core porosity measuring and log reading is essential to reach the true values. The core porosity for this study was gained from MOC for wells FQ-6, FQ-14, and FQ-19.

The porosity estimation from the studied wells pointed to the two types of porosity (primary and secondary), where a primary recorded value was in low levels of 4%-8.9%, and the secondary porosity estimated low to fair decimal fraction in values about 5%-12%. All the recorded data for the well logs and the obtained data that belong to the core measuring porosity showed that the MB21 unit of Mishrif Formation in the Fauqi oilfield had the high value of secondary porosity, but with less than MB11, and MB12 in the primary porosity.

The type of diagenesis processes that is responsible for secondary porosity in the MB21 reservoir unit are not evaluated precisely in this study according to the lack of data involving with petrographic study, but by sighting the previous registered data at the library of reservoir directorate and reviewing the last studies, all of it indicate of the dissolution process especially in the rudist facies layer of MB21 reservoir unit (AlBahadily & Nasser, 2017), the Mishrif equivalent formation in south Iran, Sarvak formation, the results were tend to the same fact (Ghafoori et al., 2009).

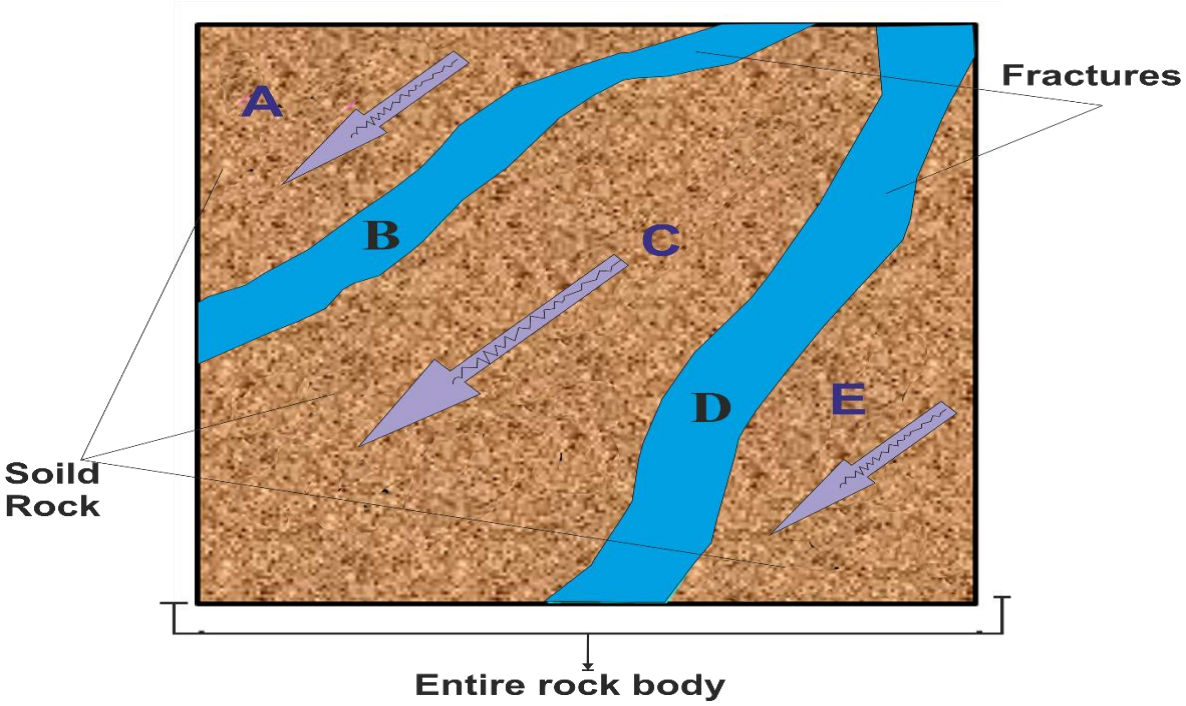

Fig. 2.8: shows the prediction of porosity fracture through density-sonic relation. Sonic waves are just transmitted through (A, C, and E) sections, but the density and neutron logs calculate the entire rock body, modified after (www.Geoloil.com, 2020).

d. Water and Hydrocarbon Saturation

Calculation of fluid saturations is still one of the main properties to the petrophysics' researcher. Since the manifest of petrophysics, the problem of saturation issues still stands as one of the major technically challenging problems. And with few exceptions, this challenge is fixed by determining water saturation by the next relationships (Pickett, 1966):

$$S_w = I^{-1/n} \quad (2.18)$$

$$I = \frac{R_t}{FR_w} = \frac{R_t}{R_0} \quad (2.19)$$

$$F = \emptyset^{-m} \quad (2.20)$$

Where;

S_w = pore volume filled with water of resistivity R_w,

I = resistivity index,

n = saturation index,

R_t = true resistivity of formation,

F = the factor of formation resistivity,

Ø = porosity factor, and

m = cementation index.

In the pre-days, to resolve this equation, the resistivity index is determined from the borehole directly and this value is used to get the Sw from the apparent value of the saturation index or for laboratory tests.

Some other functions are used to obtain water saturation in the formations that have been interesting for oil exploration. An ordinary matter is to the presence of water accompanying to the hydrocarbon deposits, so it is important to estimate its amount and take a fair view of the quantity of oil there, by subtracted water volume (Asquith et al., 2004; Schlumberger Ltd., 1984). The most used methods are:

1. **For uninvaded zone:** zones with shale ratio less than 10%, Archie's equation will be employed:

$$S_w = \sqrt{\frac{F * W_r}{R_t}} \qquad (2.21)$$

While for shaly formation with proportion exceed than 15%, depending Asquith's equation (Asquith et al., 2004):

$$S_w = \left(\sqrt{\frac{F * R_w}{R_t}}\right) - \left(\frac{V_{sh} * R_W}{0.4 * \emptyset_t * R_{sh}}\right) \qquad (2.22)$$

2. **For flushed zone:** Archie's equation is the chosen formula:

$$S_{xo} = \sqrt{\frac{F * R_{mf}}{R_{xo}}} \qquad (2.23)$$

Where: Sw = percentage of water saturation (5%),

S_{xo} = water saturation in flushed zone,

F = formation factor,

V_{sh} = Shale Volume,

$\emptyset_t$ = total porosity,

R_w = formation water resistivity,

R_t = truly formation resistance,

R_{sh} = shale resistivity,

R_{xo} = invaded zone resistivity.

Every parameter, involved with previous equations, should be mathematically calculated to employ in the calculations, as:

Formation factor (F): the directly proportion for formation water resistivity with over-saturated formation resistance (R_o) by Archie's equation, 1944 (Archie, 1950):

$$R_o = F * R_w \quad (2.24)$$

$$F = \frac{R_o}{R_w} \quad (2.25)$$

- Mud filtrate resistivity (R_{mf}): directly taken from the log and make a correction by Arps' equation according to (Archie, 1950):

$$R_{mf_{tf}} = R_{mf_{ts}} * \left(\frac{T_s+21.5}{T_f+21.5}\right) \quad (2.26)$$

- Formation temperature (T_f): while both mud and mud filtrate temperature vary according to the temperature changing with depth directly, so it is necessary to limit the formation's temperature from (Archie, 1950):

$$T_f = (G.G * d) + T_s \quad (2.27)$$

$$G.G = \frac{BHT-T_s}{T_D} \quad (2.28)$$

Where: D = depth,

T_D = the temperature at the limited depth,

G.G = geothermal gradient,

BHT = borehole basement temperature.

- Formation water resistivity (R_w): regarding (Schlumberger Ltd., 1984), could be calculated directly from cross-section plots of (R&Ø), SP log curve, or from the geochemical analysis. According to (Sadooni, 1995), by limiting the shale baseline, the distal curve deviation, and the temperature at the distal point in order to find the R_w from the equation:

$$SSP = -K\log\frac{R_{mf}}{R_w} \quad (2.29)$$

For our study, the value of formation water resistivity had been obtained from the MOC, and was equal to (0.02).

- ***Moveable Fluids Bulk Volume (hydrocarbons & water):***

Bulk volume of water (BVW): representing the amount of formation porosity added to the water saturation, and it can be used to evaluate the carbonate reservoir's potential. Be noticed, that if the volume of water is still steady for various depths means it is irreducible water and the zone is homogenous (Schlumberger Ltd., 1984).

$$BVW = S_w\emptyset \quad (2.30)$$

In the same manner can be also calculate porosity for an invaded zone (S_{xo}) by using the same equation (Schlumberger Ltd., 1984):

$$BVW = S_{xo}\emptyset \quad (2.31)$$

Bulk volume of hydrocarbon (BVH): by estimating the area and the average thickness of a reservoir, porosity, and water saturation could determine the hydrocarbon volume (Wheaton, 2016):

$$V_{xo} = Ah_v\emptyset(1 - S_w) \quad (2.32)$$

Where:

V_{xo} = hydrocarbons volume,

A = average area,

h_v = net thickness,

Ø = porosity,

S_w = water saturation.

Usually, from these parameters in addition to the recovery factor (R_F), the volume of reservoir can be obtained (Wheaton, 2016), from:

$$V_R = \emptyset AhS_hR_F \quad (2.33)$$

Where: V_R = volume of reservoir,

S_h = hydrocarbon saturation,

R_F = recovery factor*,

Ø = porosity, A= area, and h = thickness.

* **recovery factor**: hydrocarbons' volume that contained in the reservoir represents the function of pore-volume and water saturation, which is implied to determine the amount of recoverable hydrocarbons in the reservoir, and they are a various drive for this parameter (Table 2.6) (Dake, 1978).

Table 2.6: drive mechanism of reservoir and hydrocarbons recovery factor in percentage afrter (Dake, 1978).

Reservoir drive mechanism	Percent ultimate recovery	
	Gas	Oil
Strong water	30–40	45–60
Partial water	40–50	30–45
Gas expansion	50–70	20–30
Solution gas	N/A	15–25
Rock	60–80	10–60
Gravity drainage	N/A	50–70

After all, there were two interesting reservoirs for commercial purposes. The main reservoir is in the Mishrif Formation, especially at Mb.21 unit, where the secondary reservoir for our field was the Asmari reservoir (Aqrawi, 1998) (unfortunately, the researcher dose not obtain the required data for the secondary one). The water saturation (S_W) parameter usually depending Archie's equation in the calculations, which measures the relation of porosity and resistivity of the rock formation (Archie, 1950):

$$SW = \left(\frac{a*Rw}{Rt*\emptyset^m}\right)^{1/n} \quad (2.34)$$

Where: S_W is the water saturation in decimal fraction, (a, m, and n) are Archies' parameters stand for: (a) is the tortuosity factor, (m) is saturation exponent, and (n) is for cementation exponent with a value of (1, 2, 2) respectively, Rw is the

water resistivity of formation recorded from M.O.C with a value of (0.0217 Ohm.m), and Rt is the true resistivity of the formation.

The calculated Rw from the Pickett plot is ranging (from 0.0214 to 0.0217 Ohm.m). The (a, m, and n) values are0020calculated with interactive petrophysics software with the logarithmic scale (Pickett, 1966), and the true resistivity measured directly from the resistivity log (Figs. 2.9, 2.10, and 2.11).

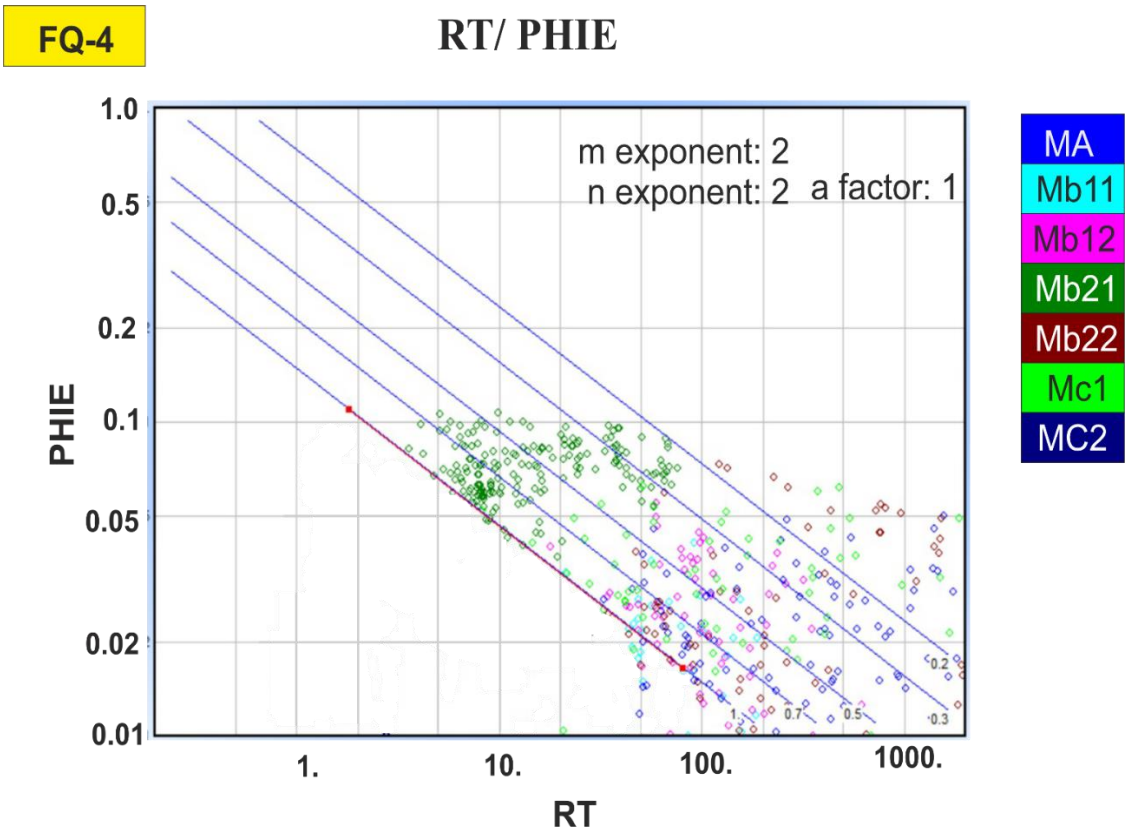

Fig. 2.9: Pickett plot of density – porosity relation to find the value of formation water resistant and saturation for well FQ-4.

The result from the well FQ-4 aimed to the best values in the main reservoir units, MB21 in dark green ticks' color which has the high value of porosity with less percentage of water saturation (Fig. 2.9).

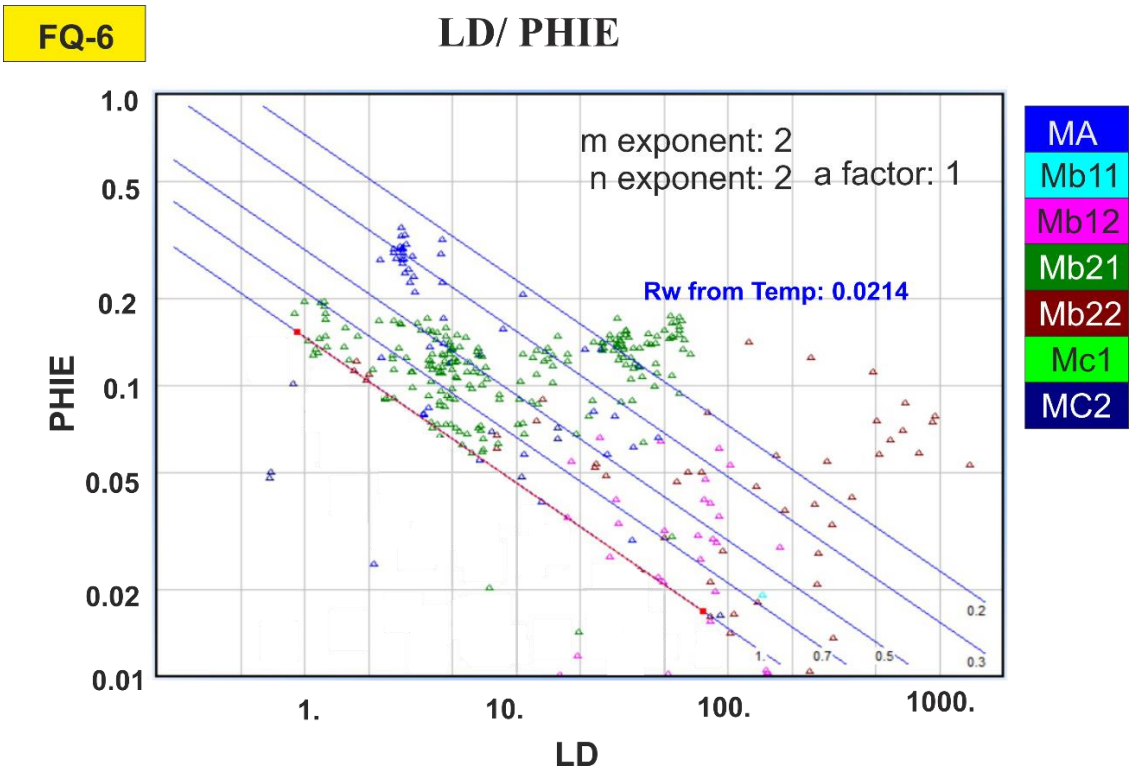

Fig. 2.10: Pickett plot of density – porosity relation to find the value of formation water resistant and saturation for well FQ-6.

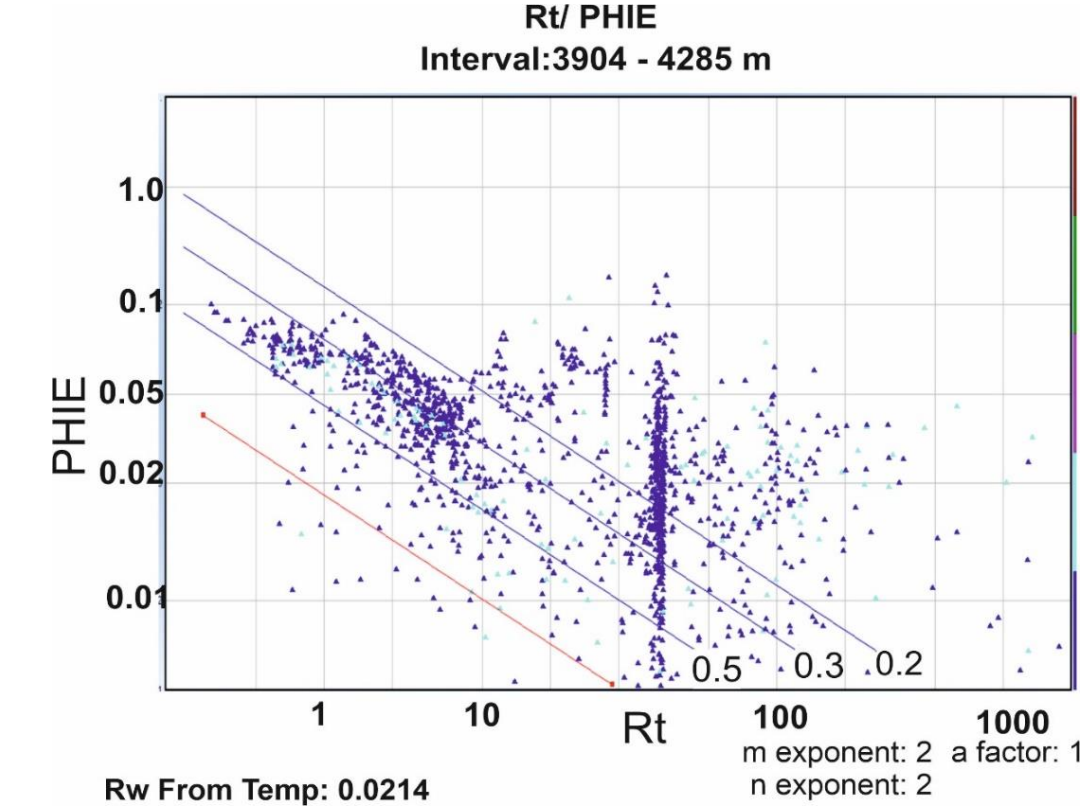

Fig. 2.11: Pickett plot of density – porosity relation to find the value of formation water resistant and saturation for well FQ-19.

The results of both FQ-6 and FQ-19 wells showed the same result for FQ-4 well. The parameter of water saturation is too important as a petrophysical character to limit the approximate hydrocarbon in a reservoir (Pickett G. R., 1973). The main dependent function to measure the water saturation in the formation is resistivity. Regarding the hypothesis of considering all the voids in rock formation will be fulfilled with fluids of water and hydrocarbons (oil and gas), may it contain one phase or two and in special cases filled with three phases of fluids (Kamel & Mabrouk, 2002).

The most important target is the hydrocarbons volume in the reservoir, but with no easy way to estimate its quantity, and where the volume of water could be estimated with more than a method, so, the hydrocarbons volume gain from the percentage of water saturation (Kamel & Mabrouk, 2002) from the equation:

$$S_h = 1 - S_w \quad (2.35)$$

Where: hydrocarbons saturation is (S_h), and water saturation is (S_w).

Applying the equations and integrating them with the results of IP logs analyses led to the main rock formation properties ending with the reservoir characteristics that are clarified forwards in this chapter of the study.

The Shale Volume can estimate the reservoir units in the formation, as such the formation was divided by previous studies into seven units by the comparison of the Shale Volume and type of fluid contents rather than the changes in the values of porosities. These seven reservoir units were represented in the Mishrif Formation which are MA, MB11, MB12, MB21, MB22, MC1, and MC2 have some changes in their thicknesses in the various studied wells.

The formations depths and thicknesses vary across the studied wells in the field relative to the well location and the thickness of Injana and Fatha formations, but the total stratigraphic is at the same details. The whole Mishrif Formation is limestone composition that varies across its reservoir units by the structure of the lime, Shale Volume, water and hydrocarbon saturation and the values of porosity.

d. Permeability (K)

Permeability is defined as a measurement of the porous medium capability to fluid transit through it, and it is the most important character to the rock units to be a reservoir when being porous effective and connected. Permeable materials permit the flow of fluids from levels of high energy to levels of low energy due to interconnected voids (Dake, 1978).

The diversity of soil grain size regarding the coarse to very fine-grained soil gives a wide range of permeability coefficient values up to 10 orders of magnitude. Most methods to calculate permeability in the field are theoretical, related to several hypotheses regarding the test involving the water head and path flow. Field permeability may be calculated through pumping tests which give a good measurement of the aquifer permeability (Elhakim, 2016). Unfortunately, the calculation of permeability for carbonate rocks is not as easy as in clastic rocks, and because of its deposition environment's nature and for the diageneses processes rather than the varying porous. So, most geologists depend on resistivity logs to calculate, in different ways, relatively to the effective porous ratio and water saturation (Jassim & Goff, 2006).

The blocked porous medium has three varied relative permeabilities, to gas, oil, and water, that mainly depend on the state of saturation by each of these fluids, and particularly on the allocation of the saturation. There is a different case for air permeability and for the reservoir. The reason for this difference between them is that relates to the sand structure itself which is regularly modified under many circumstances with the processes of cleaning and drying pre-measuring air permeability (Johnston & Beeson, 1945). The permeability of the medium could be absolute or effective.

Absolute permeability is calculated throughout Darcy's equation (Johnston & Beeson, 1945) :

$$Q = \frac{kA\Delta P}{\mu L} \qquad (2.8)$$

Where:

Q = liquid quantity in millimeter, K = Darcy's constant,

A = cross-sectional area, ΔP = pressure differentiation,

μ = viscosity, and L = long of the flow path.

To estimate the precise value of porosity, calculate the porosity values from the measured logs and compare with the core porosity analysis values of the studied wells by making a cross plot between two readings from the two sources in the linear-linear equation to identify the relationship type.

Permeability calculation (K): at the beginning of this chapter we spotted some information about permeability and its meaning in general.

As it is known, the permeability calculates from Darcy's law in the laboratory by flowing a known viscosity fluid through a sample core of porous rock with figured dimensions, then measuring the pressure's drop across the core or by another way depending on the measuring of the rate flow that produced at various pressures (Fig. 2.12) (Glover & Luo, 2020).

Darcy's formula is expressed in:

$$Q = \frac{KA(P_i - P_o)}{\mu L} \qquad (2.9)$$

Where:

Q = the flow rate in (cMB12/sec) or (MB12),

P_0 = pressure of outlet fluid in (dyne/cMB11) or (pa),

P_i = pressure of inlet fluid in (dyne/cMB11) or (pa),

K = permeability in (MB11 or darcy*),

A = the sample area in (cMB11, or MB11),

μ = the dynamic fluid viscosity (pa. sec),

L = the length tube (fluid path) in (cm, or m).

***Note**: one darcy of permeability of a sample is 1cm long and the cross-section area is 1cMB11 when the difference load pressure between the ends of the sample is 1 dyne/cMB11 causing a flow rate of 1 cMB12/sec to the fluid of I poise

viscosity (1 darcy = 0.9869*10^{-12} MB11, 1 darcy = 1000 Milli darcy) (Glover & Luo, 2020).

The other type is effective permeability, which is an important one to the reservoir calculations, represents the rock that allows a specific phase of liquids to permit, concerning the other phases and it is related to voids saturation of liquids and their physical and chemical properties.

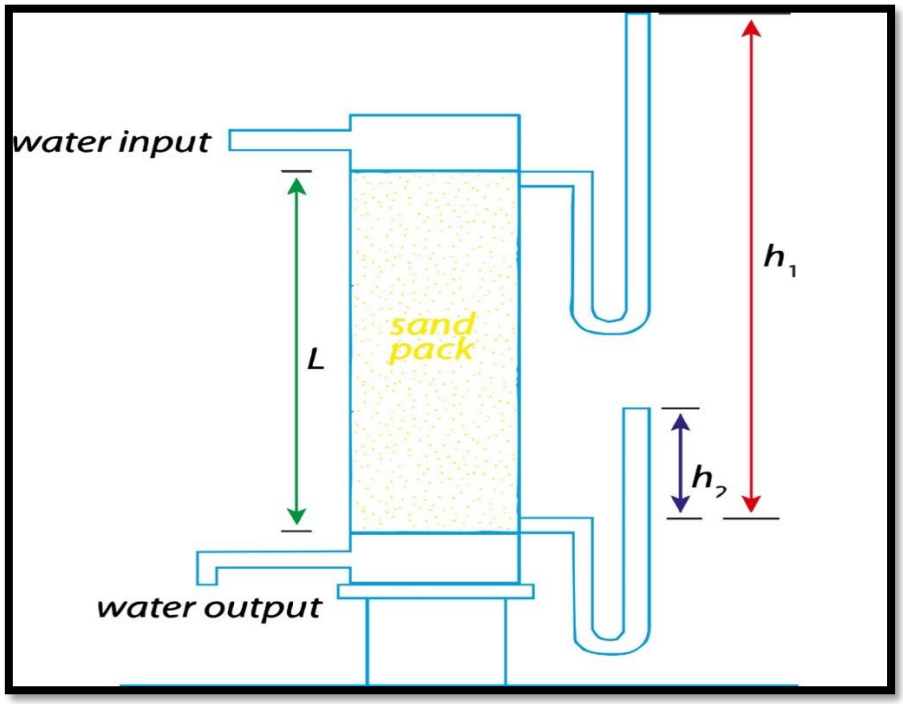

. Fig. 2.12: shows Darcy's apparatus, modified after (Glover & Luo, 2020)

So, the permeability for liquid (oil & water) and gasses could be obtained from the (equation 24) above:

- **For (oil and water):**

$$K = 1000\frac{L}{A}\,\mu\,Q\,\frac{1}{(P_0-P_i)} = 1000\frac{L}{A}\,\mu\,\frac{\Delta V}{\Delta T}\,\frac{1}{(P_0-P_i)} \qquad (2.10)$$

Where: Q = the flow rate = $\Delta V/\Delta T$ (cMB12/sec),

ΔV = flowed liquid volume in time ΔT (cMB12),

ΔT = measured flow time (sec).

- **For gases:**

$$K = 2000\frac{L}{A}\,\mu\,Q\,\frac{P_{atm}}{(P_0^2-P_i^2)} = 2000\frac{L}{A}\,\mu\,\frac{\Delta V}{\Delta T}\,\frac{P_{atm}}{(P_0^2-P_i^2)} \qquad (2.11)$$

Where: P_{amt} = atmosphere pressure.

There are several grades of permeability in rocks depending on the pore volume, compaction, cementation, and the rate of connected voids, which take a 12 by Leverson (1967) (Dake, 1978) (Table 2.7).

Table 2.7: permeability classification by Leverson, 1967 after (Dake, 1978).

Permeability Range (MD)	Class
< 1	Poor
1 – 10	Moderate
10 – 100	Good
100 – 1000	Very good
> 1000	Excellent

The calculation of permeability (K) depended on Timur's method to estimate the value without aiming to limit the type of fluids in reservoir voids (Timur, 1968). This equation considers the ratio of porosity to the irreducible water saturation in manner of Timur constant:

$$K = a * \frac{\emptyset^b}{SWi^c} \qquad (2.12)$$

Where: K is the permeability in millidarcy, ø is the porosity, S_{Wi} represents the irreducible water saturation water in the formation, and (a, b, and c) are constants.

The results showed that the best values were in the MB21 units and by comparison with values obtained for porosity, the best linear relation was also noticed in the MB21 unit (Fig. 2.13).

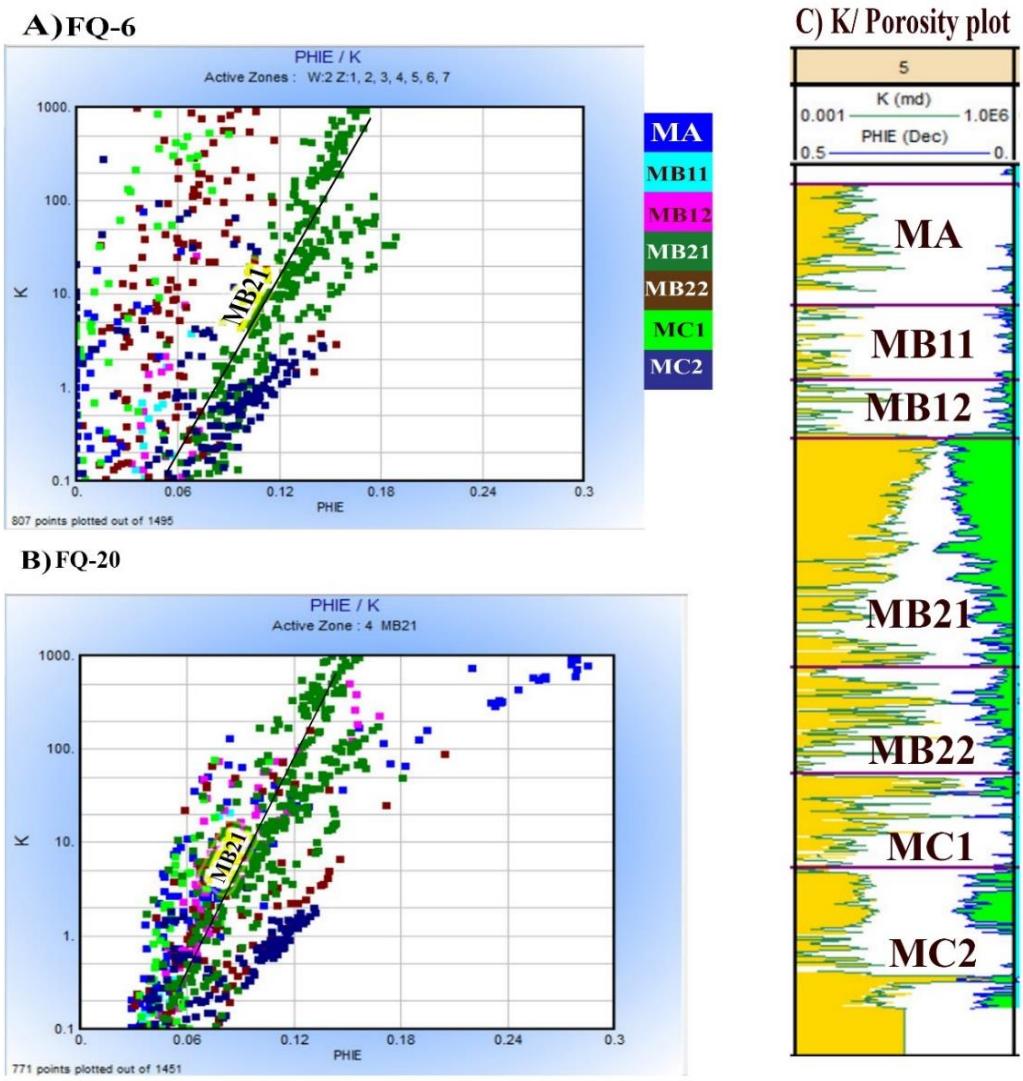

Fig. 2.13: A & B: an integration cross plots of porosity and permeability. Overall relations the best value showed in the MB21 unit as linear plotting relationship. C: shows the k log in the golden color and the porosity log in light green color, and obviously the best integer was in the MB21 unit.

Generally, the studied well showed the same comparison of porosity and permeability. Some of other units gave a good porosity but in regarding the fluid contents showed higher ratios of water saturation extracted from the saturation plots (Fig. 2.14, and Fig. 2.15).

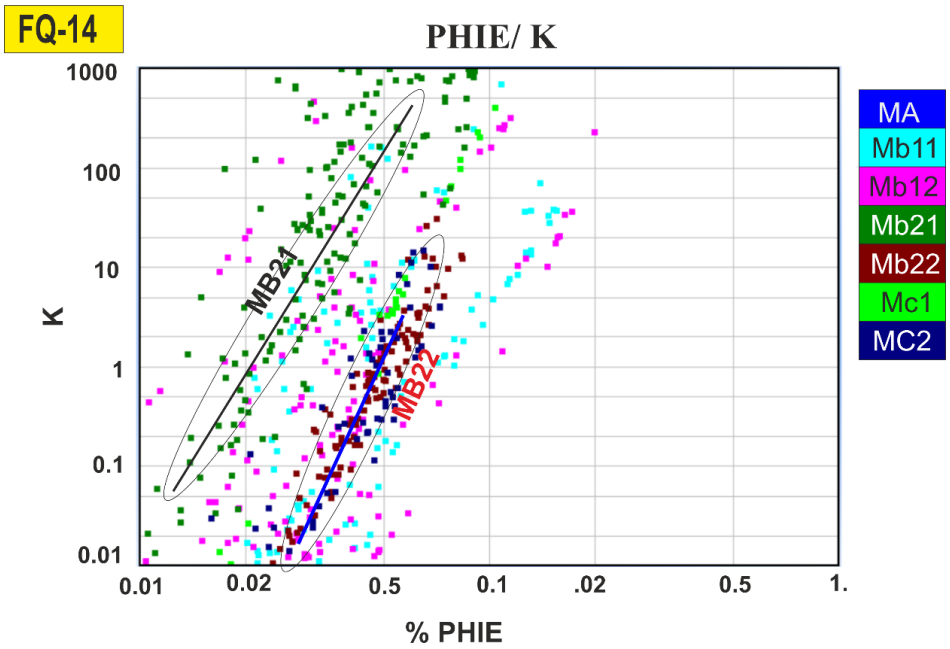

Fig. 2.14: proportional plot of well FQ-14, shows the relative relation of porosity/permeability clarifies the best linear in the MB21 unit. The unit MB22has a good linear relation but in low stage.

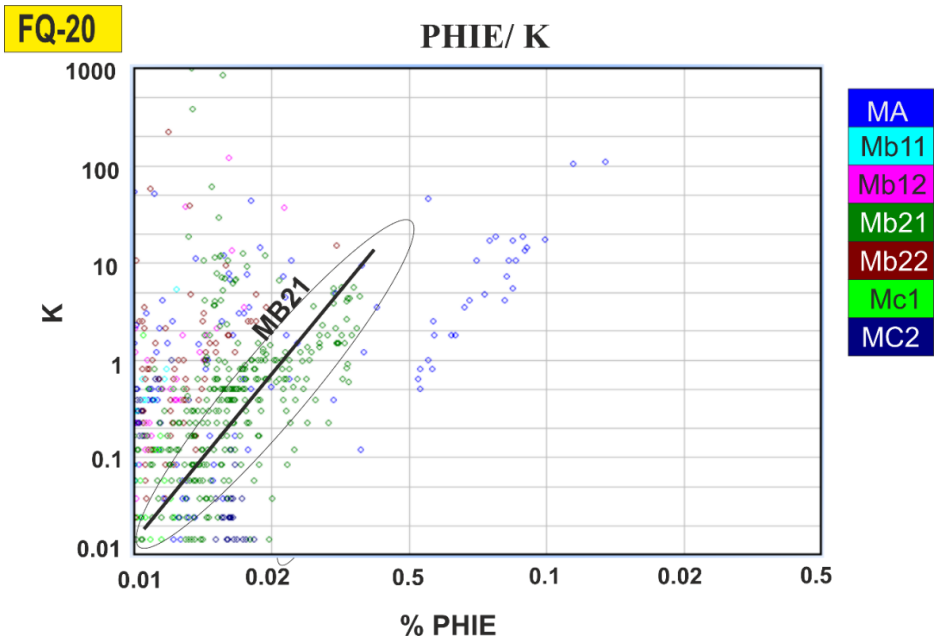

Fig. 2.15: proportional plot of well FQ-20, shows the relative relation of porosity/permeability clarifies the best linear in the MB21 unit.

Reservoir units' properties

1. MA Unit

This unit mainly consists of bioclastic limestone (packstone & wackestone). Fair to good oil shows in some parts, but poor porosity measured on CNL (6% in

average). The petrophysical properties of this layer such as porosity, water saturation and Shale Volume identify through the contour map of each parameter (Fig. 2.16, 2.17, 2.18)

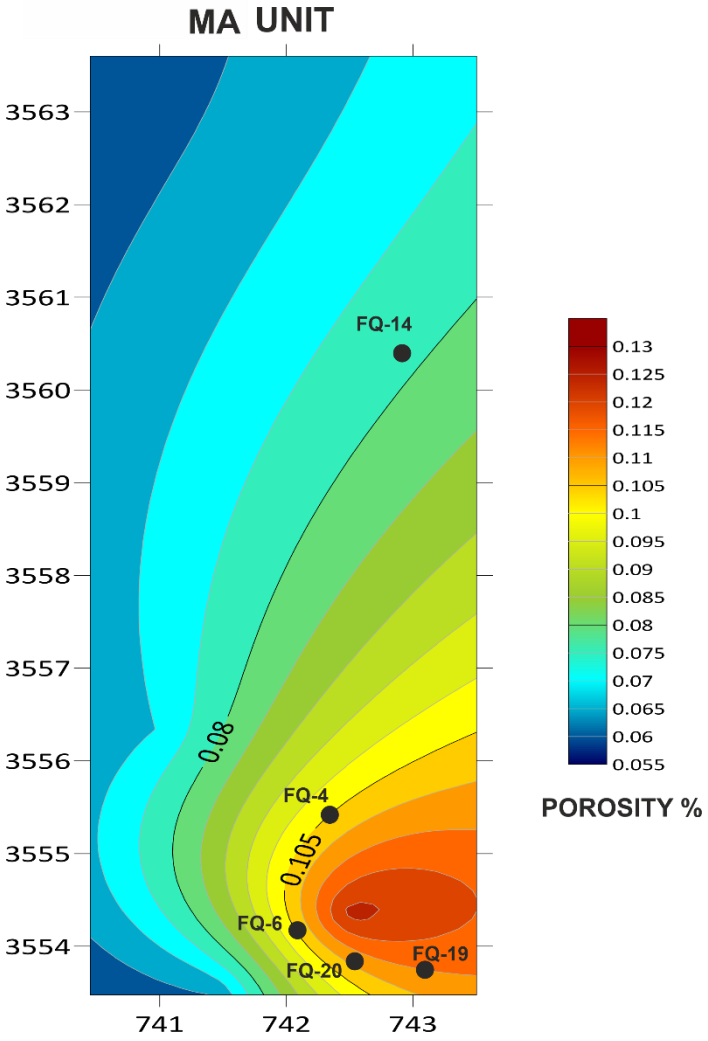

Fig. 2.16: shows the distribution of porosity for the MA unit.

The figure shows that the values of porosity ranges from fair to moderate and the high values are in the areas adjacent to the center of the south dome.

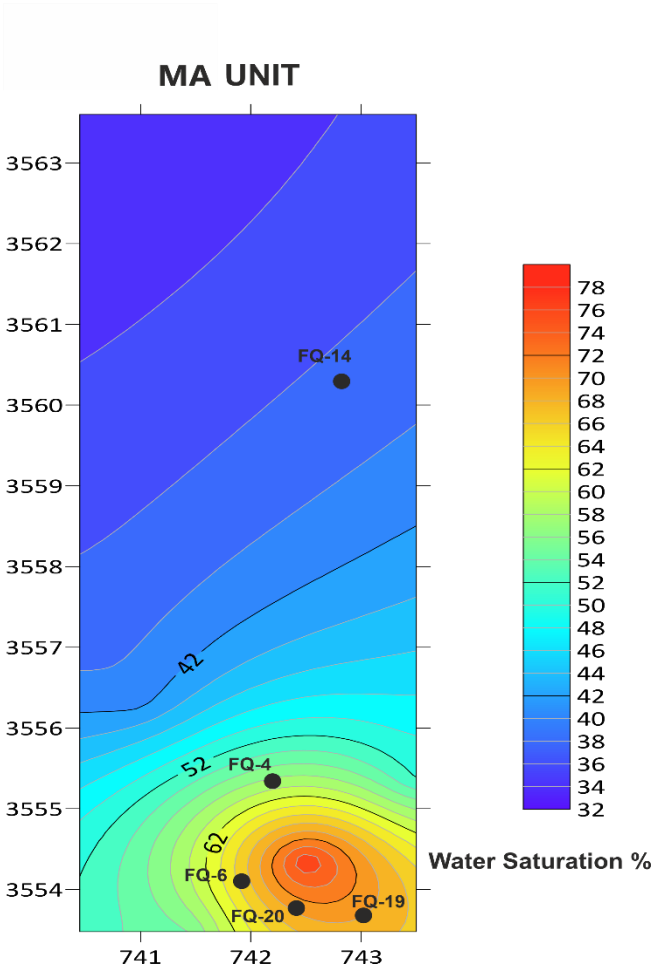

Fig. 2.17: The water saturation map in the MA unit throughout the studied wells.

The water saturation map of the unit shows high level of water saturation at most wells in ranges of 52-70% except that in the north dome was less than 40%.

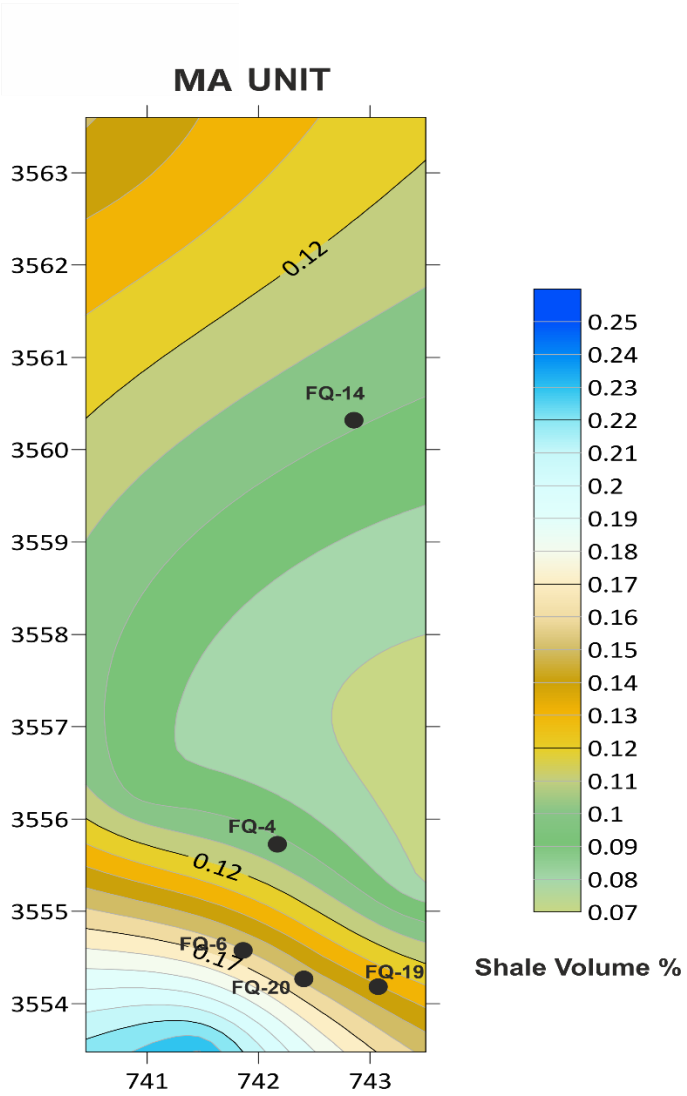

Fig. 2.18: shale map dispersion ratios within the MA unit, shows the low ranges of shales in this layer about 19% and the values decrease toward the north dome not exceeds of 10%.

2. MB11 Unit

This unit mainly consists of bioclastic limestone (packstone to wackestone) with chalky limestone in various depths. It shows trace oil with poor porosity on CNL (9% max). The petrophysical properties show in the properties contour map (Fig. 2.19, 2.20, 2.21).

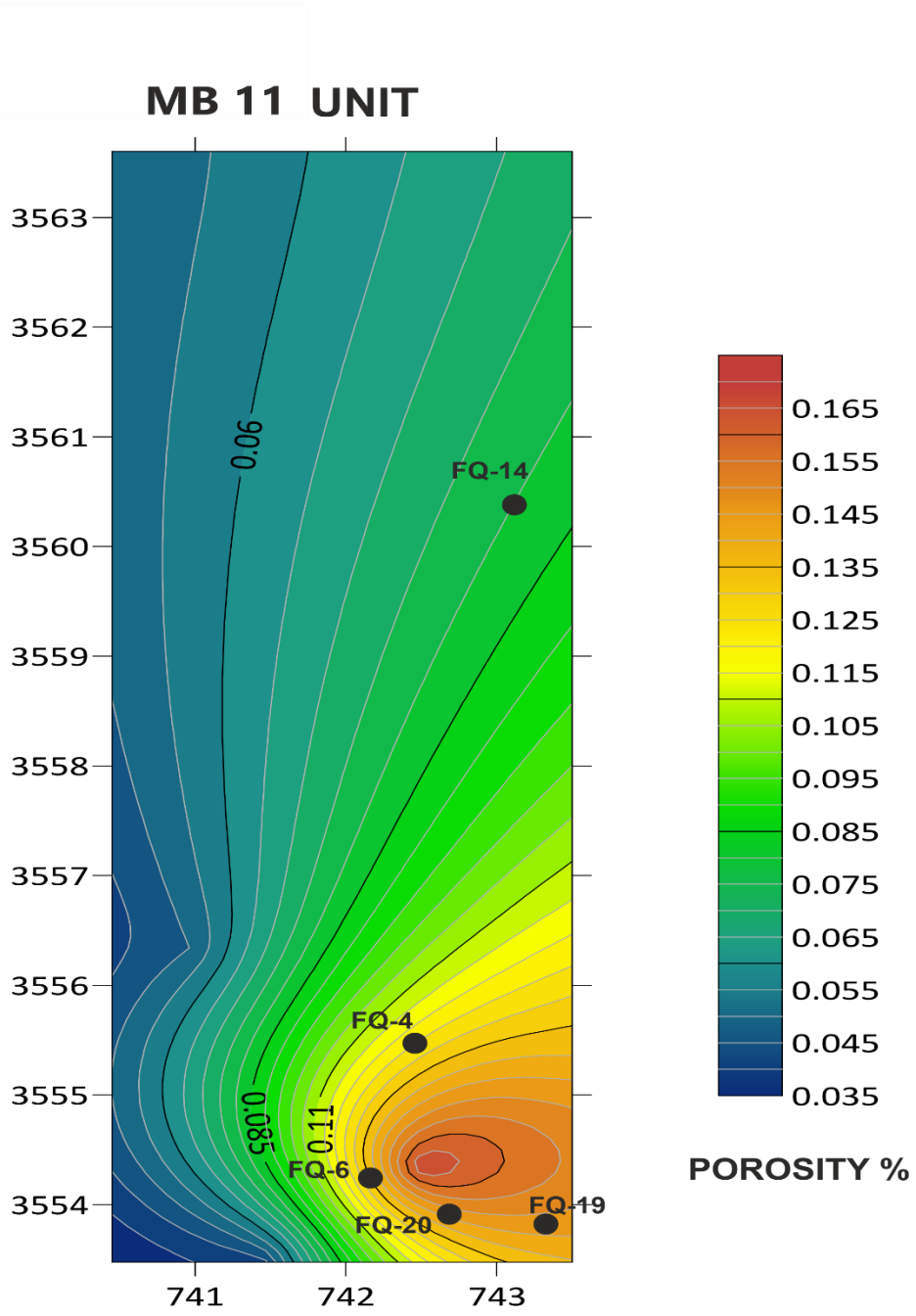

Fig. 2.19: porosity distribution in the MB11 unit within the studied wells.

The porosity in the fair ranges and it is decrease toward the north dome. The high values show in the wells FQ-19 close to 12.5% and in the well FQ-20 is 17.5%.

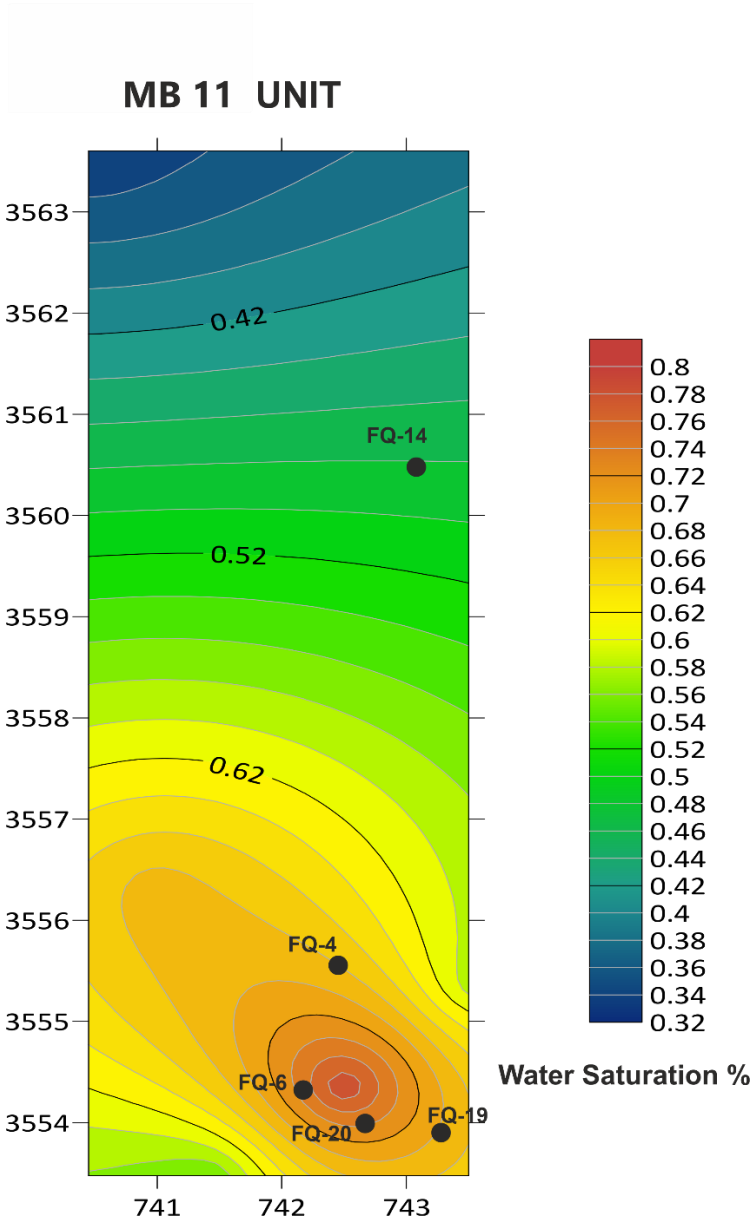

Fig. 2.20: the water saturation distribution mode for the MB11 unit within the studied wells.

The results indicate that the water saturation generally decrease towards the north dome, but with values of Sw higher than in the layer MA in ranges 70-78% at the south dome and 50% in the north.

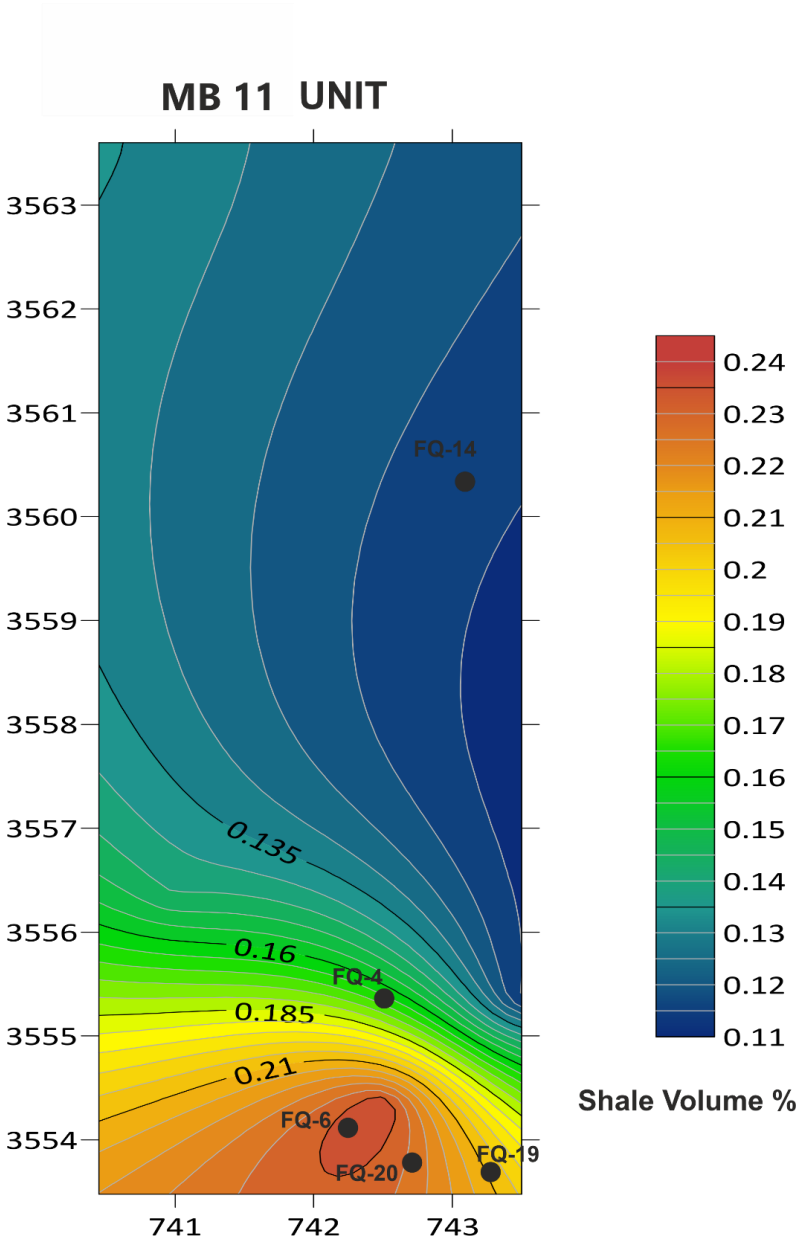

Fig. 2.21: Shale Volume dispersion values within the studied wells.

The results of Shale Volume interpretation reflect the high values of Shale Volume in the MB11 unit especially at the wells FQ-6, FQ-19, and FQ-20 to be exceeds than 24% in some parts. The values decrease to the north to be about 12% in the well FQ-14.

3. MB12 Unit

This unit is consisting of chalky limestone and wackestone with trace oil shows and poor porosity on CNL (~ 9%). The results show that the total porosity is in moderate about 15.5% at the south dome decreases towards the north to records

12% in the well FQ-14 (Fig. 2.22). The water saturation calculations show the same values of about 55% at the wells close to the dome center and in the north dome. The values in this layer increase to the west toward the Mesopotamian Basin (Fig. 2.23).

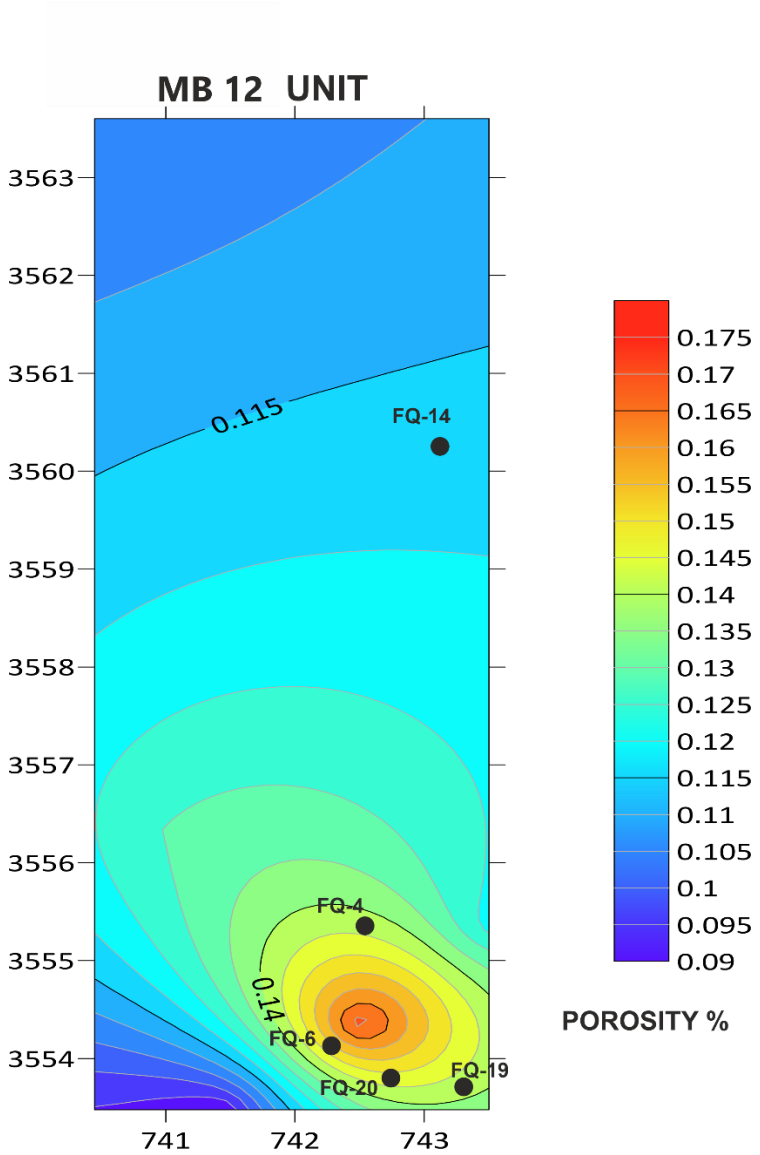

Fig. 2.22: porosity distribution contour map for the MB12 unit within the studied wells.

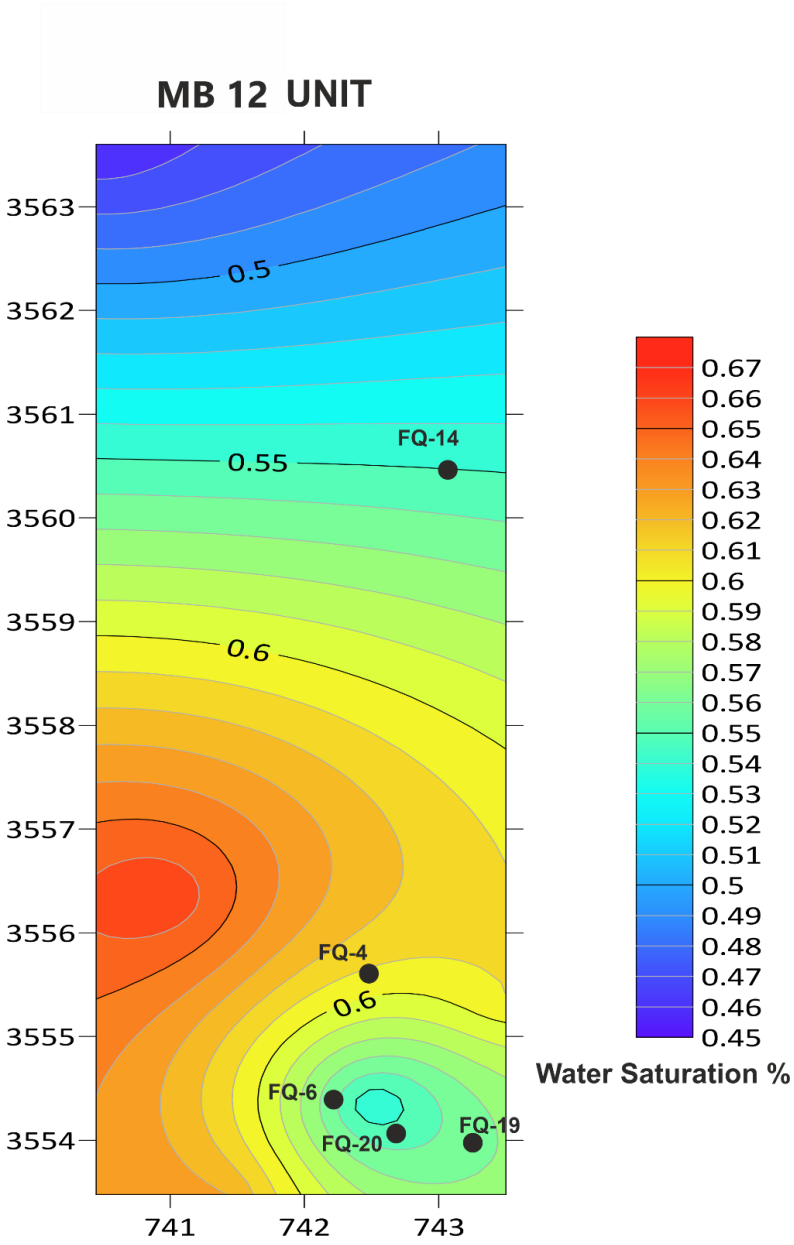

Fig. 2.23: water saturation distribution contour map for the MB12 unit within the studied wells.

For the Shale Volume calculations, the values ranged from 15% in the well FQ-19 near the Iranian territory increases in the wells FQ-20, and FQ-4 in value about 16.5% reaches 19.5% in the well FQ-6. The less value is in the well FQ-14 in less than 13%. Generally, the values of Shale Volume dispersion increase to the west (Fig. 2.24).

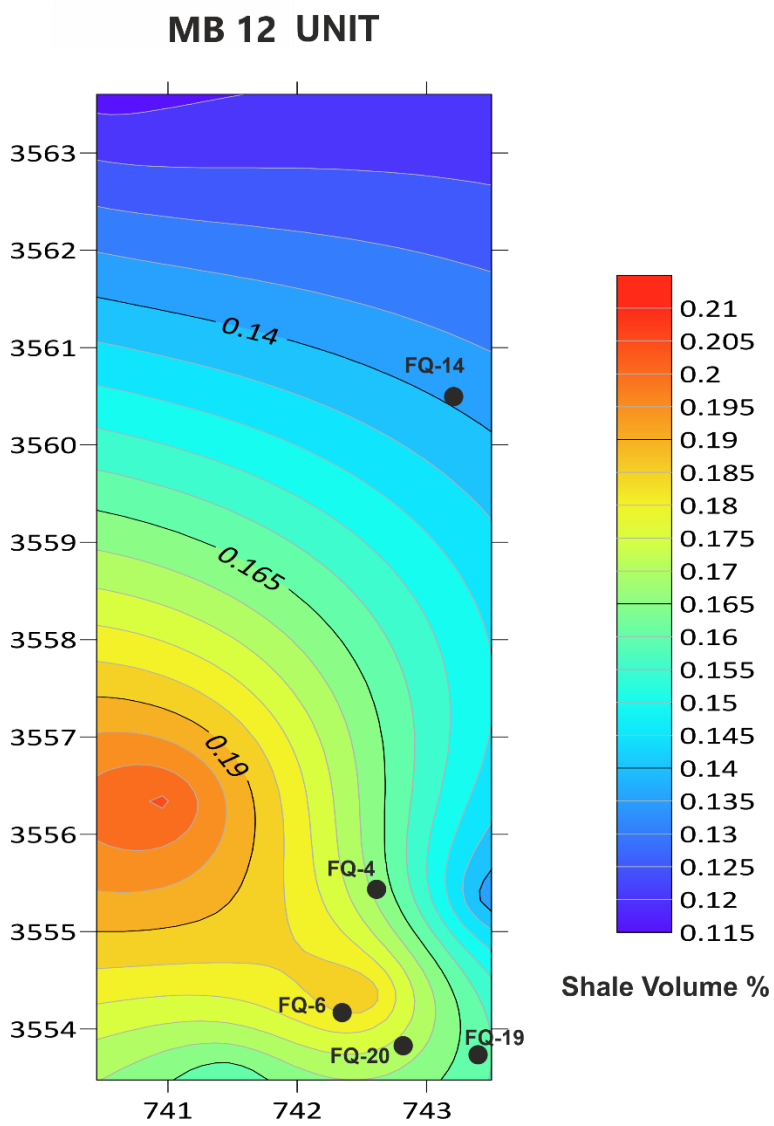

Fig. 2.24: Shale Volume dispersion contour map for the MB12 unit within the studied wells.

4. MB21 Unit

This reservoir unit represents the main productive unit in the Mishrif Formation and consists of bioclastic limestone (wackestone – packstone and mudstone). This unit shows good reservoir characteristics with good porosity of about 20% on CNL, and good oil shows. The oil produced through it over three pay zones (Abdulaziz et al, 2017).

a) Pay zone no.1, thickness (4.5) m

The maximum porosity for this part is about 20.3 % with good oil shows.

b) Pay zone no.2, thickness (4) m

For this zone, the porosity about 20% with good oil shows.

c) Pay zone no.3, thickness (3) m

The porosity measured around 18% with good oil shows.

In general, this reservoir unit was saturated with impregnated oil. The high values recorded in the wells FQ-6, FQ-19, and FQ-20 in ranges of 21-24% decrease northward in the FQ-4 is 19% and 13% in the FQ-14 within the north dome (Fig. 2.25)

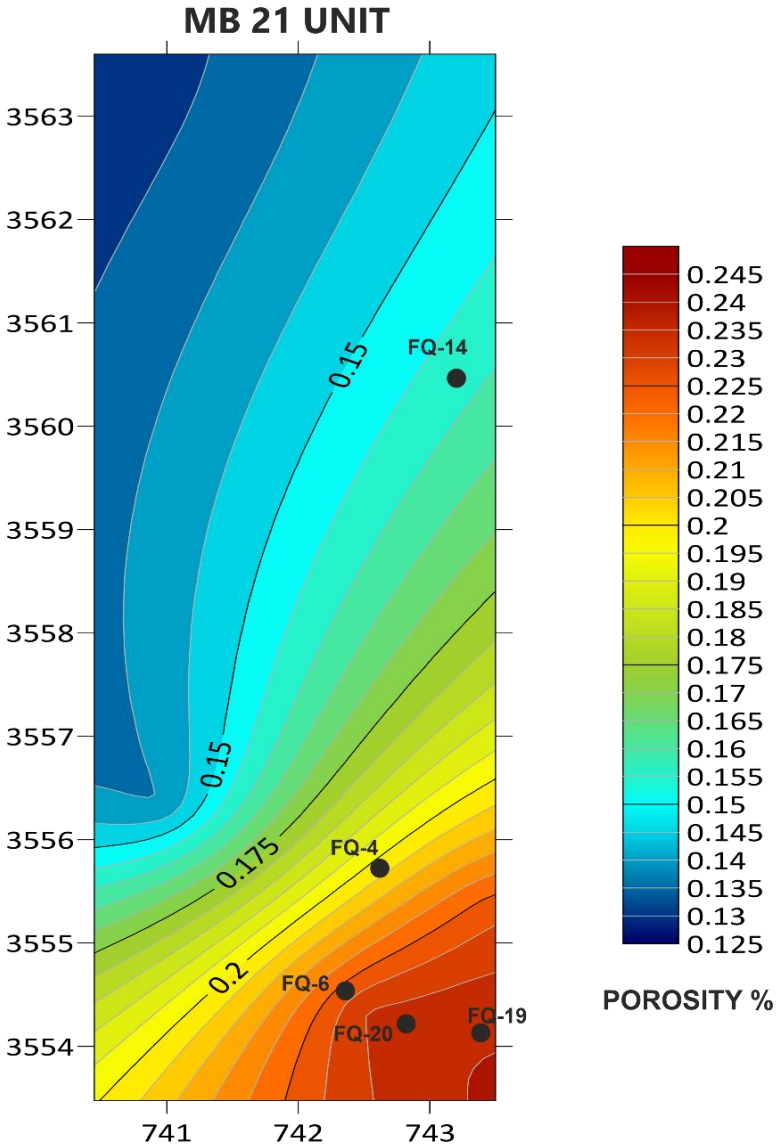

Fig. 2.25: porosity distribution contour map for the MB21 unit within the studied wells.

For the other characteristics, the water saturation records low values decreases towards the north dome 17% in the FQ-14 and to the east the value is 22.5% in the wells FQ-4 and FQ-19. The value increases westward to record 26% in the wells FQ-6, and FQ-20 (Fig. 2.26). The Shale Volume also is in low range and

the values decrease remotely from the dome center in the south part and the lowest value is in the north dome in well FQ-14 is 10.8%. the value is about 24% in the wells FQ-6 and FQ-20 and about 20.5% in wells FQ-4 and FQ-19 (Fig. 2.27).

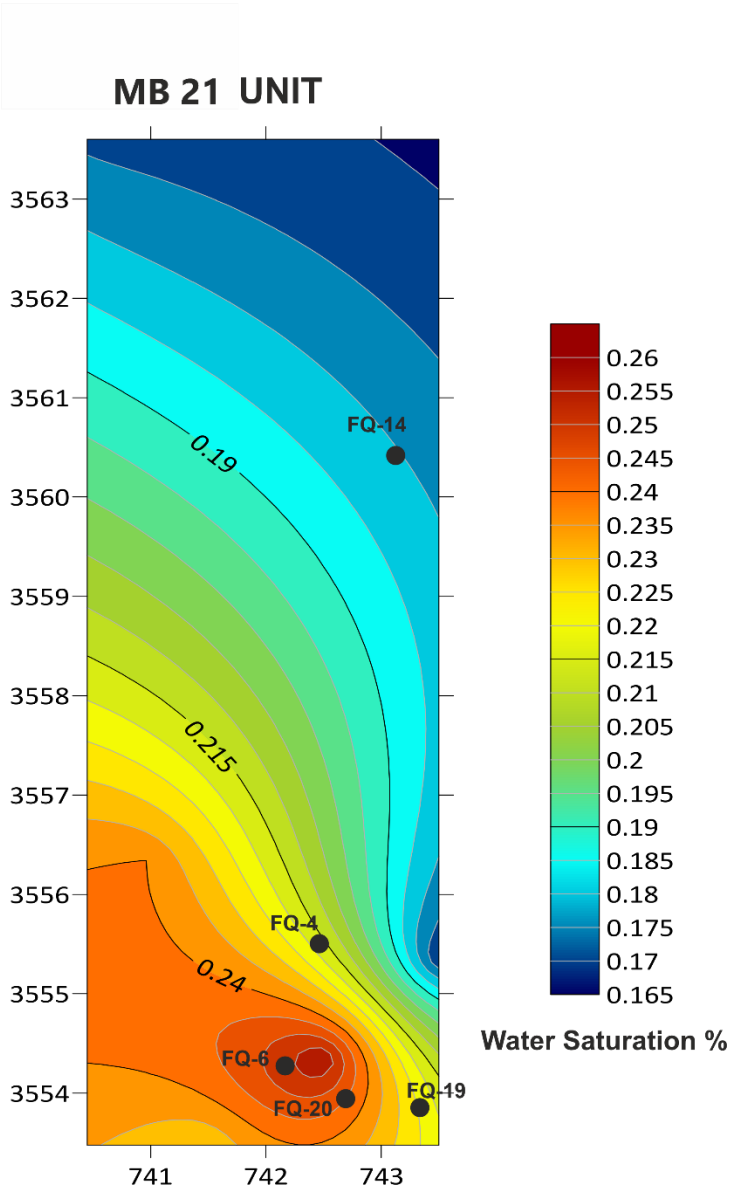

Fig. 2.26: water saturation distribution contour map for the MB21 unit within the studied wells.

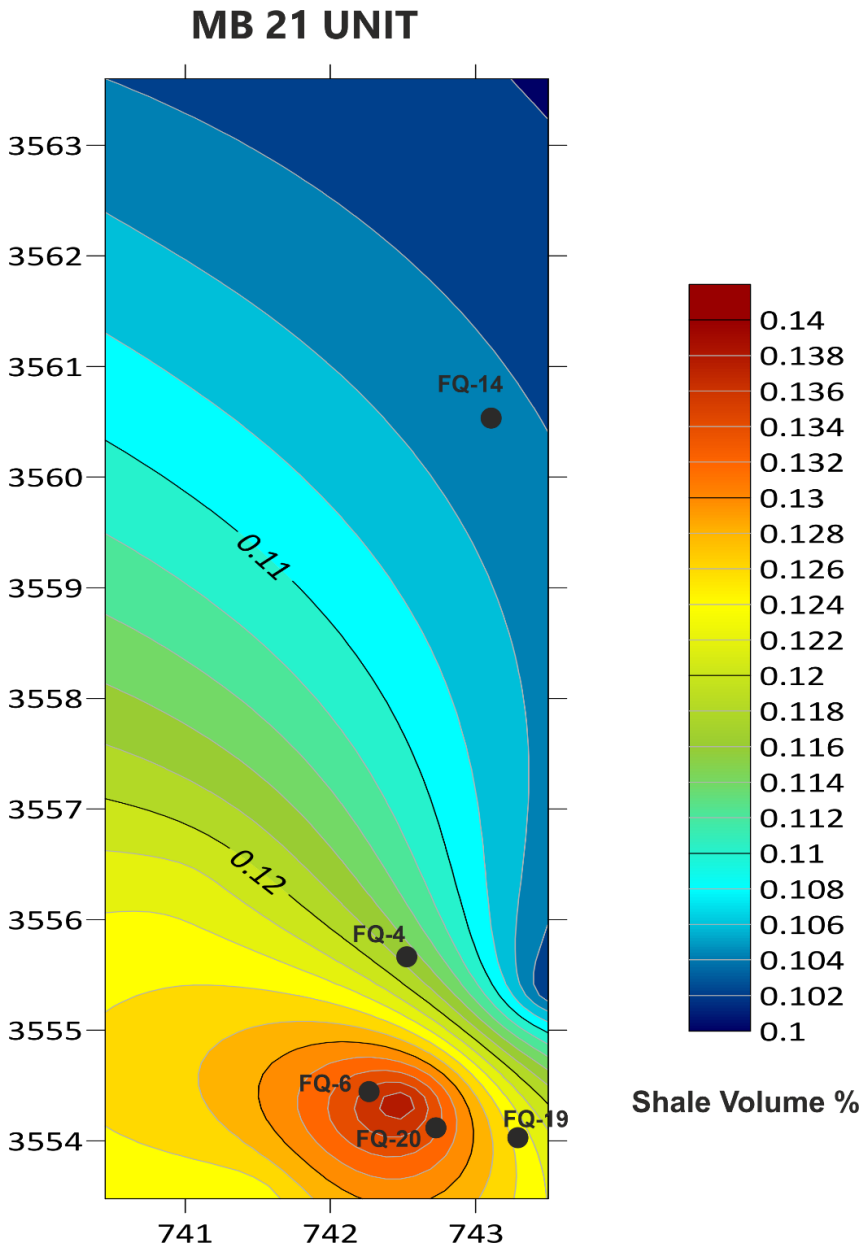

Fig. 2.27: Shale Volume dispersion contour map for the MB21 unit within the studied wells.

5. MB22 Unit

This unit consists of compact limestone with clear microcrystalline structure, but no oil shows. The porosity values are in low ranges increases westwards and northwards within values from 9% to 11% (Fig. 2.28).

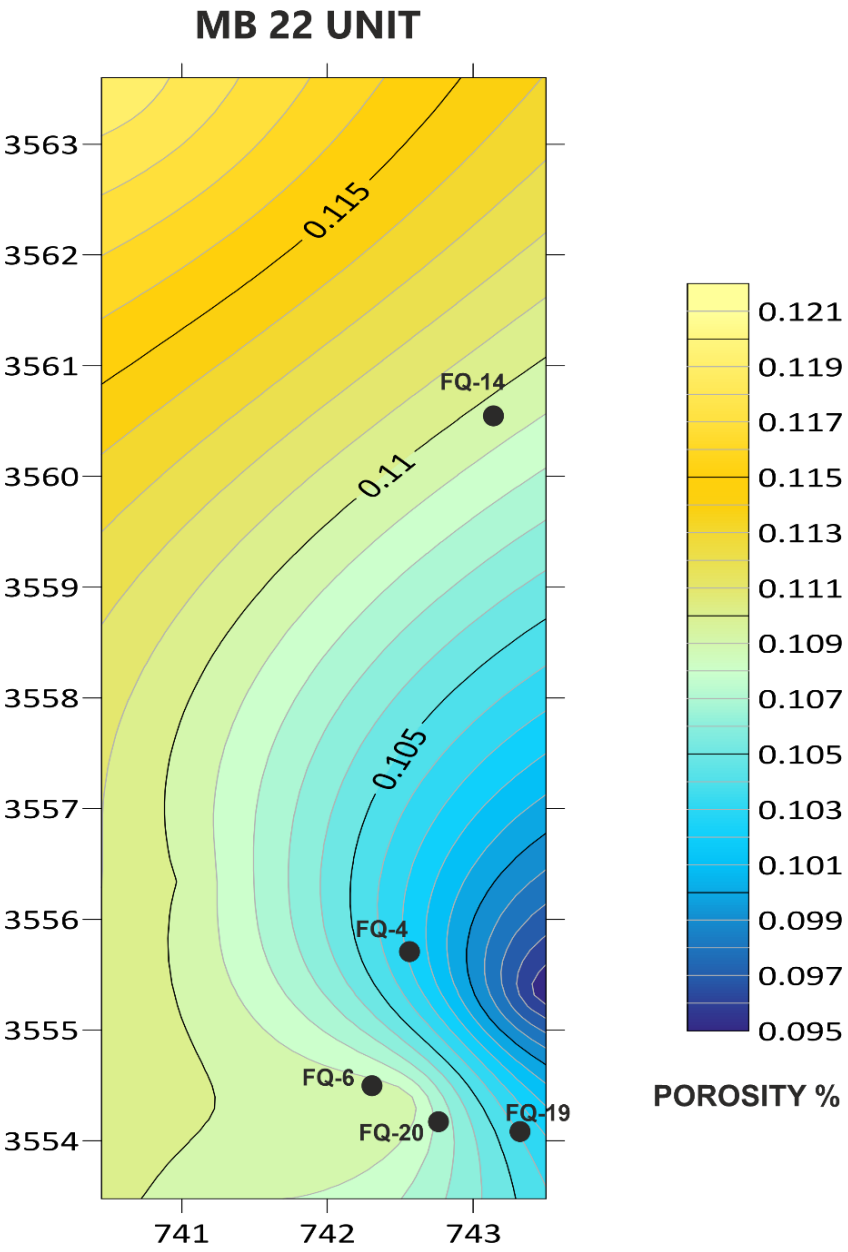

Fig. 2.28: porosity distribution contour map for the MB22 unit within the studied wells.

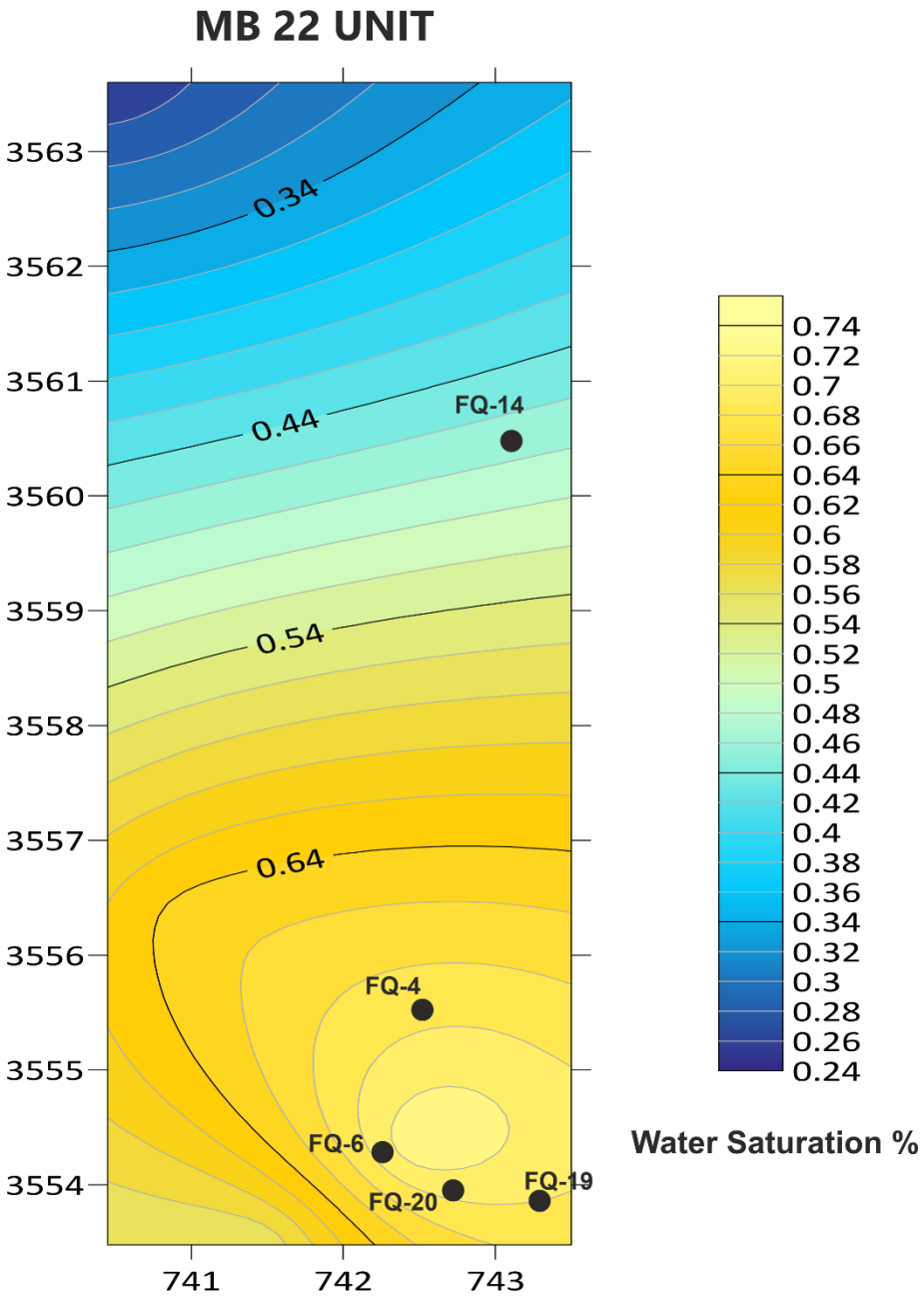

Fig. 2.29: water saturation contour map for the MB22 unit within the studied wells.

The water saturation in the MB22 unit is in high ranges 65-75% in all the wells within the south dome, while it records less content in the north dome in the FQ-14 52% (Fig. 30). For the shale content, the Shale Volume has high ranges 24-28 % in the south dome and about 19% in the north dome.

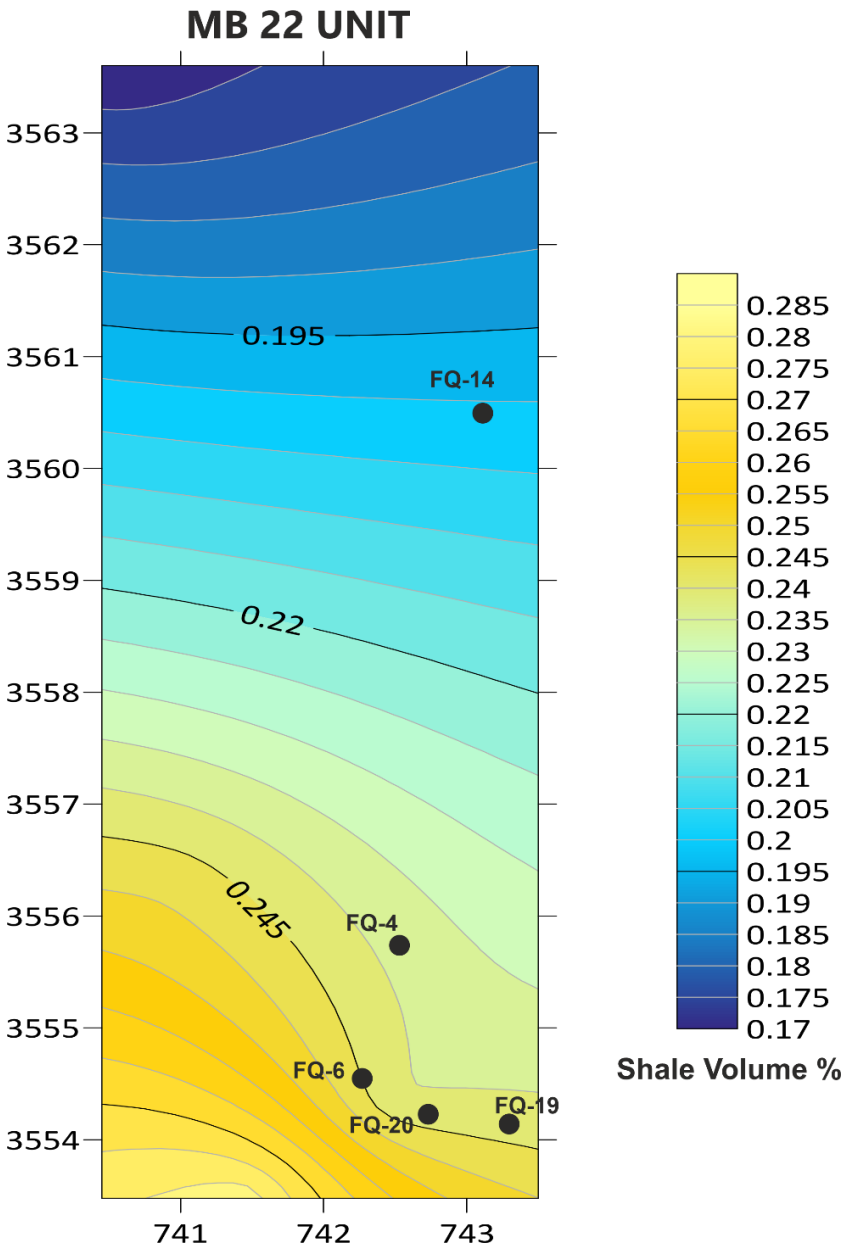

Fig. 2.30: porosity distribution contour map for the MB22 unit within the studied wells.

6. MC1 Unit

This unit is consisting of compact bioclastic limestone (wackestone to packstone) that has poor porosity especially in the FQ-14 at the north dome does not exceed 7% with no oil shows increase southward to reaches 11% (Fig. 2. 31).

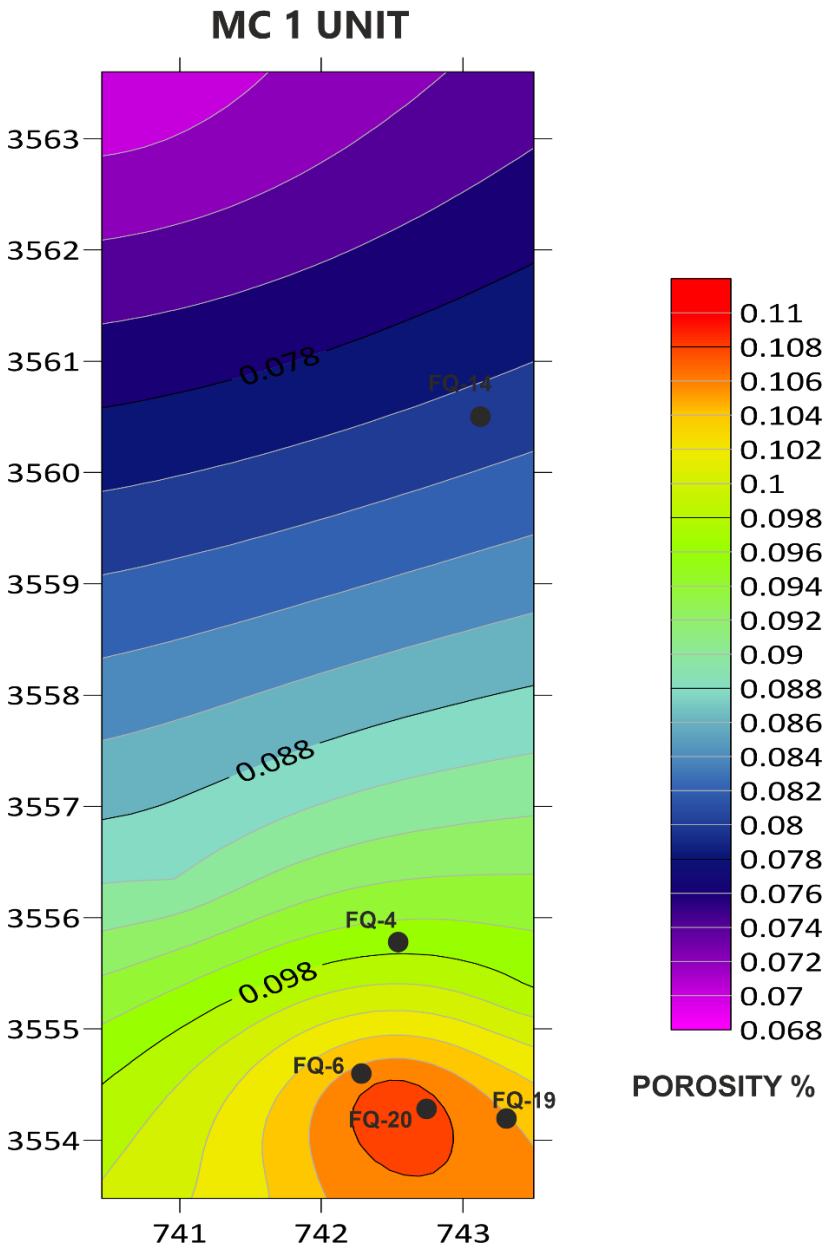

Fig. 2.31: porosity distribution contour map for the MC1 unit within the studied wells.

High water saturation in this unit exceeds than 75% in the FQ-19 decreases relatively to the north and the recorded values indicates about 72% in the FQ-14 (Fig. 2.32).

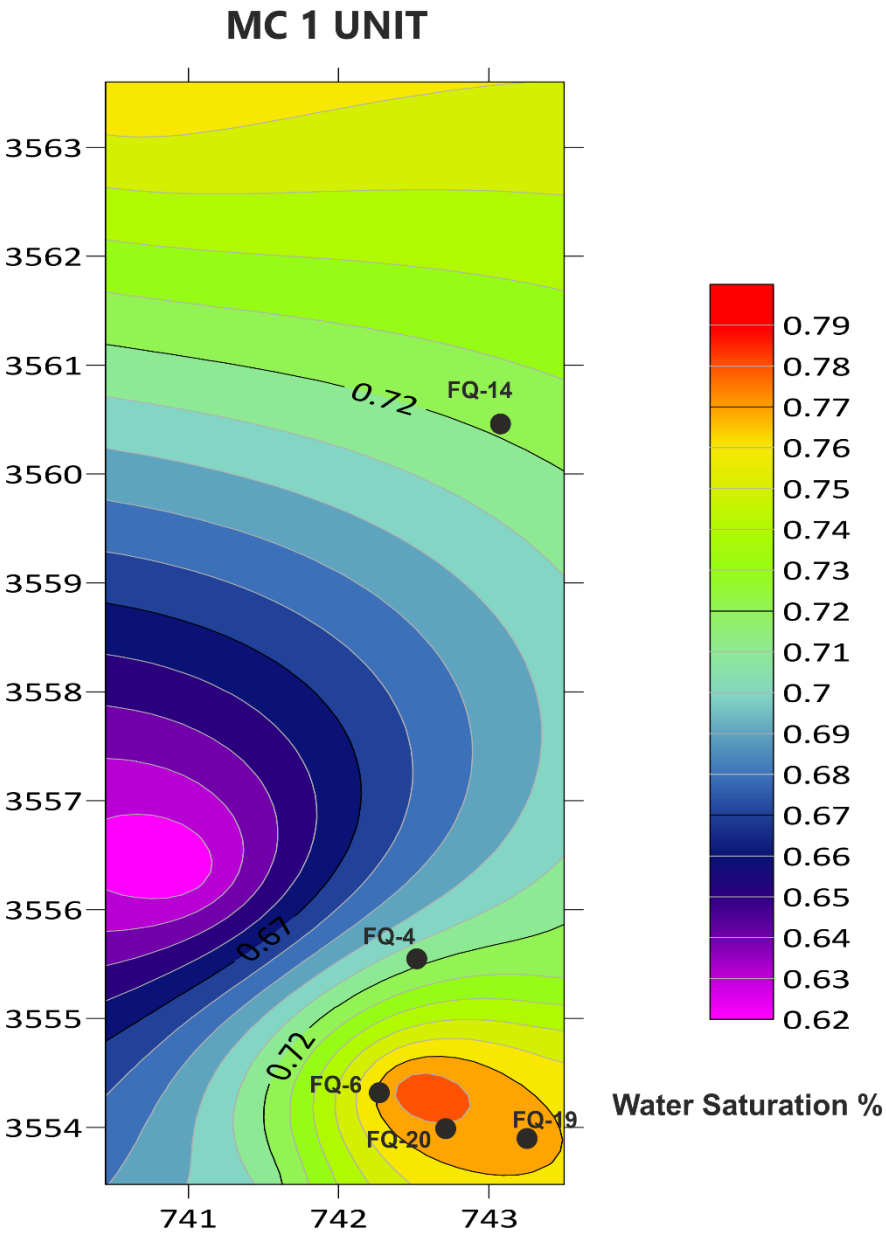

Fig. 2.32: water saturation contour map for the MC1 unit within the studied wells.

The Shale Volume reading from the Gamma Ray log shows the high shale content reaches 26% within the studied wells. These values increased downward the domes in the saddle area to reaches 28.5% (Fig. 2.33).

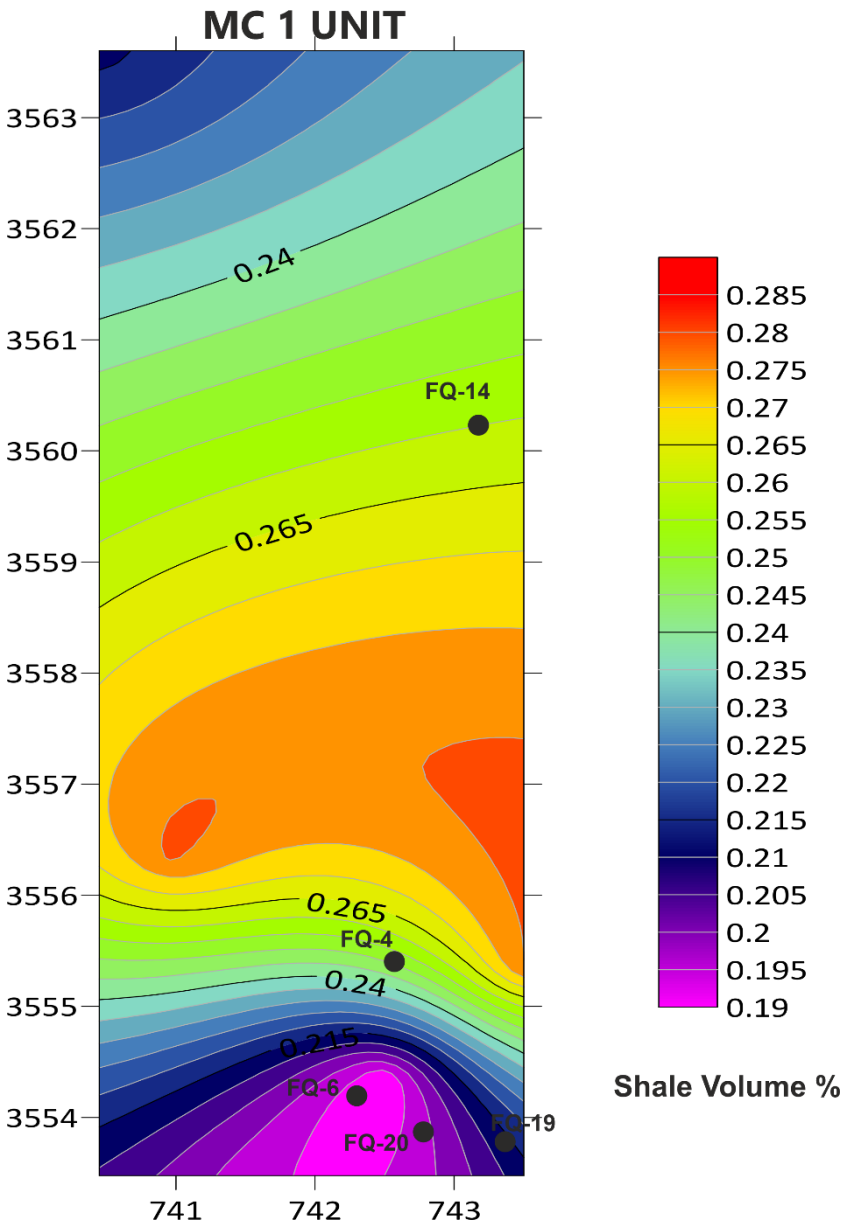

Fig. 2.33: Shale Volume dispersion contour map for the MC1 unit within the studied wells.

7. MC2 Unit

This unit mainly consists of well compacted grainstone with low porosity and no oil shows. The porosity values that recorded for this unit are relatively good increase in the wells at the south dome with value of 17% decreases to the north to be about 10.5% in the well FQ-14 (Fig. 2.34).

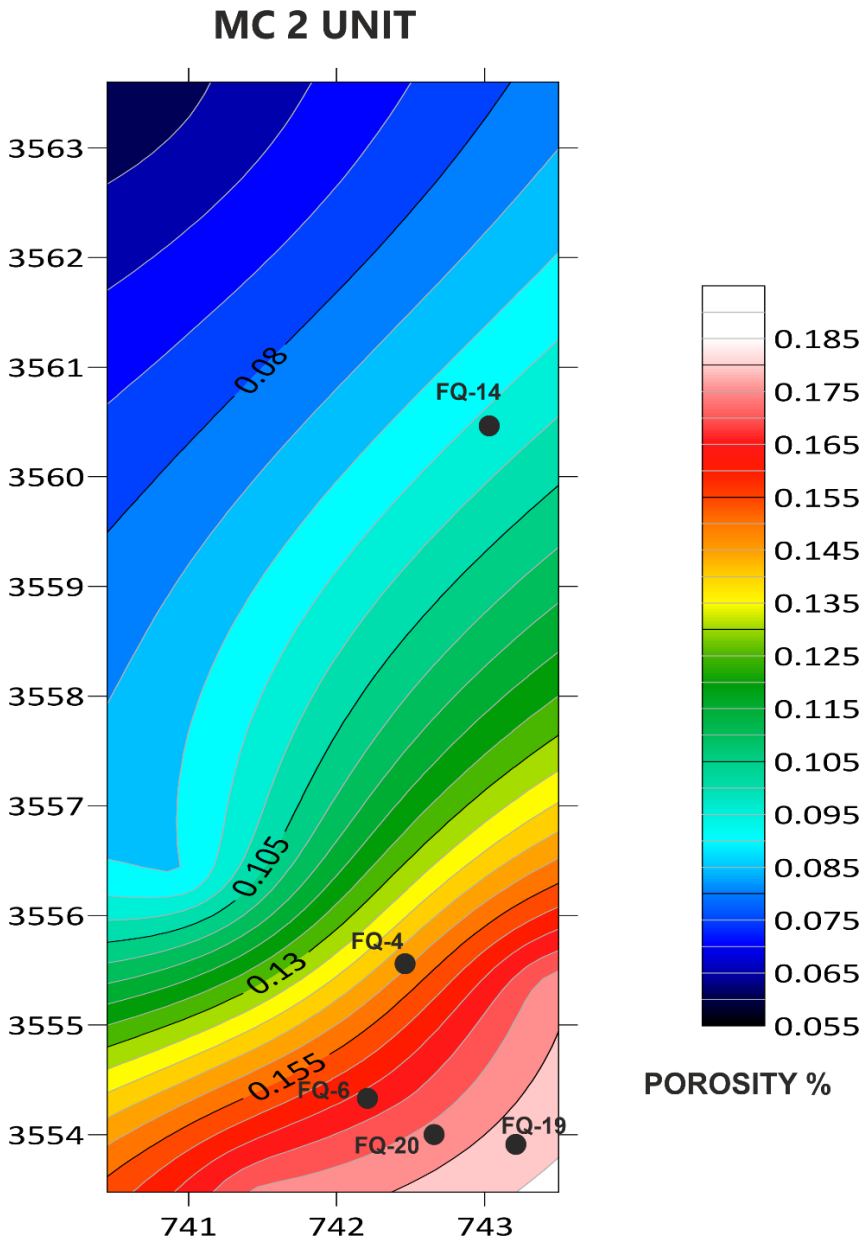

Fig. 2.34: porosity distribution contour map for the MC2 unit within the studied wells.

The water saturation in high ranges with values between 80-90% within all the studied wells (Fig. 2.35) Consequently, this reservoir unit is considered as water bearing layer.

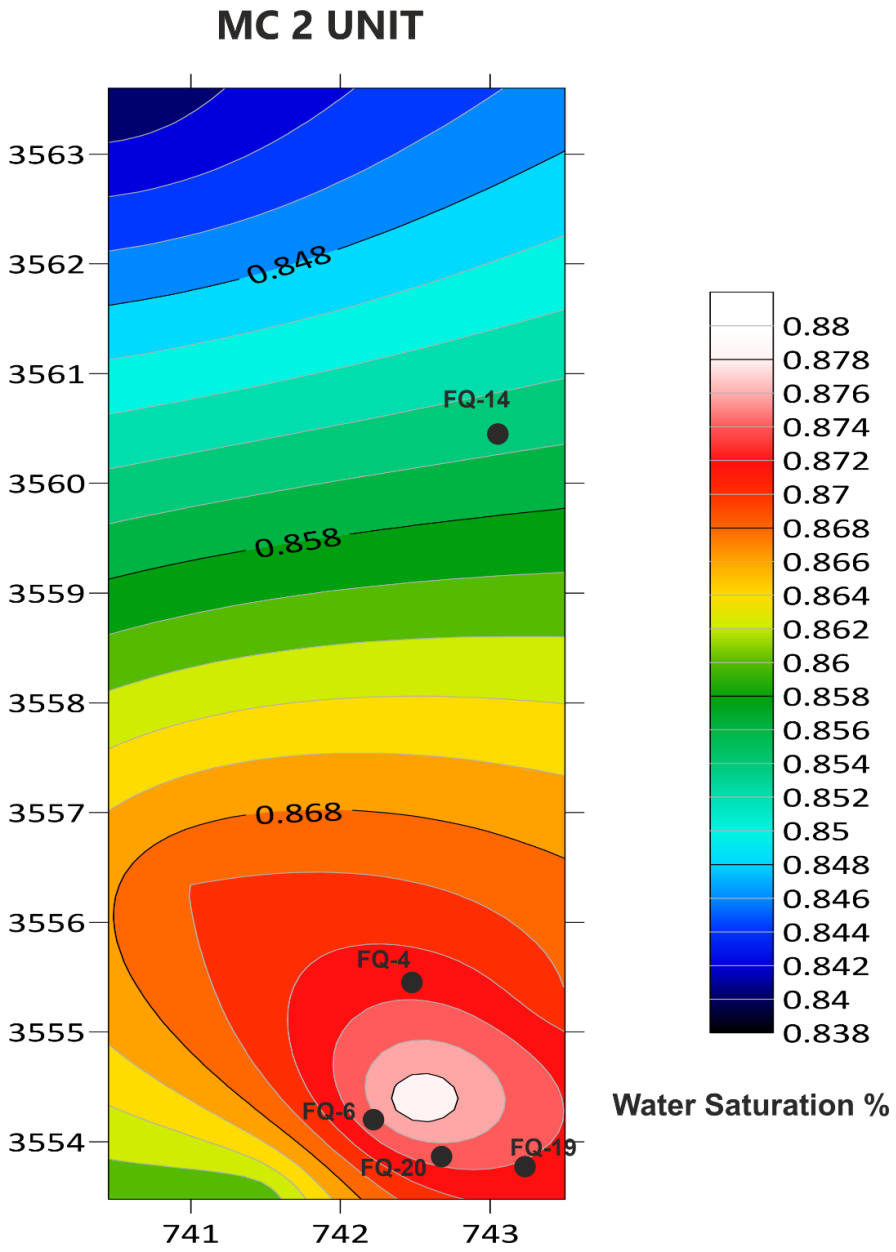

Fig. 2.35: water saturation contour map for the MC2 unit within the studied wells.

The Shale Volume in the MC2 unit shows moderate values in the south dome ranges in 14-18% increase to the north reaches 24% in the well FQ-14 (Fig. 2.36)

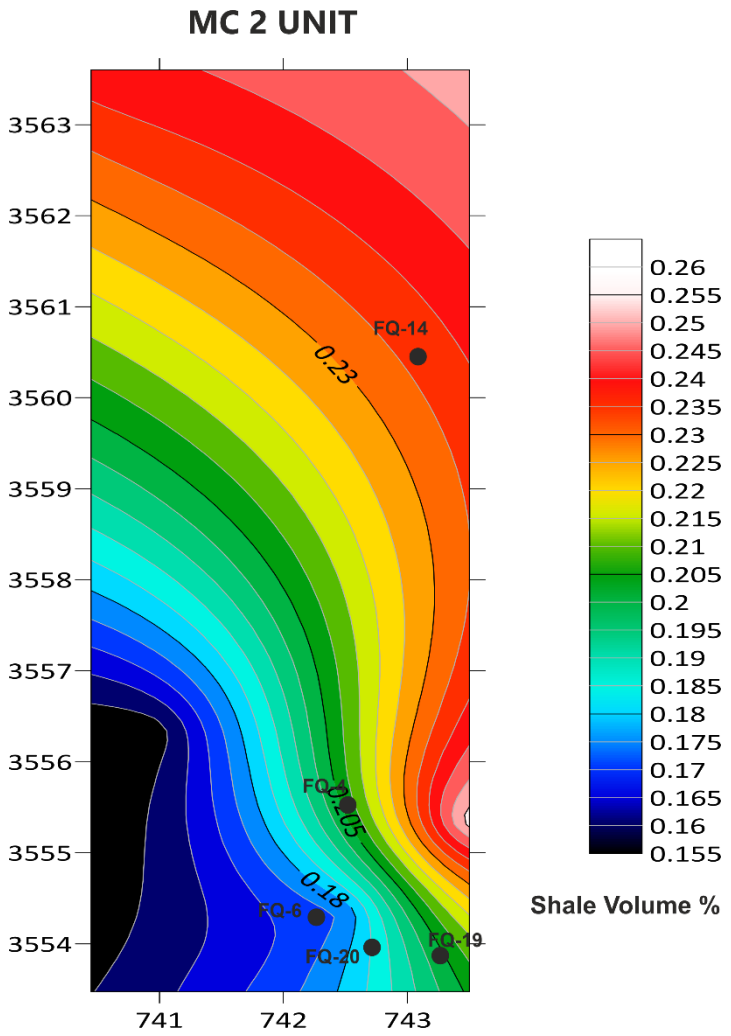

Fig. 2.36: Shale Volume dispersion contour map for the MC2 unit within the studied wells.

The variation of thicknesses for the reservoir's units are clarify in the (Table 2.8) and the correlation between them along all the studied wells showing in the correlation figure (Fig. 2.37)

Table 2.8: Reservoir secondary units of Mishrif Formation for the studied wells.

Units	Top depth m	Bottom depth m	Thickness m
Fq-4			
MA	3868.0	3893.0	25.0
MB11	3893.0	3935.0	42.0
MB12	3935.0	4000.0	65.0
MB21	4000.0	4098.0	98.0
MB22	4098.0	4137.0	39.0

Units	Top depth m	Bottom depth m	Thickness m
MC1	4137.0	4176.0	39.0
MC2	4176.0	4280.0	104.0
FQ-6			
MA	3887.5	3933.0	45.5
MB11	3933.0	3978.0	45.0
MB12	3978.0	4017.0	39.0
MB21	4017.0	4117.0	100.0
MB22	4117.0	4166.0	49.0
MC1	4166.0	4205.0	39.0
MC2	4205.0	4280.0	75.0
FQ14			
MA	3862.0	3900.0	38.0
MB11	3900.0	3941.0	41.0
MB12	3941.0	3980.0	39.0
MB21	3980.0	4073.0	93.0
MB22	4073.0	4109.0	36.0
MC1	4109.0	4144.0	35.0
MC2	4144.0	4228.0	84.0
FQ-19			
MA	3906.0	3940.0	34.0
MB11	3940.0	3983.0	43.0
MB12	3983.0	4041.0	58.0
MB21	4041.0	4142.0	101.0
MB22	4142.0	4173.0	31.0

Units	Top depth m	Bottom depth m	Thickness m
MC1	4173.0	4207.0	34.0
MC2	4207.0	4272.0	65.0
FQ-20			
MA	3875.0	3900.0	25.0
MB11	3900.0	3946.0	46.0
MB12	3964.0	4000.0	36.0
MB21	4000.0	4096.0	96.0
MB22	4096.0	4137.0	41.0
MC1	4137.0	4172.0	35.0
MC2	4172.0	4236.0	64.0

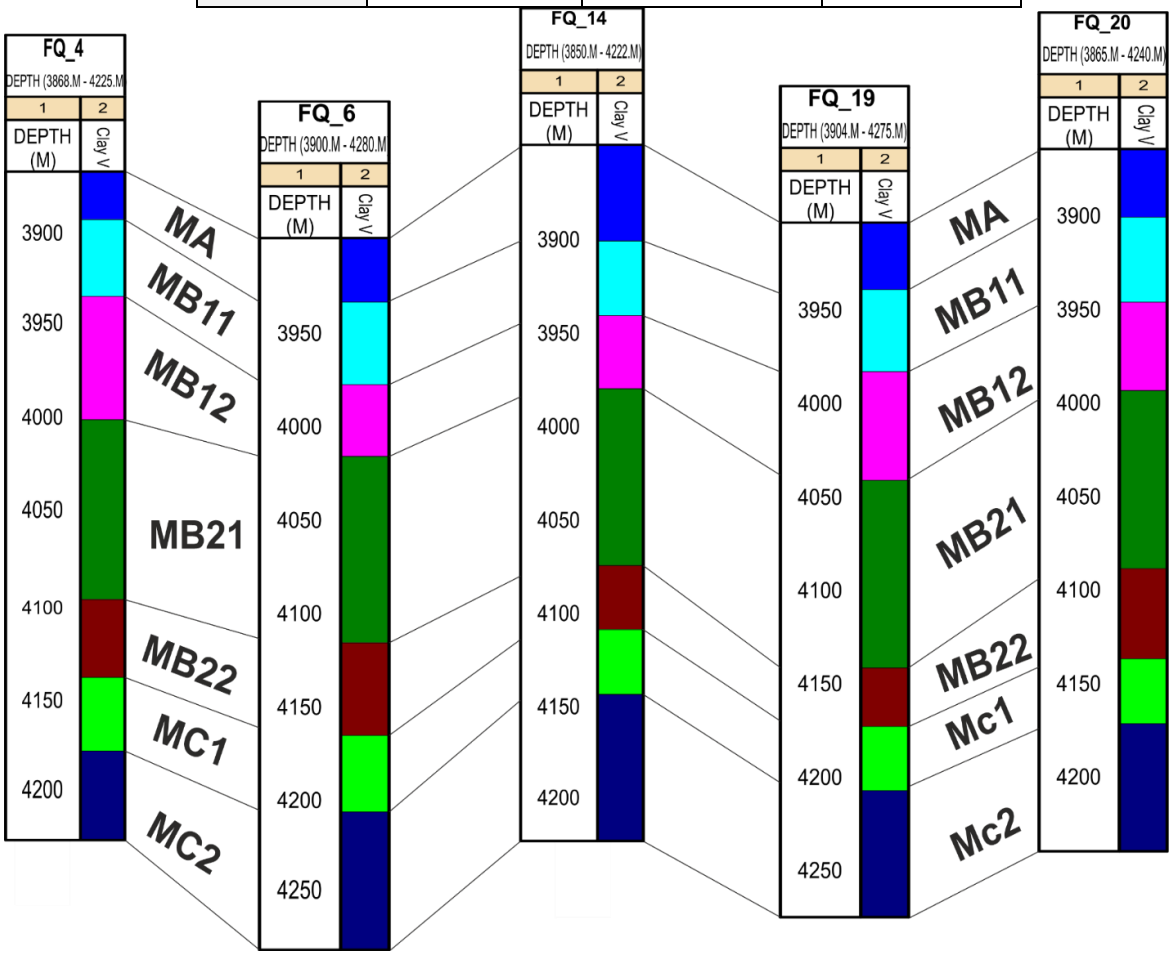

Fig. 2.37: Schematic diagram shows the depths and thicknesses of the Mishrif Formation reservoir units.

The fluid contents (water and hydrocarbons) and their characteristics in the targeted formation will appear in the basic log plots (CPI) that gather all the inputs and outputs plotted against porosity, permeability, resistivity, fluid saturation, Shale Volumes, cutoffs, …etc. All the work's results from the logs interpretation showing in the CPI plots in the figures (2. 38-2.42) considering the specific log plots that used in the evaluation of Mishrif Formation characteristics in the Fauqi oilfield. In addition to the reservoir units that have been divided according to the shale varieties.

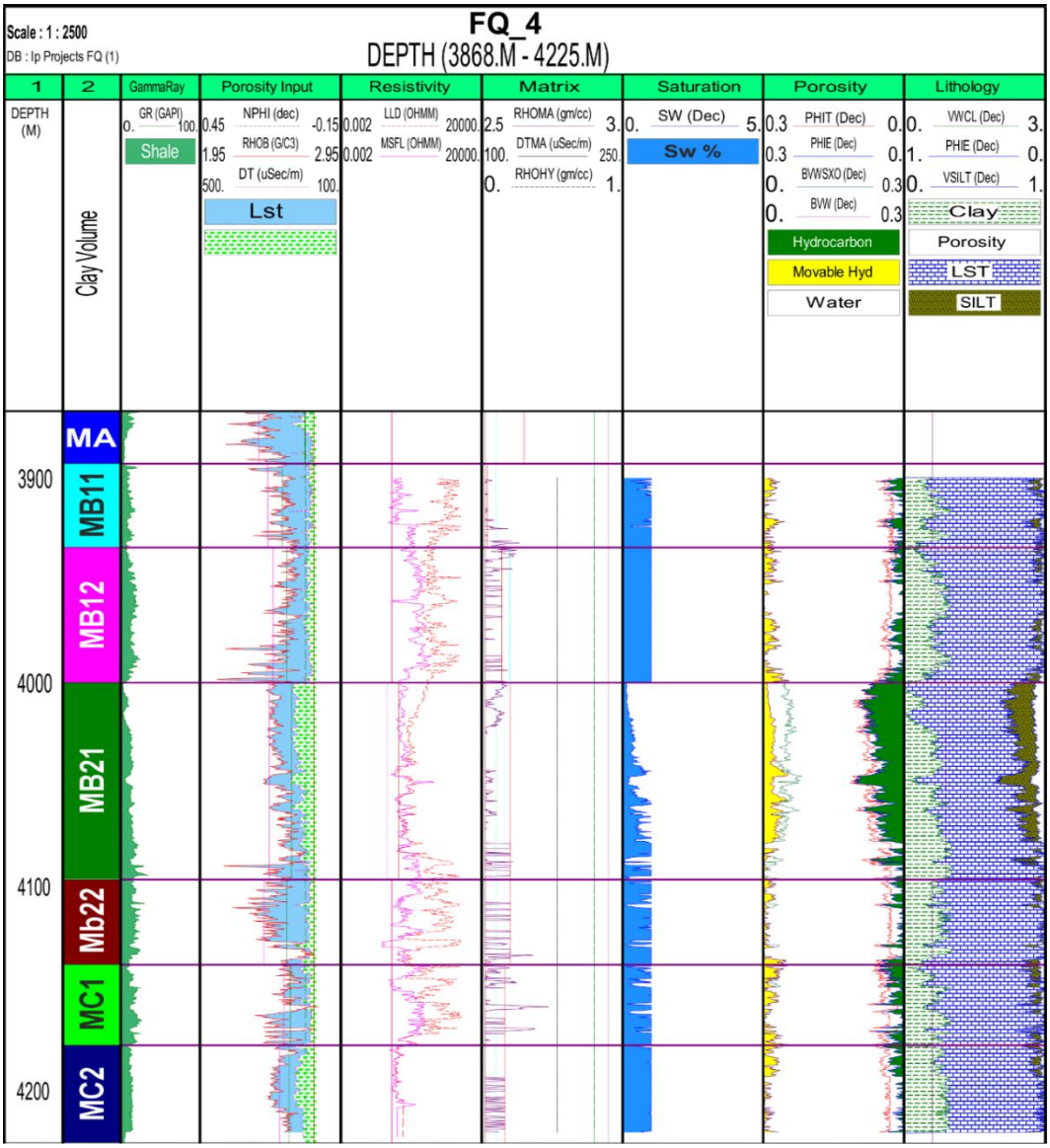

Fig. 2.38: CPI log plots of well FQ-4.

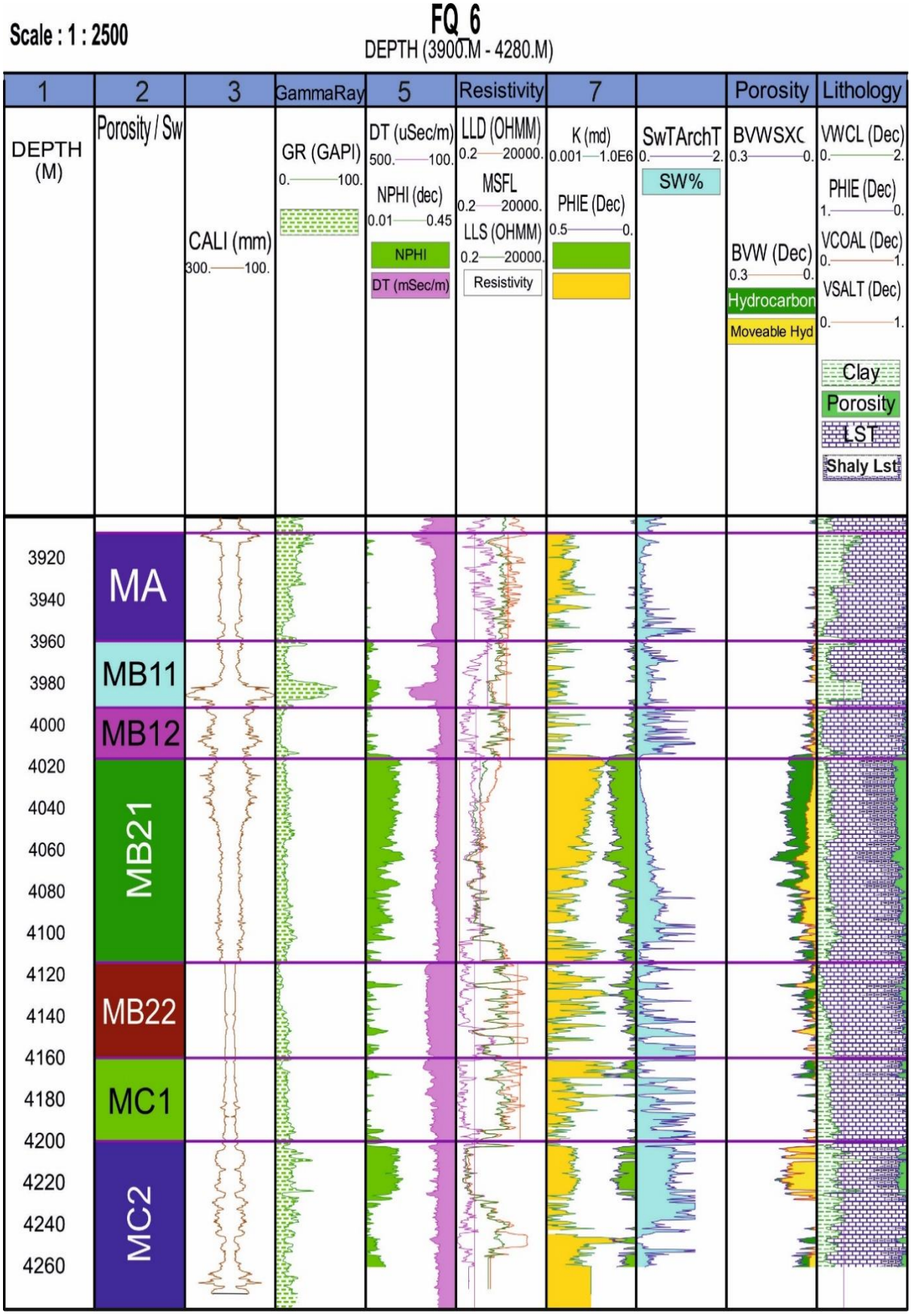

Fig. 2.39: CPI log plots of well FQ-6.

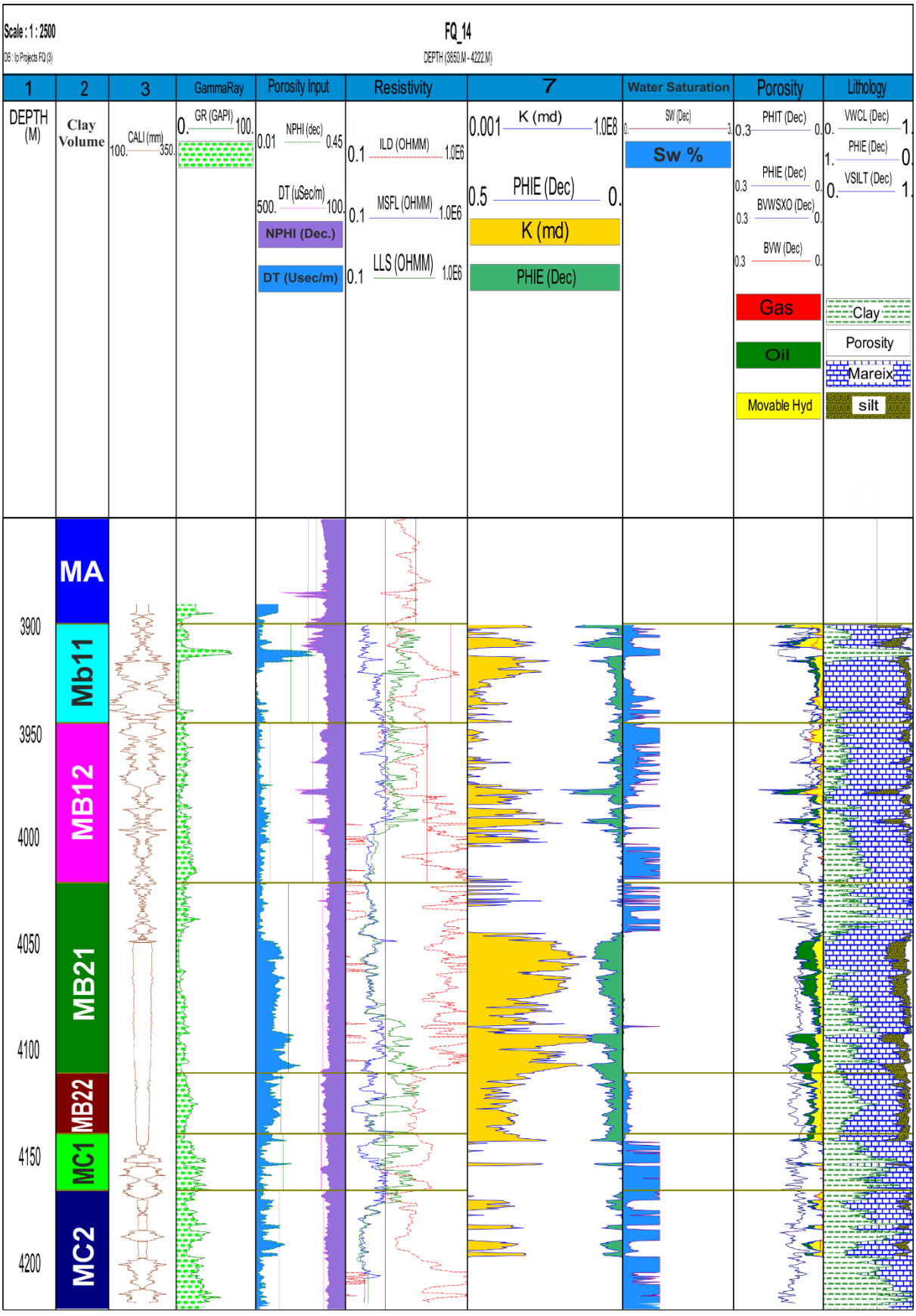

Fig. 2.40: CPI log plots of wellFQ-14.

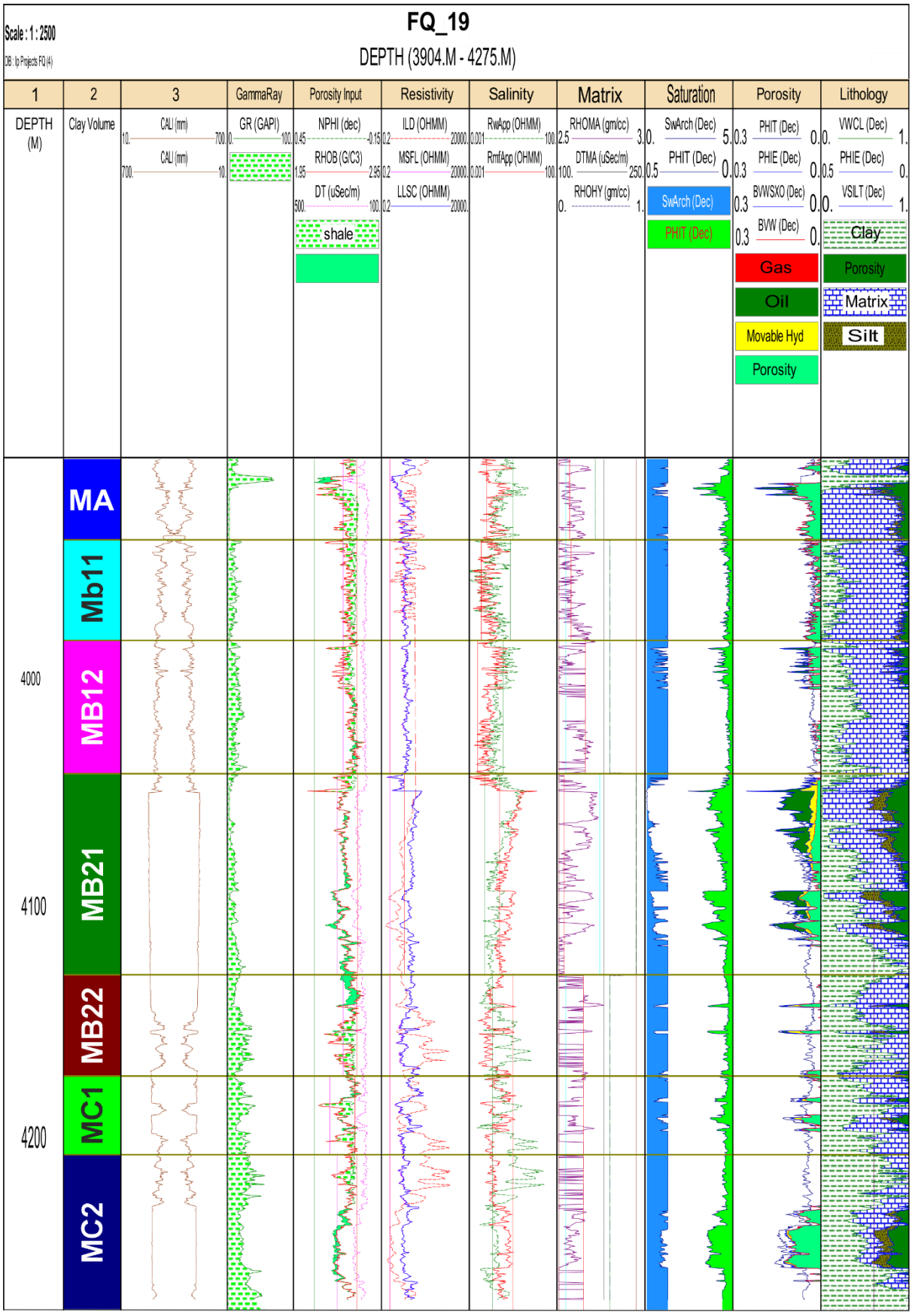

Fig. 2.41: CPI log plots of well FQ-19.

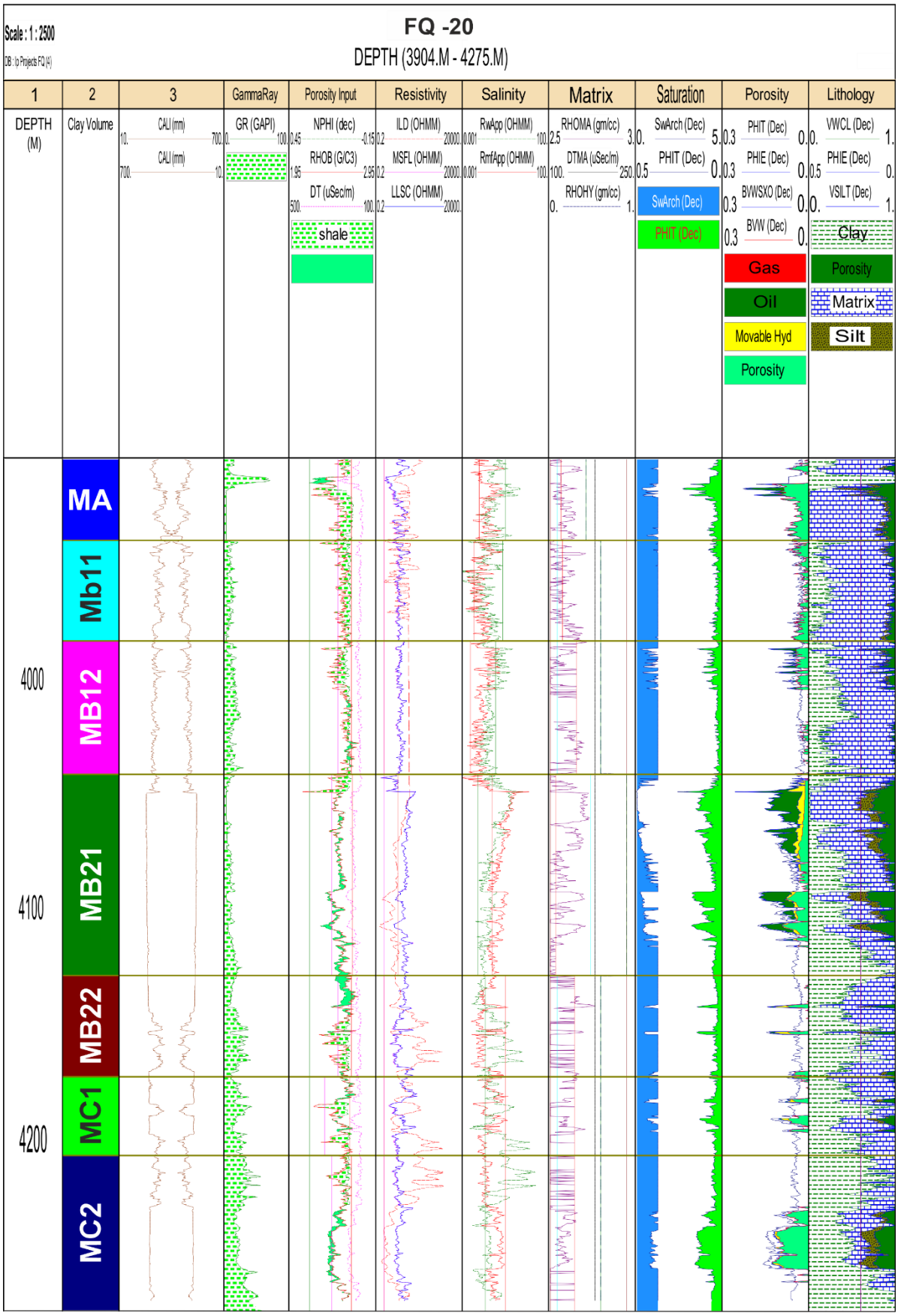

Fig. 2.42: CPI log plots of well FQ-20.

2.2. Discussion

Mishrif Formation, the main reservoir in the Fauqi oilfield, was prescribed and simulated with a computer software using log data analysis and core analyses results for five selective wells in the field. The Shale Volume varied both laterally and vertically, but in total, it is about 22% of the formation bulk volume. Evaluation of porosity was estimated by means of the consequences of both logging and core analysis. Results showed that the total porosity of the formation is ranging between 10% to 38%. The best measured porosity value in the MB21 unit of the Mishrif Formation is about 17%. The permeability estimation using Darcy's law and Timur's equation considering the porosity and irreducible water saturation gave the best results in the MB21 unit. The lowest ratio of water saturation and the highest hydrocarbon accumulations was in the MB21 unit. Good porosity and high hydrocarbon saturation indicated that the MB21 unit had the best reservoir characteristics and represented the central reservoir unit in the Mishrif Formation in this field. The default lithology equation of density/ neutron cross plot was used to discriminate the formation’s main lithology, which was organic limestone. High porosity can be attributed to the dissolution diagenesis process.

Chapter Three

Chapter Three

Organic Geochemistry of the Mishrif reservoir Crude oils

3.1. Introduction

Geochemical analytical tools have a significant role in more petroleum systems understanding. 50 years ago, organic geochemistry played a significant role in oil explorations and developments (Lawson et al, 2018). (Hunt, 1861) suggested the organic origin of the economic accumulations of hydrocarbons in the North American Paleozoic rocks and proposed that the hydrocarbon accumulations originated from marine organic matter. (Pratt, 1944) adopted the principles of petroleum geochemistry and rumored the concept of hydrocarbons origin from the organics' kerogen transformation due to thermal affect. These initial hypotheses provided a foundation for future reasoning abilities in organic geochemistry studies.

The main instruments employed for biomarker analysis in this study were gas chromatography (GC) and gas chromatography /mass spectrometry (GC/MS), and Carbon isotope analysis. Trace elements, API, and sulfur content analyses were also conducted. These parameters can be used to: (i) identify the source rock depositional environment and the type of organic matter that originates (Tissot & Welte, 1984; Peters, 1986). (ii) determination of the source rock age (Dykstra, 1987); (iii) estimation of the thermal maturity of a source rock (Waples, 1994); and (iv) biodegradation (Peters et al, 2005).

Many studies have been conducted to investigate the impact of variations in the water salinity on the depositional environment of source rocks (Gross et al, 2015). The relative abundance of n-alkanes, acyclic isoprenoids, the hopane/sterane ratio, and the gammacerane component analysis can be used to distinguish the crude oil samples that originated from source rocks deposited in hypersaline lacustrine, marine, and terrestrial environments (Peters, 1986; Peters et al, 2005).

Many biomarker and non-biomarker parameters are useful in distinguished marine or terrigenous origin for organic matters of the source rocks. Both marine and terrigenous organic source rocks could be found in marine deltaic environments. Other terrigenous oils derived from lacustrine sediments are dominated by higher-plant oils. (Isaksen et al, 2002; Peters et al, 2005). Over geological time, many different organic compounds deposited in source rocks show their potential as age-related biomarkers in crude oils (Summons et al, 1999; Moldowan & Jacobson, 2000). Many geochemical studies have confirmed the existence of a correlation between certain types of organic matter with geologic age, as shown in (Fig. 3.1) ((Peters, 1986; Moldowan & Jacobson, 2000).

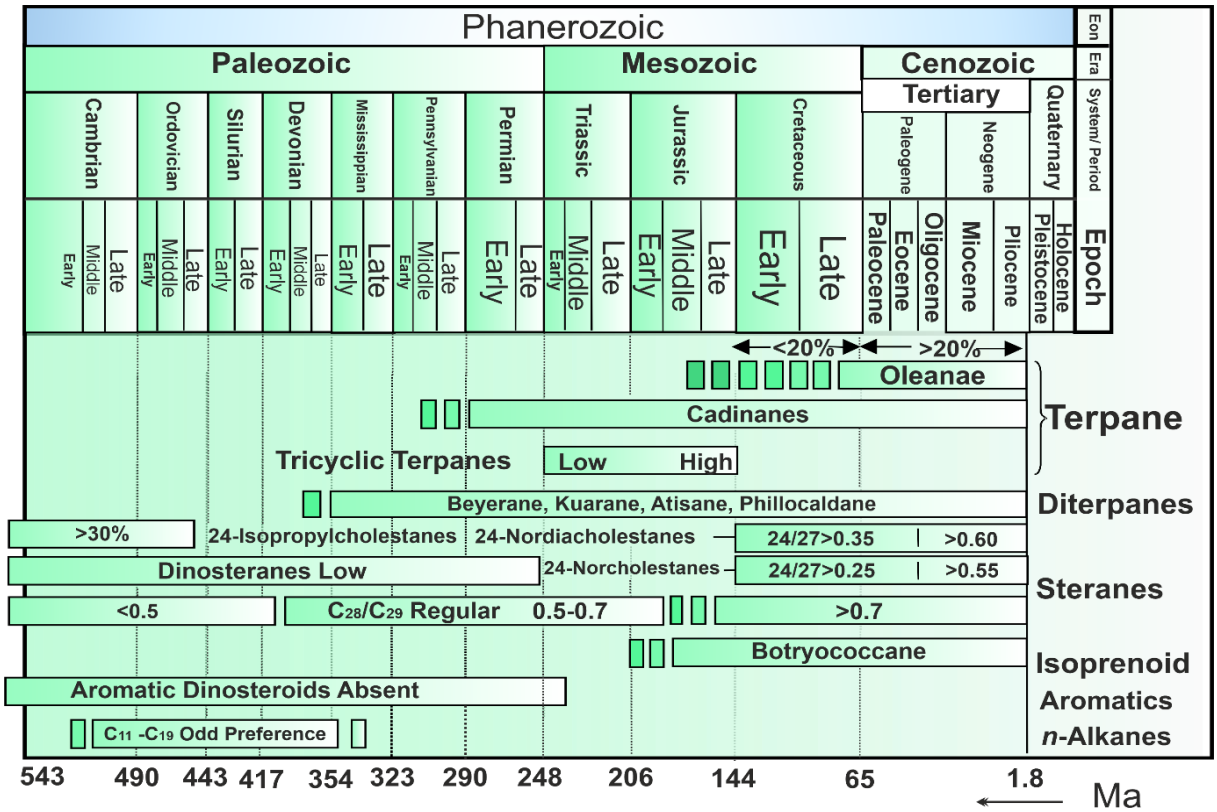

Fig. 3.1: Inferring the source rocks for crude oils through the Age-related biomarkers modified from (Peters, 1986).

The organic origin of oils came from the transformation of the essential organic matter namely kerogen (Moldowan & Jacobson, 2000).

3.1.1. Kerogen

Generally, for petroleum interest, kerogen is the widespread organic matter in the sediments (Selley et al., 1985). The kerogen is a mix of long-chain biopolymers that essentially contain hydrogen, carbon, and oxygen in addition to a few amounts of Nitrogen and sulfur (Horsfield & Rullkotter, 1994). Both kerogen and bitumen are organic residuals, but kerogen is insoluble in the petroleum solvents per contra of bitumen which is dissolved with these normal petroleum solvents (Selley et al., 1985).

There are four main sources of kerogen: marine, terrestrial, lacustrine, and recycled kerogen. The most known oils were come from marine and/or lacustrine kerogen. Depending on the ratios of H/C, and O/C in the organic compounds, the kerogen was classified into three types I, II, and III (Table 3.1) (Tissot & Welte, 1984), or four types I, II, III, and IV (Peters & Cassa, 1994).

In general, the first two types are known as sapropelic (rich lipid) kerogen which forms from the decomposition and polymerization of algae and spores that are enriched with fats and lipids, and usually produces oil according to the high (H/C) proportion (Table 3.1). The third class (III) is Humic kerogen (which contains almost carbon and oxygen) typically formed from the lignite of higher plants, and generally produces fatty oil and gas (Fig. 3.2) (Tissot & Welte, 1984; Selley et al., 1985).

Table 3.1: kerogen types, ratios of C-H and C-O, and oil produced type, after (Selley et al., 1985).

Kerogen type	H/C ratio	O/C ratio	Petroleum type
I, Algal	1.65	0.06	Oil
II, Liptinitic	1.28	0.1	Oil and gas
III, Humic	0.84	0.13–02	Gas

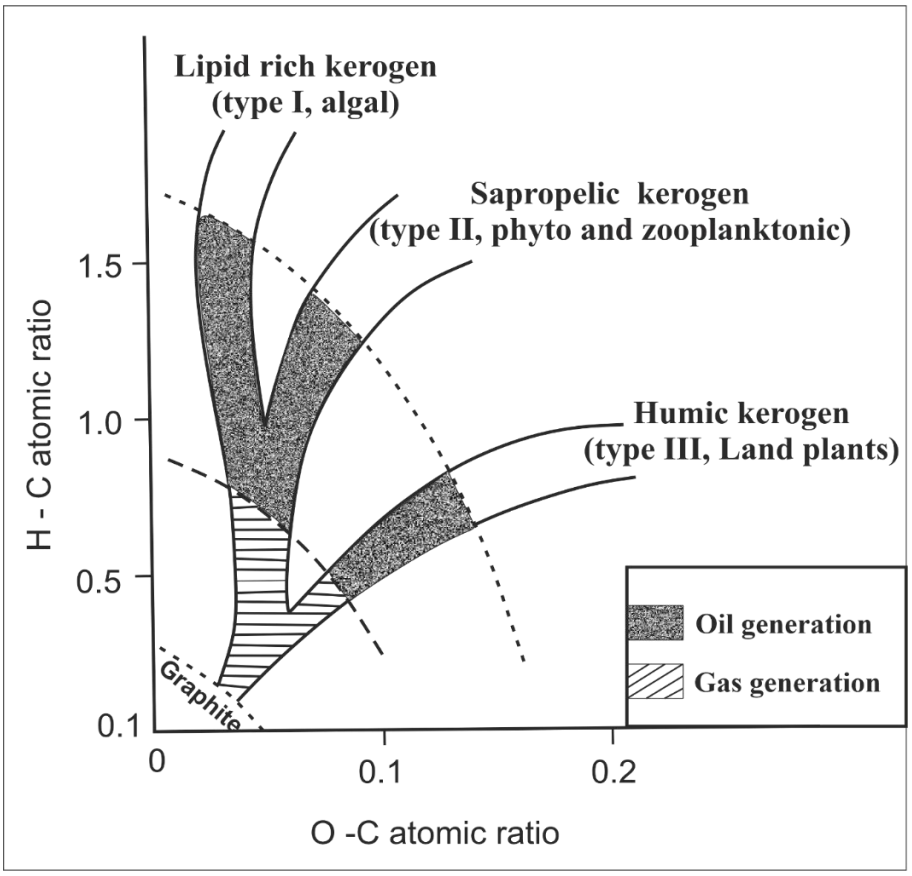

Fig. 3.2: kerogen types scheme plotting on the relation of O-C/ H-C ratio, after (Tissot & Welte, 1984).

3.2. Results and discussion

3.2.1. Lithology and depositional environment of the Source rock

Organic-rich consolidated sediments could be generative as potential source rocks or active source rocks that previously generated great petroleum amounts. Several ways of geochemical analysis of organic matter can be used to describe expelled oils source rocks that interesting for evaluating basin conditions, emigrants' oils, and their source type (Peters, 1986; Zumberge, 1987).

1. **Carbon isotopes ratios**

The deviation of aromatics and saturates of $\delta^{13+}C$ could infer the age and the environments of the source rocks, where the second part of isotopes are the fraction ratios (saturates, aromatics, resin, and asphaltene) are figured in polarity and polarizable. Saturates conclude linear, branched, and cyclic compounds that

have polar properties such as paraffin. Aromatics, mostly cyclic aromatic ring compounds tend to be polarizable (Horsfield & Rullkotter, 1994).

Resin and Asphaltene are polar substituents, the resin concludes (NSO) and separates from the Asphaltene by subjecting to heptane and pentane as it dissolve in these compounds while the Asphaltene is non-soluble in these compounds (Sofer, 1984). The two parameters of saturate and aromatics are based on two equations each one reflects a different type of organics source rock environment, and the difference between these equations is known as a canonical variable (Fig. 3.3) (Sofer, 1984):

Terrigenous originates

$$\delta^{13}C_{aro} = 1.12\delta^{13}C_{sat} + 5.45 \quad (3.1)$$

Marine originates:

$$\delta^{13}C_{aro} = 1.10\delta^{13}C_{sat} + 3.75 \quad (3.2)$$

Canonical variable:

$$CV = -2.53\delta^{13}C_{sat} + 2.22\delta^{13}C_{aro} - 11.65 \quad (3.3)$$

Where, CV is the canonical variable, C_{aro} is the aromatics fraction of isotope, and C_{sat} is the status saturation of isotope.

The analyzed crude oil samples have values of $C_{saturates}$ ranging from -27.36 to -27.81, and the $C_{aromatics}$ values were between -27.53 and -27.73 (Table 3.2). From the relation between saturates and aromatics fraction of the carbon isotopes and Sofer canonical variable inferred that all samples derived from the marine environment where all samples indicate the non-terrestrial environment of source rocks originate (Fig. 3.3).

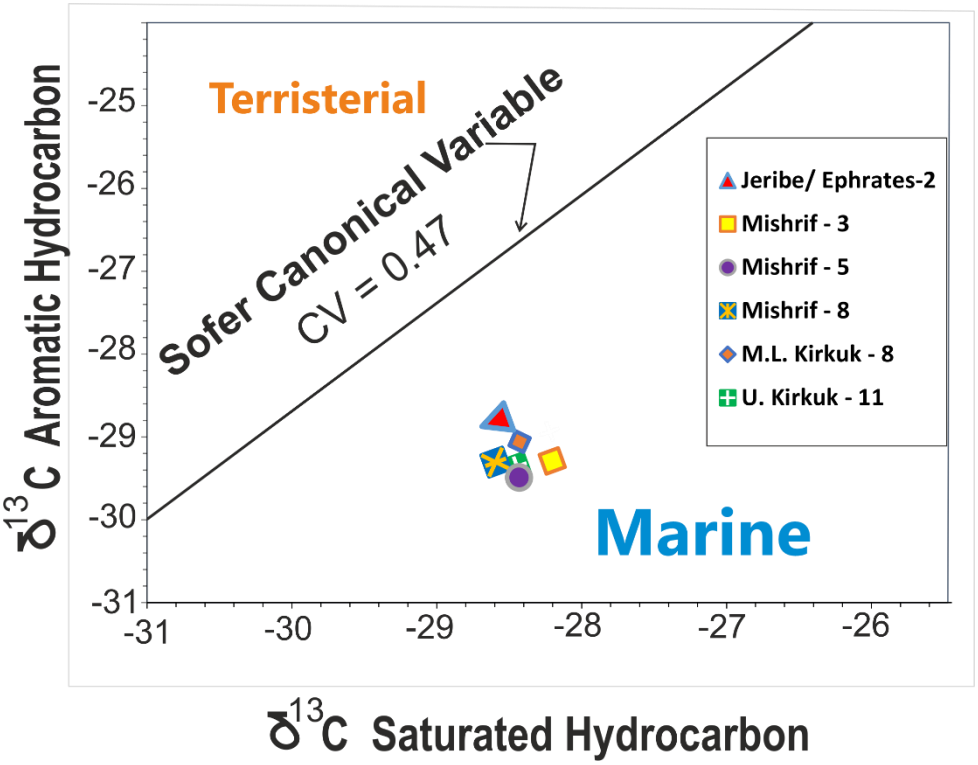

Fig. 3.3: plotting saturates against aromatics of $\delta^{13}C$ isotopes shows the period forming of source oil of Mishrif and Asmari reservoirs in Fauqi oilfield in the Upper Jurassic to Lower Cretaceous, after (Peters et al., 2005).

Table 3.2: concludes the carbon isotopes saturate, aromatics, resin, asphaltene, and Paraffins ratios in the crude oil samples.

Oilfield	Formation	Type of analysis								
FQ	Jeribe/ Euphrates 2	C13+ Saturate	C13+ Aromatic	C.V.	% Sat	% Aro	NSO	Asph	Sat/Aro	n-paraffin /Naphthene
FQ	Mishrif 3									
FQ	Mishrif 5									
FQ	Mishrif 8									
FQ	M/ L. Kirkuk 8									
FQ	U. Kirkuk 11									

2. Pristane/n-C_{17} and phytane/n-C_{18}

Pristane and phytane ratio in the geochemical analysis is a good biomarker indicator to infer the variation of oxic and reductive conditions upon the time when the source rock was deposited, and the early stages of biodegradation in the organic matter. Phytanic acid is the initiative compound forming precursor of

pristane, so it supposes to be found in large amounts at the beginning of plant decay on the land reflecting the oxic condition more than in the aqueous environment where anaerobic conditions are more reductive. The increasing Pristane/n-C_{17} ratio relative to phytane/n-C_{18} reflects the terrestrial origin of the organic matter. Generally, phytanic acid considers a marker of oxidizing conditions (Cummins & Robinson, 1964). The results of crude oil analysis were pristane/nC17 ratio ranges from 0.19 to 0.31, and phytane/nC18 ratio ranges from 0.31 to 0.42 (Table 3.3). Plotting the phytane to pristane ratios cleared the type of environment to be reduced and the origin of organic matter is an open marine. The low maturity can be seen from the samples placed (Fig. 3.4).

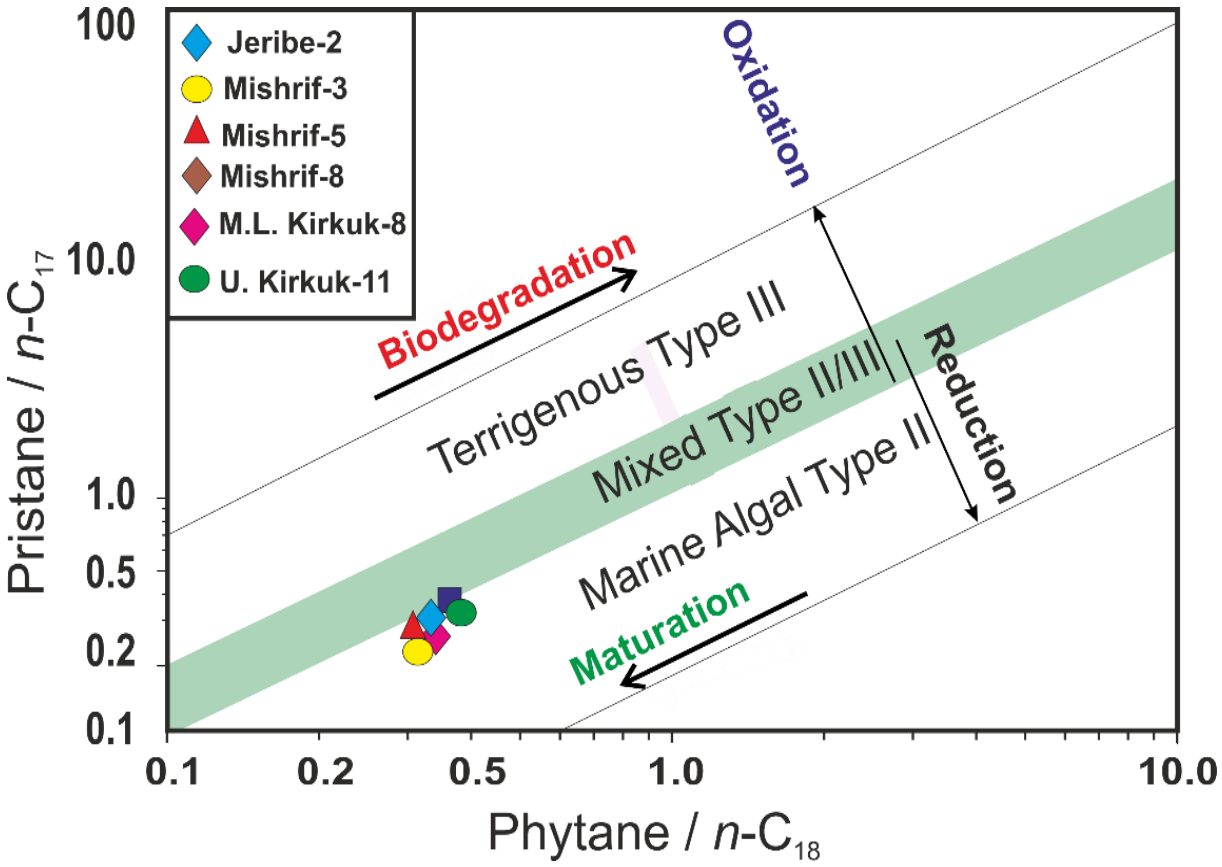

Fig. 3.4: pristane/n-C_{17} to phytane/n-C_{18} ratios relationship reflects the nature of the deposition environment and the type of organic matter that originates the petroleum source rocks, after (Peters et al., 2005).

3. Terpene (C_{19}, C_{23} and C_{24}) indices

Tricyclic terpenes are more abundant in terrigenous originates oils, with a dominance of C_{24} tetracyclic terpene. Saline lacustrine and marine sources of

petroleum are dominant with higher carbon number tricyclic terpenes, especially C_{23} tricyclic terpenes relatively parted in crude oil (Tao et al, 2015). The order of amount content, in relative of C_{23} tricyclic terpene of originates crude oils in maximum, refer to saline lacustrine oils, and less from marine oils, and freshwater lacustrine oils respectively, while the increasing of $C_{19–23}$ tricyclic terpenes indicate to terrigenous oils (Tao et al, 2015).

Low abundance of tetracyclic terpanes C_{24} found in crude oils, and in the ancient sediments that could be reflects from the bonds fission to C_{17} and C_{21} affected by thermal effects or microbial activity, or from microorganisms de-cyclization to the terrestrial triterpenes (Connan et al, 1980). Most of the tetracyclic terpene compounds found in both sediments and crude oils could be either in single C_{24} C_{21}, and C_{17}-Secohopane compounds that are widely employed in crude oil source rock investigations or as C_{24}–C_{27} -Secohopane homologs that are found in most sediments and environment, so it is useless in the petroleum source rock correlation (Connan et al, 1980; Peters, 1986).

In the investigation of the lithology of the origins of crude oils, using the plotting diagram of tricyclic terpenes. All the samples reflect marine carbonates originate that are enriched with the C_{22}/C_{21} with values between 0.93 and 1.05 and a lesser amount of tricyclic terpene C_{24}/C_{23} in the range of 0.25 to 0.28 (Table 3.2) (Fig. 3.5). The carbonates generally came from open marine platforms.

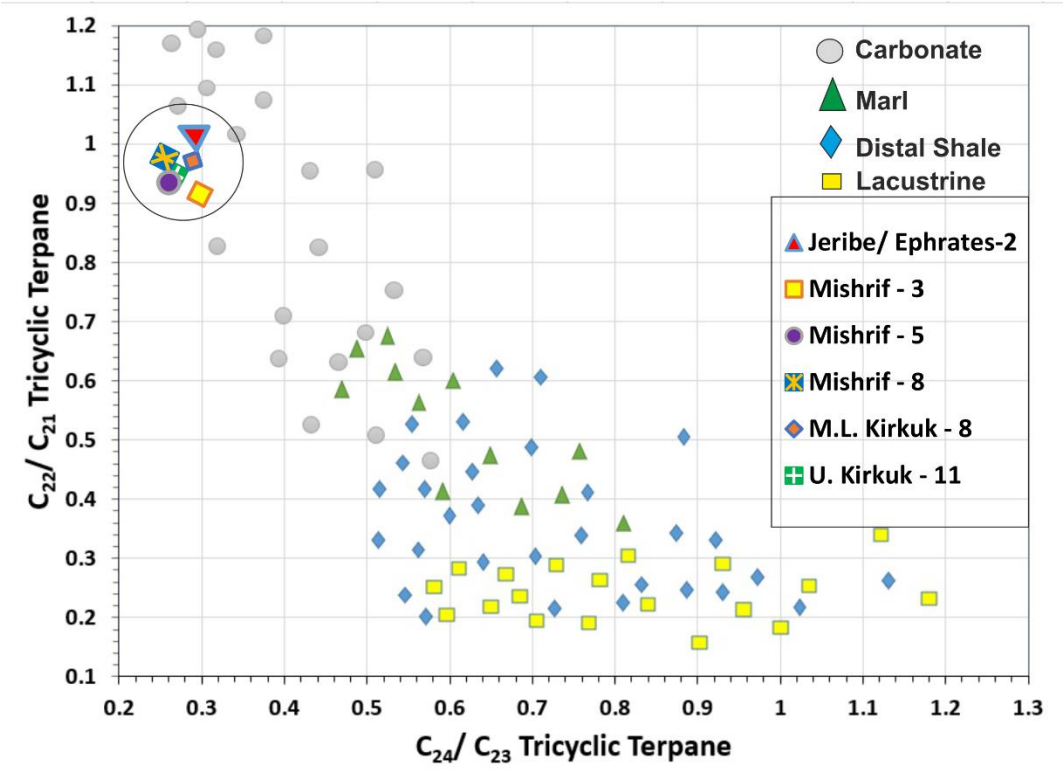

Fig. 3.5: terpenes indices shows that the type of originates oil source were carbonates for all samples examined in Fauqi oilfield, after (Peters et al., 2005).

Table 3.3: numerous bulk properties of the GCMS analyzing to the crude oils' samples.

Oilfield	Fauqi	Fauqi	Fauqi	Fauqi	Fauqi	Fauqi
well no.	2	3	5	8	8	11
Formation	Jeribe/ Euphrates	Mishrif	Mishrif	Mishrif	M/ L Kirkuk	U. Kirkuk
Depth m.	3040	3860	4000	3890	3370	3150
C19/C23	Xx	xx	Xx	xx	xx	xx
C22/C21	Xx	xx	Xx	xx	xx	xx
C24/C23	Xx	xx	Xx	xx	xx	xx
C26/C25	Xx	xx	Xx	xx	xx	xx
Tet/C23	Xx	xx	Xx	xx	xx	xx
C27T/C27	Xx	xx	Xx	xx	xx	xx
C28/H	Xx	xx	Xx	xx	xx	xx
C29/H	Xx	xx	Xx	xx	xx	xx
C30X/H	Xx	xx	Xx	xx	xx	xx
OL/H	Xx	xx	Xx	xx	xx	xx
C31R/H	Xx	xx	Xx	xx	xx	xx
GA/C31R	Xx	xx	Xx	xx	xx	xx
C35S/C34S	Xx	xx	Xx	xx	xx	xx
Ster/Terp	Xx	xx	Xx	xx	xx	xx

Rearr/Reg	Xx	xx	Xx	xx	xx	xx
C27%	Xx	xx	Xx	xx	xx	xx
C28%	Xx	xx	Xx	xx	xx	xx
C29%	Xx	xx	Xx	xx	xx	xx
C29 20S/R	Xx	xx	Xx	xx	xx	xx
C27 Ts/Tm	Xx	xx	Xx	xx	xx	xx
C29 Ts/Tm	Xx	xx	Xx	xx	xx	xx
DM/H	Xx	xx	Xx	xx	xx	xx
TAS3 (CR)	Xx	xx	Xx	xx	xx	xx

4. Oleanane/ C_{30} hopane

The pentacyclic triterpene (Oleanane), is a biomarker present in two isomeric habits of 18α (H)-oleanane and 18β (H)-oleanane. The source of both forms is recognized as the alpha (α) compartment plants that have maximum thermodynamic stability to verify it as the most ascendant structure in oil originating rocks with thermally matured crude oil. So, the 18α (H)-oleanane considers one of the most significant diagnostic biomarkers on the terrestrial plant of angiosperms (Fig. 3.6 a & b) (Moldowan & Jacobson, 2000; Al-Khafaji et al., 2019).

So, in order to predict the sediment type, an Oleanane plotted against the C29 Ts/Tm, while to estimate the organic species the plot will be against tricyclic terpene C19/C23.

This biomarker is an index to the dominant of angiosperm taxa during the period of source rocks deposition, and by plotting it against other terpenes compounds could reflect the paths of higher plants or the type of lithology if it is rich or poor in clay content. The average value of all samples of Ol/C_{30} is about 0.01, and the C_{19}/C_{23} average was 0.15 -0.17 which reflects the reduced environment condition synchronized deposition period of source rocks (Fig. 3.4 a). Oleanane indices can be used to investigate the clay content in the environment and sediments of source rocks by plotting with C_{29} trisnorneohopane/ trisnorhopane (Ts/Tm) which has values in the average of 0.09 (Fig. 3.4, b).

The Ts /Tm ratio is plotted for the oil sand of Cretaceous period, and it increases than (0.5) to reflects the portion of Shale Volume in calcareous rock facies (Peters, 1986).

Relatively, the results in this term showed that the source rock related to an environment with low angiosperm dominance and lithology of low clay content reflects the marine environment.

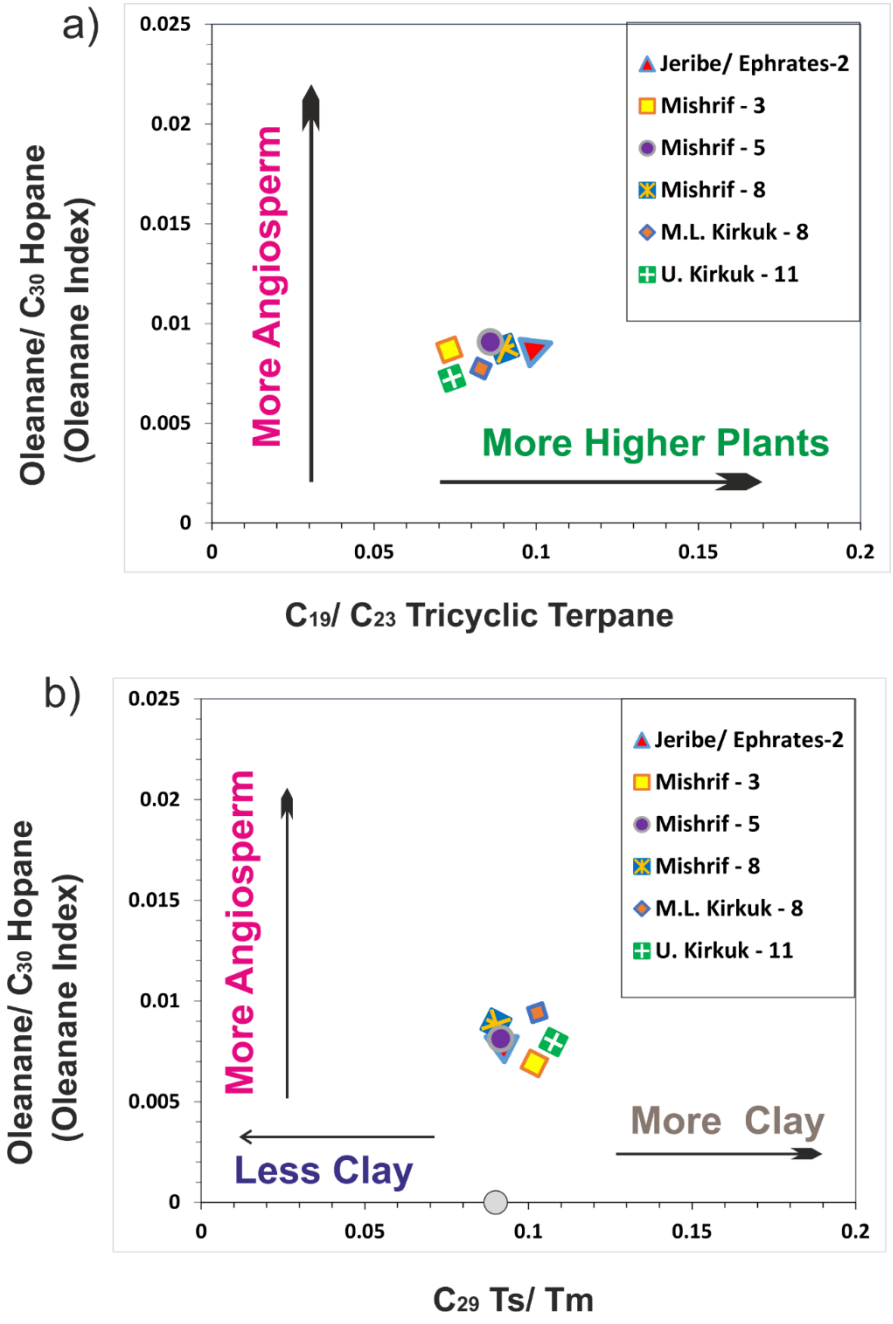

Fig. 3.6: the oleanane biomarker. a) in relation with tricyclic terpene (C_{19}/C_{23}) shows the samples placed in the higher plants' region. b) plotting against C_{29} Ts/Tm terpane, shows the less contents clay origin of the source rocks oil, after (Peters et al., 2005).

5. Sterane Ternary Diagram

The C_{27}-C_{29} sterane abundance could be utilized as an indicator of the nature of terrestrial and aquatic chlorophyllin biota. The dominance of C_{29} steranes is usually reflected in the land plant. The presence of stable sterane compounds infers the high contribution of terrestrial plants, especially from resin-produced species, the dipterocarpacceae. If, the presence of steranes fits in values of $C_{29} > C_{28} < C_{27}$, then the origin of the source rock is interpreted as a mixing of organic matter between algae and terrestrial plants (Huang & Meinschein, 1979).

Steranes that perhaps formed throughout diagenesis and catagenesis processes rearranged in diasteranes within no biological precursors. The quiet dominance of diasteranes in the crude oils reflects the clay mineral enriched environment of deposition of the oil source rock, whereas the Triaromatic sterane is used to investigate the thermal maturity of the source rocks (Horsfield & Rullkotter, 1994).

The stable steranes compounds of $C_{27,}$ $C_{28,}$ and C_{29} in values of 34.4 – 35.6, 22.2 – 24.4, and 41.2 – 42.8 respectively (Table 3.2). The ternary diagram that was employed in the biomarker evidence depending the tri-relation of these three steranes compounds.

The results, in total, reflected an open marine environment as the origin of the source rocks, and the condition of sedimentation in these environments tend to be more reducing leading to ensuring the expectation of forming source rocks of oils in reductive medium (Fig. 3.7).

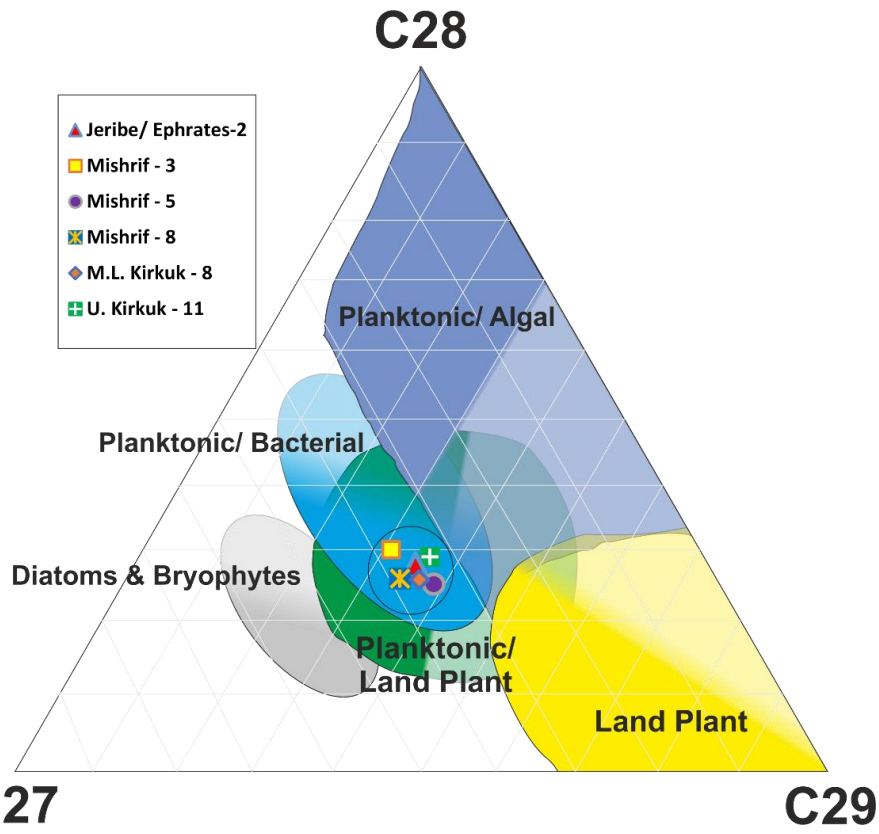

Fig. 3.7: the ternary diagram of steranes compounds showed that the samples originates in an open marine environment where the planktonic dominant, after (Peters et al., 2005).

6. Hopane/ terpene relation

Hopane structure had an indication of two paths: one for the increase in the carbonate contents in the oil source rock, and the other for the range of the relative reduction of deposition circumstances during forming the source rocks (Moldowan & Jacobson, 2000; Al-Khafaji et al., 2019).

Relative to their good abundance in the crude oils, $C_{34,}$ and C_{35} were used in plotting diagrams to evaluate the results ratio of C_{31}/ C_{30} hopane with an average value of 0.36 can be plotted versus the terpene ratio of C_{26}/ C_{25} which has a value an average of 0.78, in order to limit the rock source mineralogy. The results of all samples were in carbonate lithology, except the Jeribe formation which showed a good content of marl as shown in (Fig. 3.8). As a result, the carbonate is the main lithology which reflects an open marine origin of the source rock.

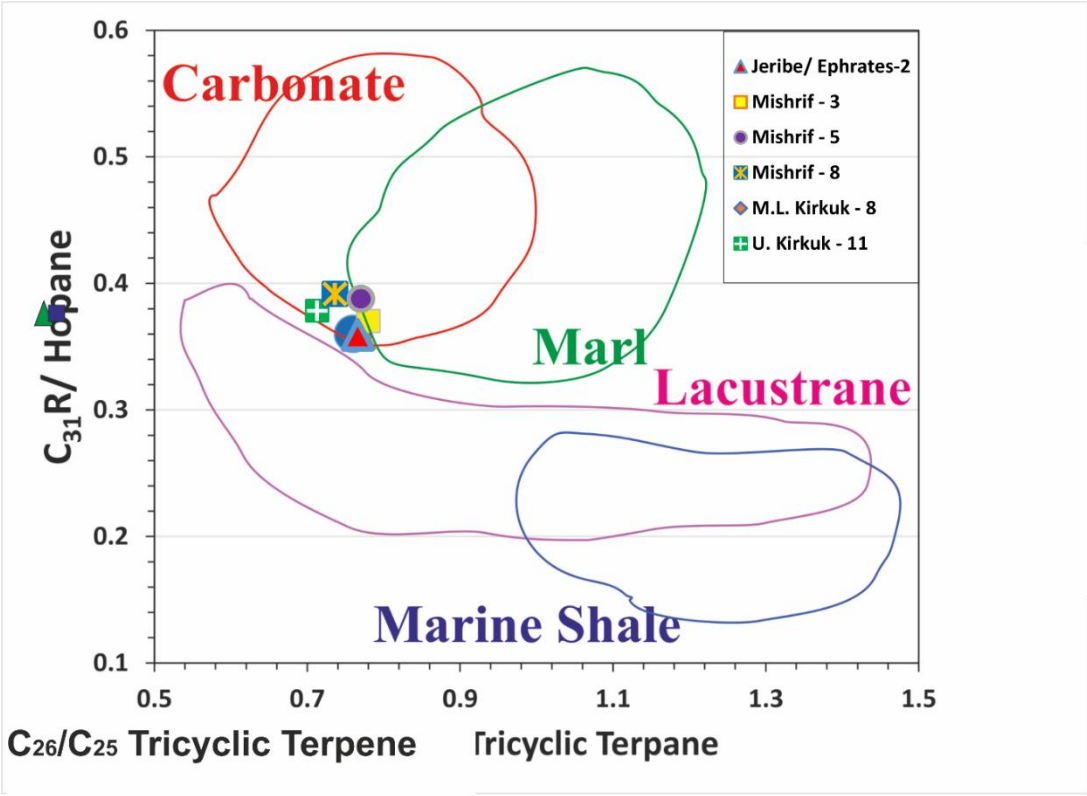

Fig. 3.8: the relationship between hopane ratio to terpene shows the carbonate origin of the source rocks of the samples of studied wells after, (Peters et al., 2005).

3.2.2. Thermal maturity

Thermal maturity of petroleum source rocks can be defined through several relations of biomarker indices, especially from the most biodegradation resistant compounds like steranes and terpenes.

1. **Triaromatic Sterane**

The Triaromatic steranes were employed to evaluate the maturity range of the source rocks over cross plot relation with the C27 Ts/Tm terpene. The value of Triaromatic ranges from 0.3 to 0.4, with a low value of C_{27} Ts/Tm at about 0.24. The result is aimed at the low maturity of the source rocks of the Mishrif Formation (Fig. 3.9).

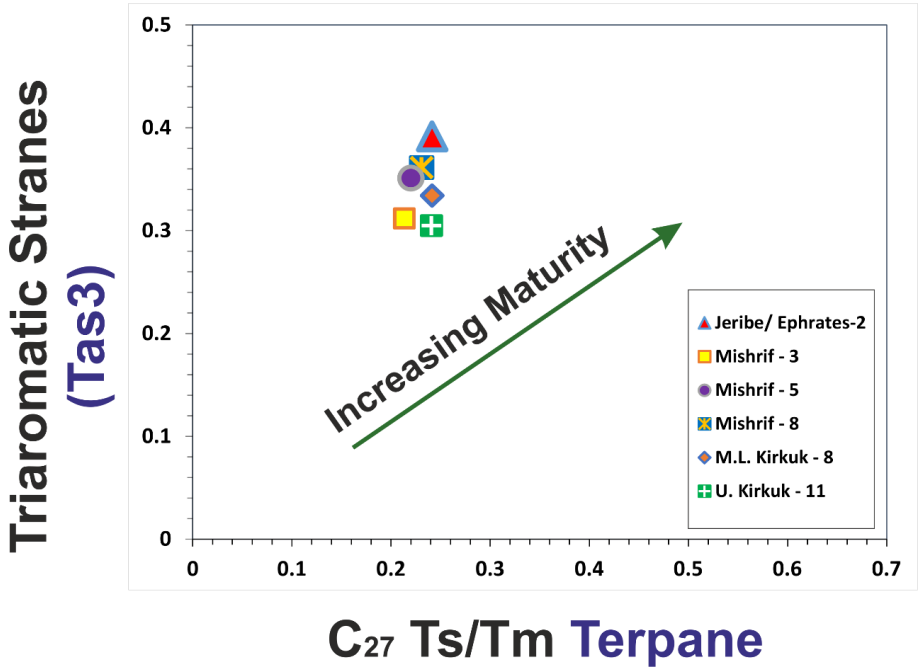

Fig. 3.9: plotting of Triaromatic sterane against C_{27} Ts/Tm terpene shows that the samples indicate a low maturity origin, after (Peters et al., 2005).

Also, can infer the maturity from Triaromatic steranes (Tas3) by plotting the C_{27} Ts/Tm against C_{29} Ts/Tm which has an average value of 0.09. This relation reflects the low maturity of the source rocks for all analyzed samples of crude oil (Fig. 3.10).

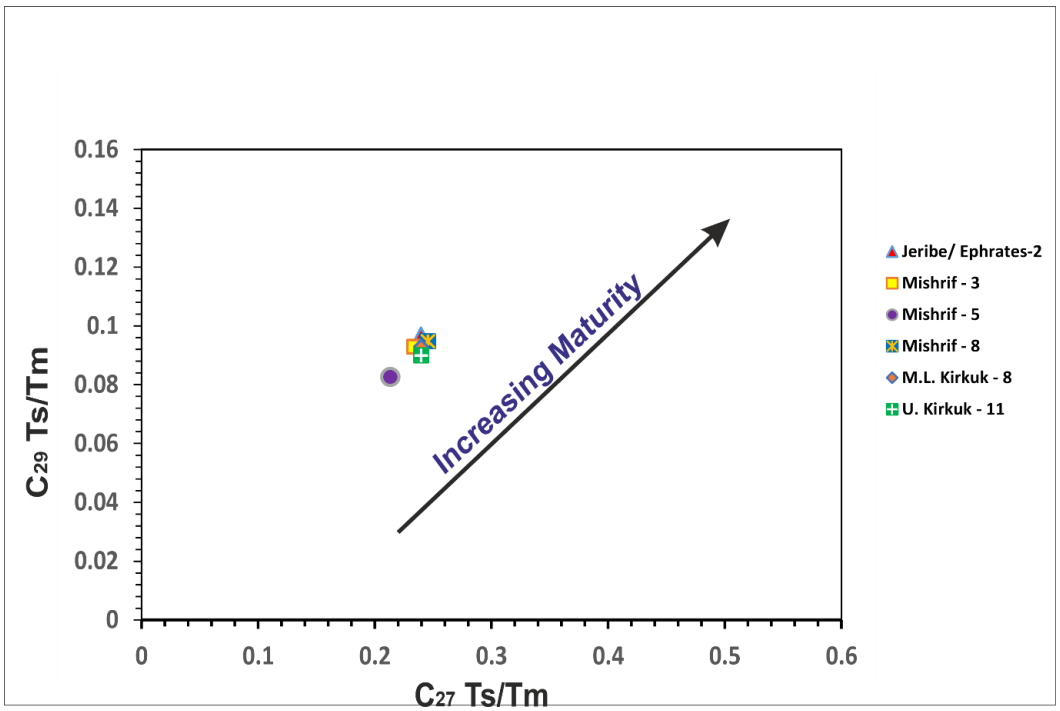

Fig. 3.10: Steranes compound relationship shows the low maturity of the oil source rocks of the studied wells, after (Peters et al., 2005).

2. API and sulfur content

This integration plot deals with the temperature maturity of the crude oil samples. Where the AP gravity represents the measuring item for petroleum quality. The value of API measures the temperature maturity and can calculate the specific gravity of the crude oil regarding by the American Petroleum Institute Formula (API) through the equation (Demirbas et al, 2015):

$$SG_{oil} = ({}^{141.5}/_{API + 131.5}) \quad (3.2)$$

Where: SG is the specific gravity of the oil, and API is the American petroleum institute value. The high value of API means the better crude oil, and the rang of it is (10 – 50) and most the oils placed in range of (20 -45) and in manner considering the petroleum with API> 30 are light and heavy for the < 20 ones. The ratios of (S% and V%) as a weight portion decrease of the oil quality and in the same time the sulfur percentage weight used to estimate the deposit environment as the large amount indicates of reducing situations and premature thermal. The weight ratio of sulfur ranging in values from 0.05 %wt. to more than 10% wt. with an average of 1-5 %wt. The crude oils with <1% consider a sweet oil and >1% called sour oil (Demirbas et al, 2015).

Sulfur content is a general bulk parameter that used in the evaluation of economical refinery operations of crude oil throughout plotting cross sections with API gravity indices or carbon isotopes against the sulfur as weight fraction (%wt.). The knowledge of sulfur origin considers important to estimate the paleo depositional environment and the inputs' source. Organic origin sulfur expelled from organic matter's amino acid and can be found in sediments. Generally, the origin of sulfur in crude oils is a mix of organic matter origin and aqueous sulfide compounds, such as hydrogen sulfide (H_2S) due to the effect of sulfate-reducing bacteria in the anoxic marine sediments (Fig. 3.11) (Francois, 1987).

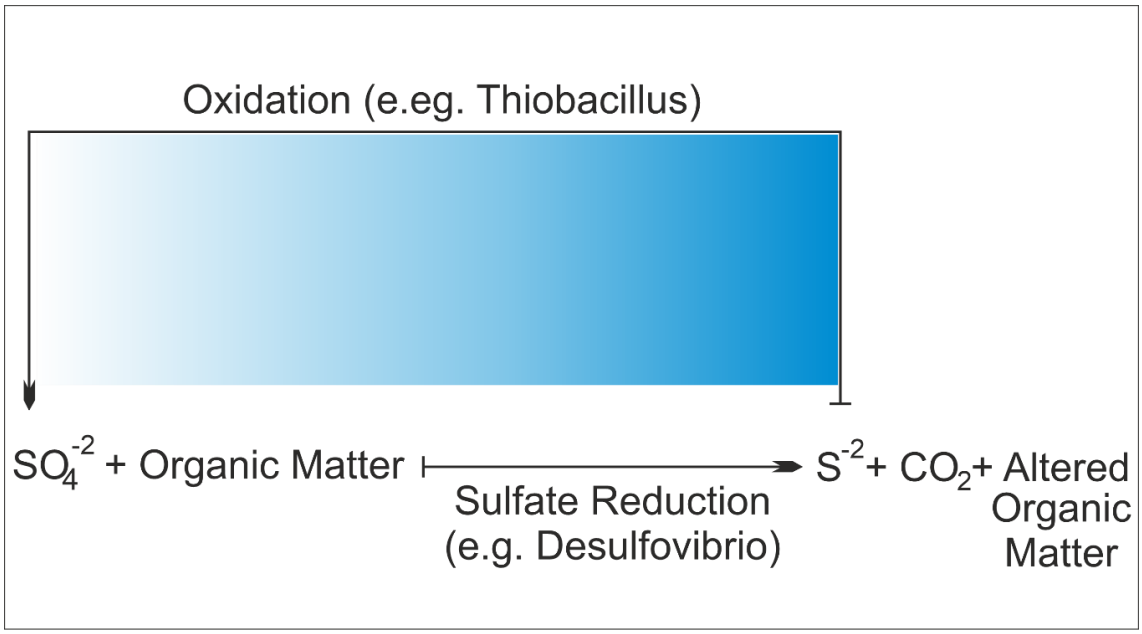

Fig. 3.11: Sulfur species typical reactions throughout sediment diagenesis processes. Through reduction reactions to anoxic condition, sulfate-reducing bacteria generates an excess sulfide. Metals, like iron, and organic matter rival sulfides. In carbonate (clay-poor) sediments, excess sulfides gone integrated into the immature kerogen due to the poor metal content in this environment, after (Peters, 1986).

The result shows the samples of crude oils with values of API at the bottom grade at values 17 to 20 API (Table 3.4) to consider heavy oils that reflect low thermal maturity, on the other hand, the high abundance of Sulfur in weight fraction of about 4% wt. In average, reflecting the reducing state of source rocks forming within carbonate marine origin (Fig. 3.12).

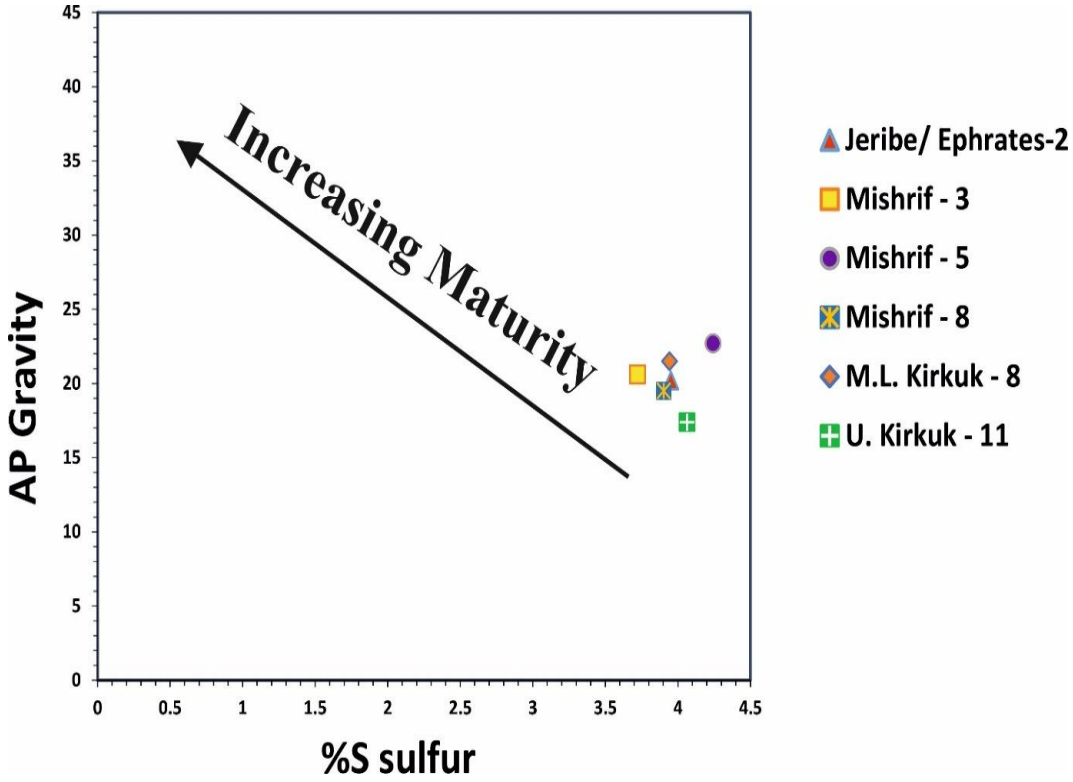

Fig. 3.12: API gravity plotting against Sulfur weight fraction diagram, shows all samples in low maturity, after (Peters et al., 2005).

Table 3.4: shows the AP gravity, non-organic materials, Pr/Ph ratios, and CPI of the crude oil samples.

Oilfield	Formation	API Gravity	% S	% C_{15}	V ppm	Ni ppm	Pr/Ph	Pr/n-C_{17}	Ph/n-C_{18}	n-C_{27}/n-C17	CPI
FQ	Jeribe/ Euphrates 2	xx	Xx	Xx	Xx	xx	xx	xx	xx	xx	xx
FQ	Mishrif 3	xx	Xx	Xx	Xx	xx	xx	xx	xx	xx	xx
FQ	Mishrif 5	xx	Xx	Xx	Xx	xx	xx	xx	xx	xx	xx
FQ	Mishrif 8	xx	Xx	Xx	Xx	xx	xx	xx	xx	xx	xx
FQ	M/ L. Kirkuk 8	xx	Xx	Xx	Xx	xx	xx	xx	xx	xx	xx
FQ	U. Kirkuk 11	xx	Xx	Xx	Xx	xx	xx	xx	xx	xx	xx

3. Dia./Reg. Steranes and Ts/Ts ratios

The Dia./Reg. Steranes ratios and the Ts/Ts ratios are used to estimate the source rocks maturity where the high values of the diatomic steranes reflects a high maturity level and the high values of the Ts/Tm ratios also reflects a high maturity. The results clarify the early maturity stage where the values of Ts/Tm are about 0.2 where the Ts/Tm ratios begin to increase quite during late maturation. and in range of 0.18- 0.21for the Dia./Reg. Steranes ratios (Fig. 3.13).

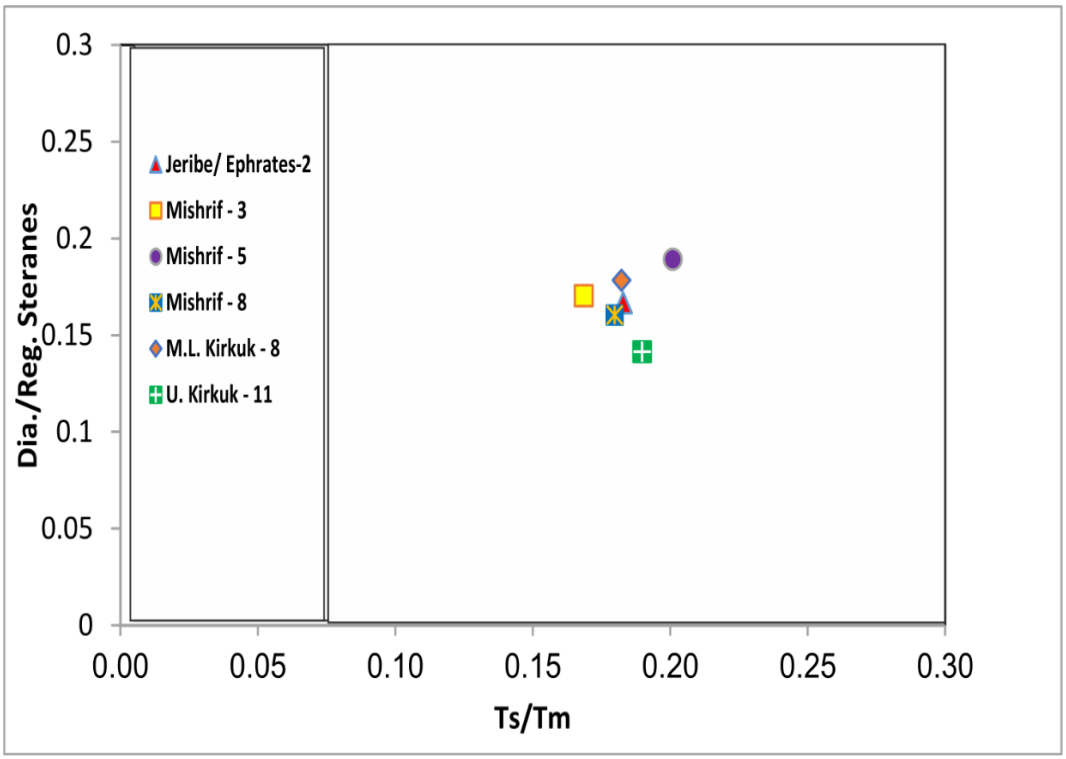

Fig. 3.13: shows the relation between The Dia./Reg. Steranes ratios and the Ts/Ts ratios to estimate the maturity of the source rocks, after (Peters et al., 2005).

3.3. Age Prediction

1. Carbon Isotopes relation

The relation between saturates and aromatics fraction of the carbon isotopes and Sofer canonical variable inferred the approximate age of deposition of the source rocks (Al-Khafaji et al., 2019). The results showed that most of the samples belonged to the upper Jurassic period and part of it indicated an Upper Jurassic to Lower Cretaceous period (Fig. 3.14).

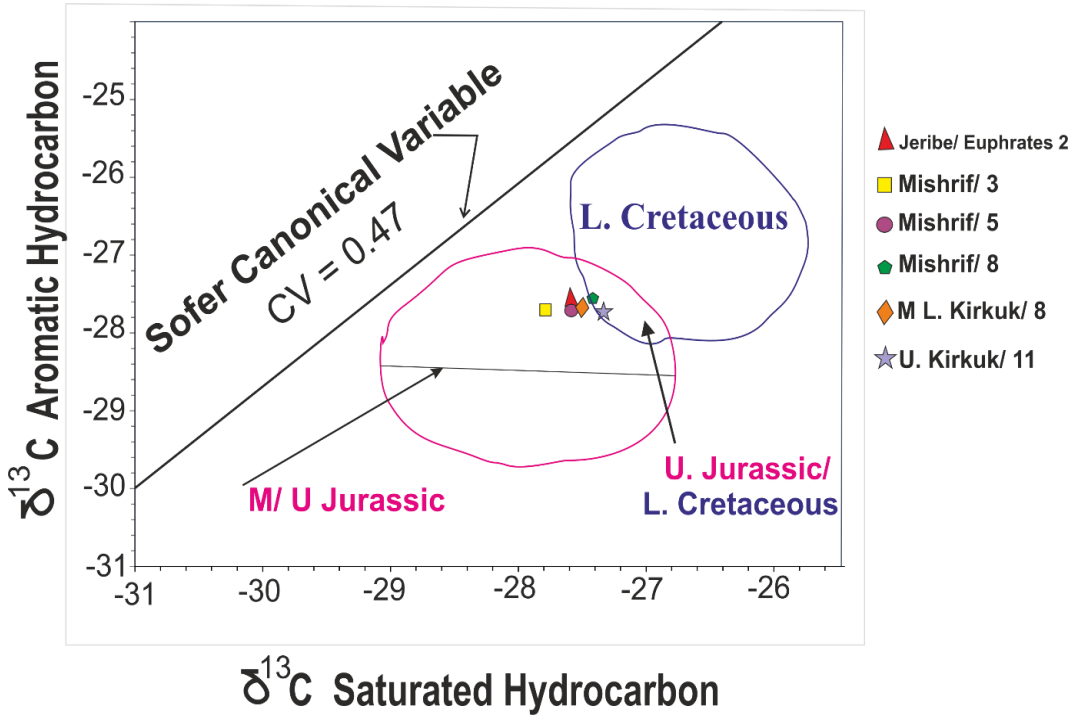

Fig. 3.14: saturates and aromatics $\delta^{13}C$ isotopes plotting shows the period forming of source oil of Mishrif and Asmari reservoirs in Fauqi oilfield in the Upper Jurassic to Lower Cretaceous, after (Peters et al., 2005).

2. Sterane, C_{28}/C_{29} ratio

The sterane compounds can be used to infer the age of the petroleum source rocks where there are relative variations in the C_{28} and C_{29} through geologic time. Noticing the relative increase of C_{28} in the marine environment synchronizes with decreasing in C_{29} during a significant period. For that, C_{28}/C_{29} ratio can be used to predict the age of deposition (Peters et al, 2005). The C_{28}/C_{29} ratio of the analyzed samples takes values between 0.52 and 0.59 which reflects an age from middle/upper Jurassic to the Cretaceous period (Fig. 3. 15)

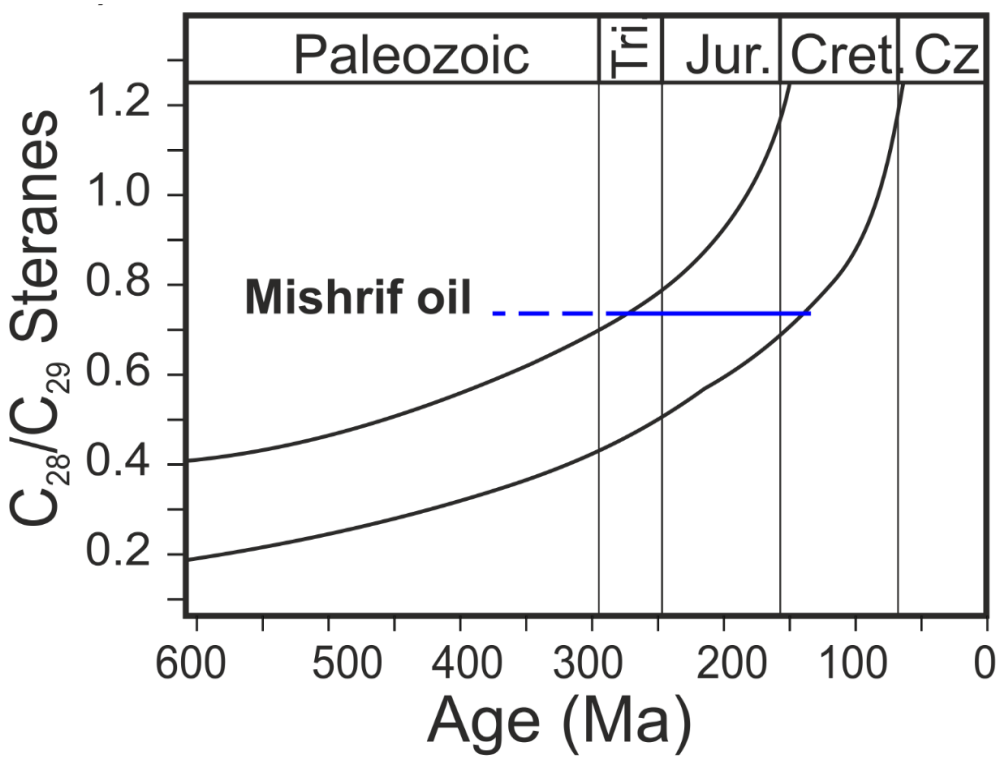

Fig. 3.15: shows the ratio of C_{28}/C_{29} steranes reflects the upper Jurassic-lower Cretaceous age for the source rocks of Mishrif Formation oils, after (Peters et al., 2005).

3. Carbon isotopes values

The stable carbon isotope ^{+13}C is generally used to give the ages while there is no decay for another isotope and oil age investigation could be inferred from the negative value of the isotope. The age of Cretaceous has isotope ^{+13}C with negative values nearly -27, whereas the older ages has negative value of about -28 or less (Al-Ameri & Zumberge, 2012; Al-Khafaji et al., 2019). All analyzed samples of crude oil have values ranging in -27.3 to -27.8 (Table 3.2), which reflect the age from mid-upper Jurassic to Cretaceous (Fig. 3.16).

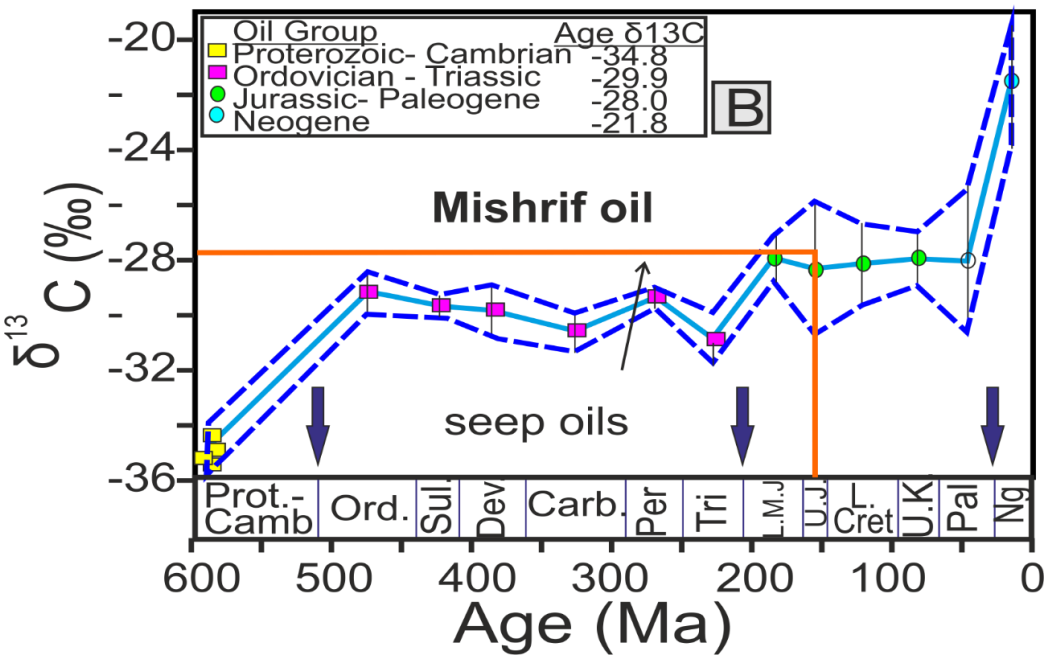

Fig. 3.16: shows the ratio of carbon isotopes ratios reflects the Upper Jurassic-Lower Cretaceous age for the source rocks of Mishrif Formation oils, after (Peters et al., 2005).

3.3. Discussion

Gas chromatography (GC) and gas chromatography/mass spectrometry (GCMS) were used to determine the saturated hydrocarbons. API/ %S wt., Pristane/phytane (Pr/Ph), isoprenoids/n-alkanes, homohopane, diasteranes, Oleanane indices, C_{27}-C_{29} regular steranes, and Ts/Tm are determined. The studied crude oils over the analyzed samples result in the suggestion of an open marine oil source and estimation to be characterized by the low level of maturation mainly sourced from organic matters, with non-organic contents, of reduced marine origin with few terrestrial inputs, and the mineral that forming the source rocks initially of carbonates. The results also suggest that the oils belong to the Upper Jurassic and lower Cretaceous in essential of Sulay and Yamama formations, and the probability source of the Middle-Upper Jurassic period of source rocks formations.

Chapter Four

Chapter Four

Fauqi Oilfield Petroleum System Modeling

4.1. Introduction

The main concept of infield 1D, 2D, or even 3D modeling heat flow mimicry and all the infra geochemical models is to rebuild the pre-environment in seeking the petroleum source rocks' maturity. Calculating and calibrating the temperature throughout the evolution stages of the interested basin is the key role in this mission. One of the main keys in these calculations is the heat flow. Many formulations and equations were used to conduct the solutions (Ungerer, 1990).

If the paleotemperature is known, chemical kinetic equations can be utilized in thermal cracking rate estimation for oil generation. Pore fluid pressure also has an important role in analytical procedures. Integrating the predicted pressure with the sedimentation rate is engaged to estimate the sediments' compaction. The compaction with porosity can ease the bulk thermal conductivity evaluation and calculate heat flow. In the beginning calculation, only 1D simulation can be done according to the capability of the computer tools used in the previous times (Ungerer, 1990; Hunt, 1996).

At the end of the past century, new computer developed software helped perform 3D simulation for more precise modeling that gave the required interpretation of the petroleum source rocks, heat flow, sedimentation rate, and sedimentation condition concept of basin modeling expressed the erection of the geological model to all the sedimentary processes synchronized basin forming and the post processes along the geological time (Ungerer, 1990).

There are good orders of hydrocarbon distribution within the basin and petroleum gravity decreasing downward in the depths. Vertically, heavier oil tends to be found in the shallow regions, whereas the lighter oil is in the deep following the porous layers ending with gas accumulations at the base bar with the non-porous layers. In the same manner, lateral distribution takes a similar

pattern where the heavy oils accumulate around the basin margin, and the lighter oils condense in the center of the basin (Nandakumar & Jayanthi, 2021).

Implied physical and geochemical parameters with the hydrocarbons cycle of generation, migration, and preservation are the key to understanding the causes of such patterns of oil distribution, and later to evaluating the sedimentary basin history. In this study, the PetroMod software is used in the reconstruction of the thermal history of the basin (Welte et al, 1997).

Basin modeling software needs essential parameters as input data to be able to reconstruct the paleoenvironment. A wide range of input data is requested, e.g.: basin mechanism and the rate of uplifting and subsidence, type of the sediments and organic input as a depositional environment; lithostratigraphic and petrophysical properties, such as; porosity, permeability, thermal conductivity, etc.; basin thermal history; chemical and physical properties of fluids (water, oil, or gas); organic matter input kinetics; the age, type and the thickness of the formations; tectonic events, erosion periods so as the eroded amounts of layers (Welte et al, 1997).

Construction of basin modeling can be erected in one dimension for a single well or may be in a two or even three dimensions model as a multi-wells geologic profile in aiming to integer the resulting form of the basin with seismic data to evaluate the oil accumulations region in the fields. The thermal maturity of the source rocks can be predicted from the data of inclusion fluids in order to build geothermal modeling for oil through applied software (Nandakumar & Jayanthi, 2021).

Reconstruction of basin modeling through computer software is most wanted because the events that involving in sedimentary basin forming are irreversible operations and not possible to reverse these processes lending to a reversing model (Poelchau et al., 1997). The simple definition of a petroleum system, as shown in (Fig. 4.1), is a system concluded of all the elements, events, and

processes relating to all hydrocarbons (oils & gases) had been generated from the probable source rocks and migrated and accumulated to reservoirs (Magoon & Dow, 1994).

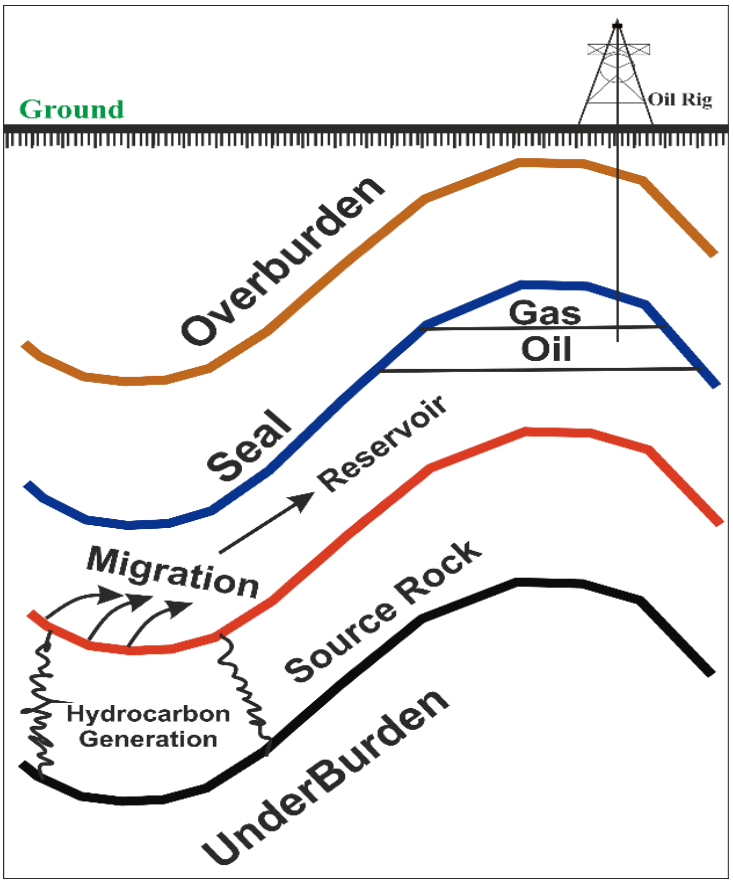

Fig. 4.1: the petroleum system elements, after (Demaison & Huizinga, 1991).

4.2. Total petroleum system

4.2.1. Source rocks

Depending on the biomarker results that obtained in the previous chapter that deals with the maturity and the age of the source rocks, the Middle-Upper Jurassic (Sargelu & Najma) formations are the main source rocks that expelled their Hydrocarbons and fed up the Late Cretaceous and the Tertiary reservoirs (Pitman et al., 2004) Many studies suggested that the Mishrif Formation oil could be derived from the Upper Jurassic-Early Cretaceous (Sulay and Yamama) formations (Al-Ameri & Zumberge, 2012; Al-Khafaji et al., 2019).

4.2.2. Reservoirs and seals

In the Fauqi oilfield, the main reservoirs belong to the period of the Upper Cretaceous. The secondary reservoir, Asmari reservoir, represents the Tertiary period. The Late Cretaceous reservoirs has a high production percentage within a ratio exceeds on 70% of the total production from this field (Pitman et al., 2004).

The main reservoir is the Mishrif Formation of the Cretaceous depth exceeds 4km and the secondary reservoirs (Asmari reservoir) of the Tertiary periods are in the average of 3km depth. Generally, the primary porosity is not so good, but the great porosity locally comes from the dissolution of the carbonate rocks and from the fractures that were affected by the folding movements (Fig. 4.2) (Beydoun., 1988).

The Mishrif Formation, the main reservoir, is divided into three rock units which are A, B, and C and seven reservoir units subsequently depending on the porosity and the shale content. The main reservoir unit according to the good characteristics obtained from the core registers and well-log data is MB21 within three pay units 1, 2 and 3. These units are sealed with compacted non-porous limestone layers. The Whole formation is ended at the top of a shaly compacted limestone layer as a trap. The bottom of the formation is represented in the MC2 unit which has high water saturation (Sepehr et al., 2006).

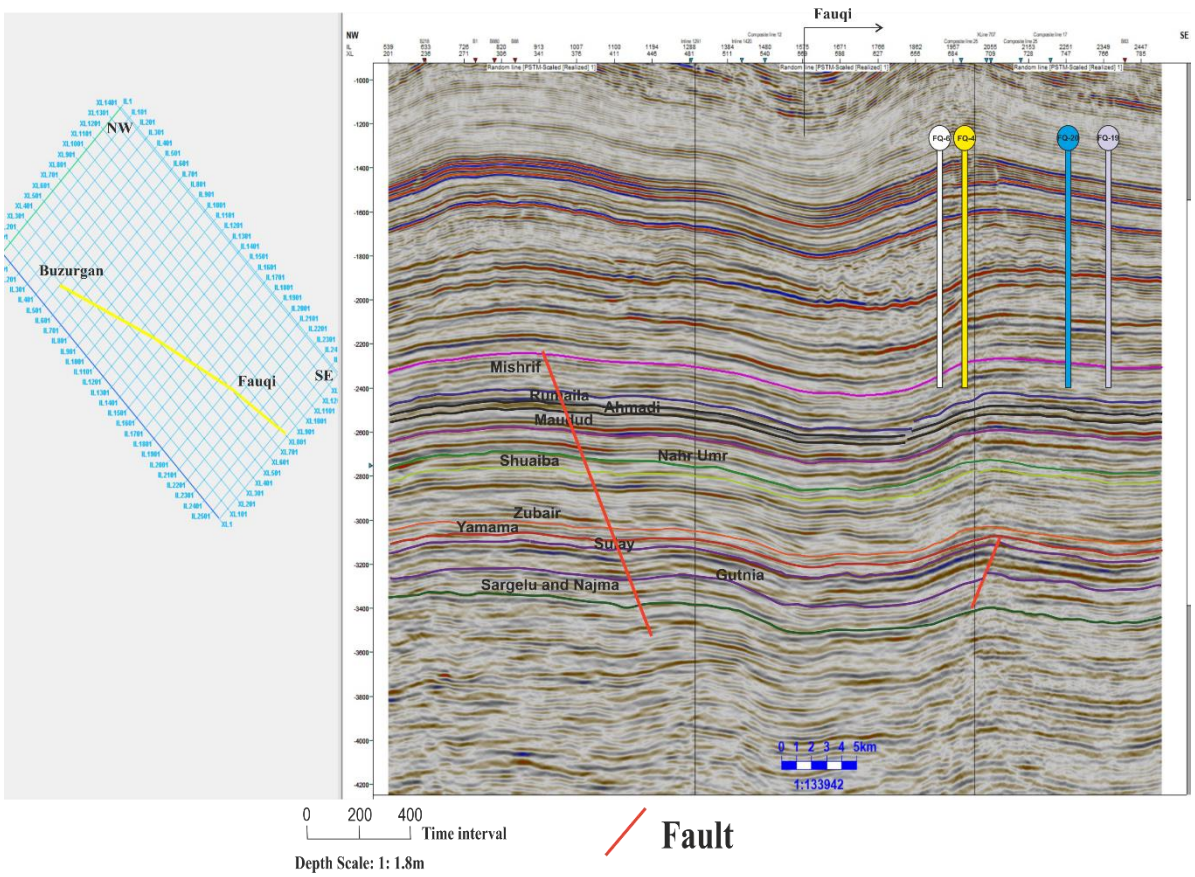

Fig. 4.2: NW-SE Seismic section extends from Buzurgan oilfield to the Fauqi oilfield shows the stratigraphy and the structural nature of the studied area, pointed on it the studied wells except for the FQ-14 well which is placed in the north dome out of the survey data, edited after Explorations Oil Company (EOC).

4.2.3. Traps

Generally, the column stratigraphy in the foreland and fold belt regions within the Zagros basin is controlled by two main seals that sustain the traps forming, the bottom Gotnia Formation and the top Fatha Formation (Beydoun., 1988). Gotnia Formation is a regional seal that consists of two distinct layers, salt and anhydrite. The Gotnia Formation was deposited during the Upper Jurassic period within the Gotnia-Garau basin across Oman, Dubai, Qatar and Zagros basin overlying the middle-upper Jurassic Sargelu and Najma formations which controlled the oils from being expelled except the fugitive hydrocarbons through the faults and salt diapirs that cause top layer fractures (Beydoun., 1988).

For traps, there are two essential types in the region of the Zagros fold belt basin, stratigraphic and structural. Many compressional folds are formed due to the orogeny movement that trended NW-SE as stratigraphic traps ending with non-porous strata. The traps mostly are structurally forming represented in the reverse and thrust faults diverse in the surrounding imbricated zone which belong to the Late Cretaceous stages. Locally traps are represented in the massive caprock like carbonates, shale, and evaporites as seen in the Mishrif reservoir. The early Tertiary epoch represents the major deformation period and traps forming (Pitman et al., 2004). The top seal in the studied area is the Fatha Formation which is considered a regional seal that enhances the Asmari reservoir traps and helps in confine the oils and prevents upward seepage.

4.3. Basing modeling

4.3.1. Heat flow

Heat flow analysis is used to determine the temperature to investigate the rate of geochemical reactions. In this analysis step, the preparation is conducted to the heat conduction, heat convection, and emitted heat due to the radioactive decay (Fig. 4.3). The thermal transition could be presented as a reflectance of the igneous intrusions (Demaison & Huizinga, 1991). Basal thermal boundary conditions of sediments should be performed for heat flow calculations. Boundary heat is calculated as separated geological events through the basin geometry (Beardsmore et al, 2001). The Surface Water Interface Temperature (SWIT) considers the main factor in heat flow analysis (Allen, 2005). This variant parameter is inferred throughout the radiation and conduction in the sediments (Beardsmore et al, 2001). The basal heat flow and the SWIT are the essential boundary conditions for heat flow estimation and analysis in sediment (Magoon & Dow, 1994). The SWIT parameter can be calculated automatically according to Wygrala formula (Poelchau et al., 1997) (Fig. 4.4) in PetroMod software by

limiting the international region and the latitude for the study area. Calculating heat flow inferred from the equation (McCullough et al, 1989):

$$Q_z = K\frac{d_t}{d_z} \qquad (4.1)$$

Where Q_z is the heat flow vertical component in (MW/m), K is the thermal conductivity in (W/m.^{o}c), and d_t/d_z is the geothermal ingredient.

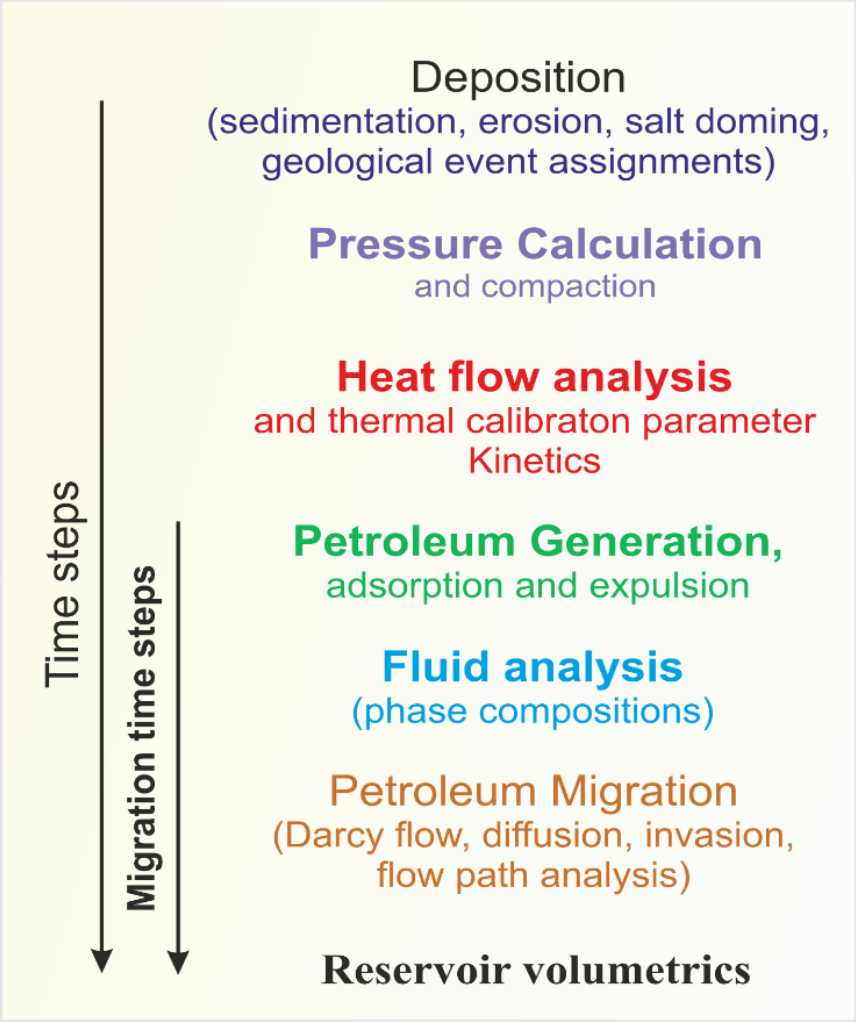

Fig. 4.3: typical basin modeling essential geological processes, after (Hantschel & Kauerauf, 2009).

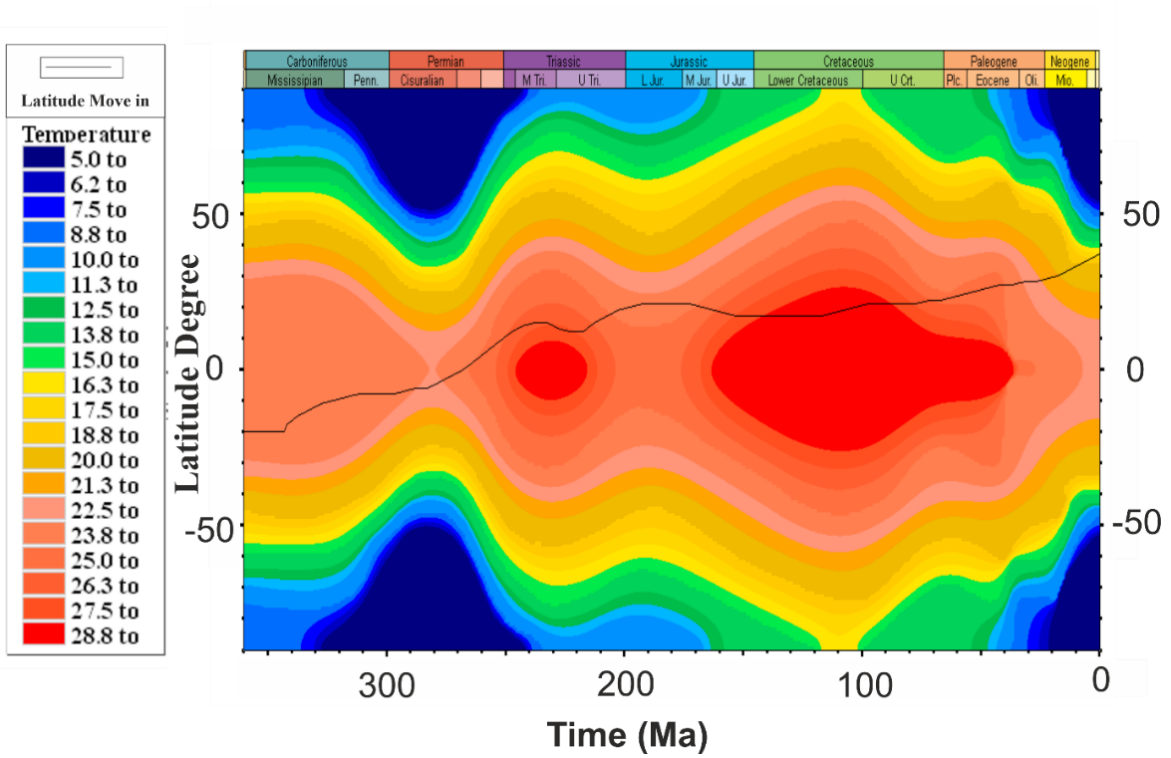

Fig. 4.4: the surface water interface temperature (SWIT) according to Wygrala, 1989 (Poelchau et al., 1997) from the PetroMod software.

While, thermal conductivity is calculated from another equation (Selley, 1998):

$$K = K_m^{(1-\emptyset)} * K_w^{\emptyset} \qquad (4.2)$$

Where k is the bulk thermal conductivity, K_m is rock conductivity in constant values (1.45 for shale, 2.56 for limestone, 2.64 for sandstone, 3.75 for dolomite, and 5.4 for anhydrite), K_w is the water conductivity (0.59 W/m.^{o}c), and ø is the porosity that measured from well logs data.

The age of heat flow evaluations is accomplished through (i) porosity values obtained from the Neutron, density, and sonic logs. (ii) rock conductivity K_m values are gathered from the well section and column stratigraphic an assignment of lithotype units. (iii) the geothermal ingredient inferred from the surface temperature, maximum recorded temperature T_{max}, and borehole temperature from well registers. Usually, thermal maturity indicess (%VR_0, T_{max} pyrolysis, …. etc.) are employed to gain the paleo heat flow (Hakimi et al, 2010). The vitrinite reflectance modeling that is obtained from the T_{max} value is used here to estimate

the heat flow in the study area by comparing the measured and modelled $\%VR_0$ (Haddad & Amin, 2007; Hakimi et al, 2010).

The results of the heat flow profile show the cooling state that continued during the Upper Jurassic to the Early Cretaceous with a value of about 40-50 Mw/MB11. After that, a significant increase in heat flow value was nearly about 60 Mw/MB11 noticed during the middle Cretaceous period which is back to the stable ranges (Fig. 4.5) from the top of the middle Cretaceous to the mid-Miocene. At the beginning of the Pliocene period, another increase in the heat flow value reaches 70 Mw/MB11 which is considered a reflectance of the convergence of Arabian-Iranian plates and the collision event which is formed the Zagros fold and thrust basin and the maximum heat flow recorded value was considered to the Zagros foreland region (Pitman et al., 2004; Hakimi et al., 2018). Nowadays, the constant value of heat flow for the Zagros foreland basin was recorded at about 50 Mw/MB11 and was calculated from the vitrinite reflectance measurements (Sweeney & Burnham, 1990).

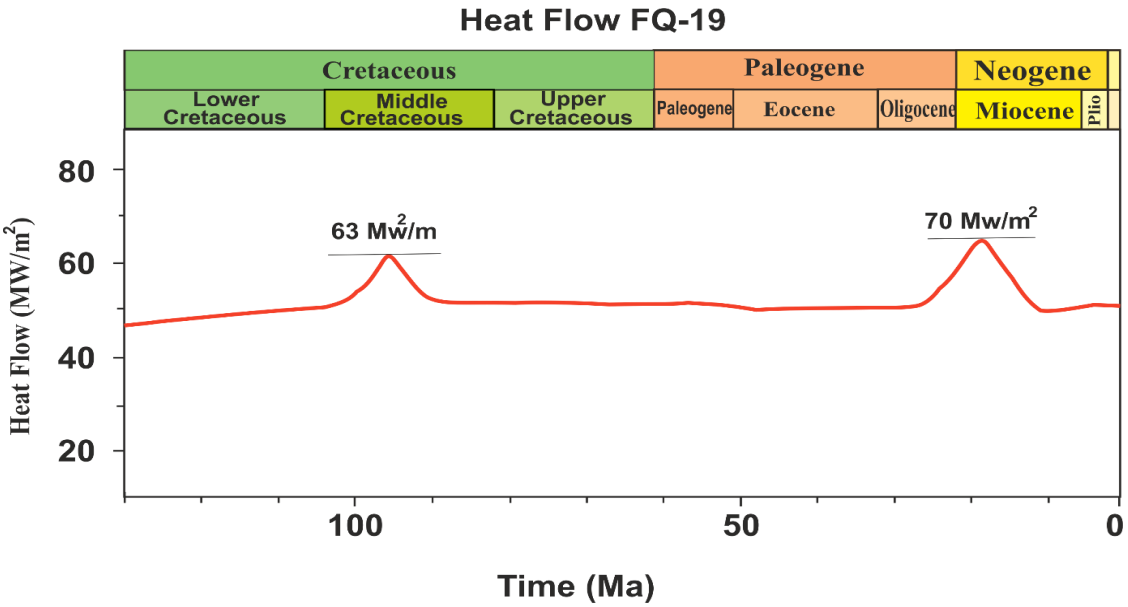

Fig. 4.5: heat flow result of the studied well FQ-19 in the Fauqi oilfield.

An evaluation of the petroleum system gained after simulating Petromod software representing porosity, thermal conductivity, pore pressure, burial history, and vitrinite reflectance of each formation.

Transport processes are including the sum of pressure and compaction, migration, and diffusion that follow basic equations in calculations. Two essential parameters are represented in the core issue, the state and the flow. The flow parameter effect influences all neighboring sites from any point. Grand computing potent is necessary for transport processes modeling.

The relation between these variable parameters is shown in (Table 4.1). In the example, the variables of thermal conductivity are (temperature and heat flow). Where temperature represents the state variable and heat flow is the relative variable. Changing in temperature (grad T) leads to heat flow, and the heat flow effects are reflected in temperature decreasing. The response to the temperature depends on the medium heat capacity, while the heat flow is affected by the thermal conductivity (Table 4.1) (Hantschel & Kauerauf, 2009).

Table 4.1: Fundamental state and flow variables with laws of transport processes, after (Hantschel & Kauerauf, 2009).

State variable	**Flow variable**	**Flow equation**	**description**
Temperature T	Heat flow q	$q = -\lambda * \text{grad } T$ (4.3)	λ= thermal conductivity
Pressure P	Water flow V_w	$V_w = -\frac{K}{V} * \text{grad}(P - Pgz)$ (4.4)	K= permeability, V= viscosity
Fluid potential u_p	Fluid flow V_p	$V_p = -\frac{K K_{rp}}{V_p} * \text{grad } u_p$ (4.5)	K K_{rp}= relative permeability V_p= viscosity
Concentration C	Diffusion flux J	$J = -D \text{ grad } C$ (4.6)	D= diffusion coefficient

Generally, mass-energy can be employed to designate boundary events in addition to the boundary conditions and conduct the result in the calculation of state and flow variables at the scale of geologic time. Boundary conditions values estimation is required to make basin units separated and reconstruct the whole matrix. The elements of the matrix reflect the state variable change affected by the flow variable variant between two adjacent units. The matrix reflection showed as the parameter's vector after simulation, just like the temperature contents in each unit (Hantschel & Kauerauf, 2009).

In order to put the circulation of petroleum from the beginning of its generation with the circumstances related to source rocks forming, the periods and the way of hydrocarbons migration, reaching the traps and all the events synchronized (Magoon & Dow, 1994) gathered all these concepts in guidance of "Petroleum System".

This petroleum system was figured and classified in tri-basics function by (Demaison & Huizinga, 1991): forming, migration, and trapping. The studying in this term could detect the oil in place (OIP) and/ or the emigrant oils.

4.3.2. Timing and erosion amount

The value of $\%R_o$ reflectance which is 1D modeling versus depth in the modeling of studied wells was about 0.250% R_o (Fig. 4.). For all the sedimentation periods the value is the same nearly the Cenozoic period reflecting the hard surface condition after comparison to this value with the recent surface value of vitrinite reflectance, and the amount of eroded section was estimated to be about 1.5km initiative in the Late Tertiary to recent days (Pitman et al., 2004).

- **Erosion**

The eroded thickness as input parameter for PetroMod software will be determined through:

$$\text{eroded}_{\text{thick}} = T_o * \frac{\text{age of erosion}}{\text{age of deposition}} \qquad (4.7)$$

Where $\text{eroded}_{\text{thick}}$ is the thickness of eroded layer, T_o is the original thickness of sediments.

- **Vitrinite reflectance (VR)**

This factor represents the measure in percentage unit to the reflectance of the incident light via the vitrinite particles' surface and calculated in ($\%R_o$), and it is considered as an optical parameter indicating the quantity of the organic matter in oils is expressed as (VR or R_o) (Sweeney & Burnham, 1990). Where the origin of this material is coming from the mature substance that formed from the lignin and plant cell cellulose (Smith & Cook, ,1980). Using of vitrinite in oil evaluation

depends on the chemical properties of the kerogen and vitrinite in the same line. The integral relation between hydrocarbon maturity and the percentage reflectance of vitrinite was defined in a Table by Sweeney and Burnham (Peters & Cassa, 1994) (Table 4.2) and (Fig. 4.6).

Table 4.2: the easy vitrinite reflectance after Sweeney and Burnham (Peters & Cassa, 1994).

No.	% R_o Vitrinite	Oil Maturity
4.	0.25 – 0.55	Immature
5.	0.55 – 0.7	Early oil
6.	0.7 – 1.00	Main oil
7.	1.00 – 1.30	Late oil
8.	1.30 – 2.00	Wet gas
9.	2.00 – 4.00	Dry gas
10.	> 4.00	Over mature

According to the study results, the reflectance of maturity throughout the vitrinite reflectance, the maturity state reflects an immature for all the formations in the studied well above the Mishrif Formation and Rumaila Formation which show an early maturity of the oil window (Figs. 4.6 & 4.7).

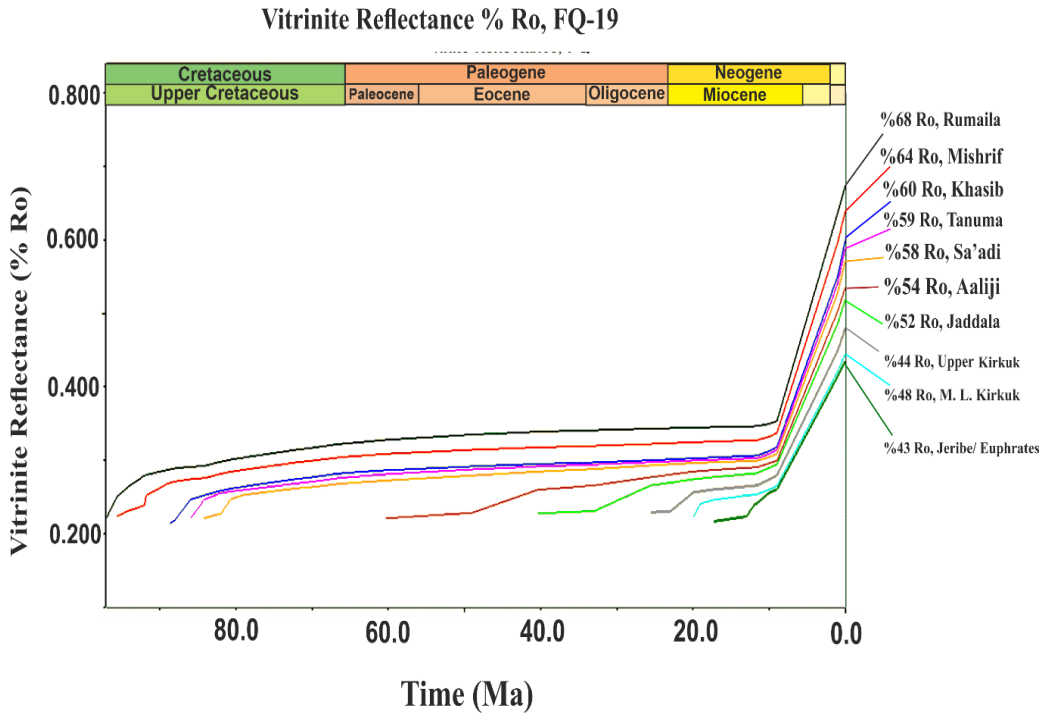

Fig. 4.6: vitrinite reflectance (% Ro) of the studied well.

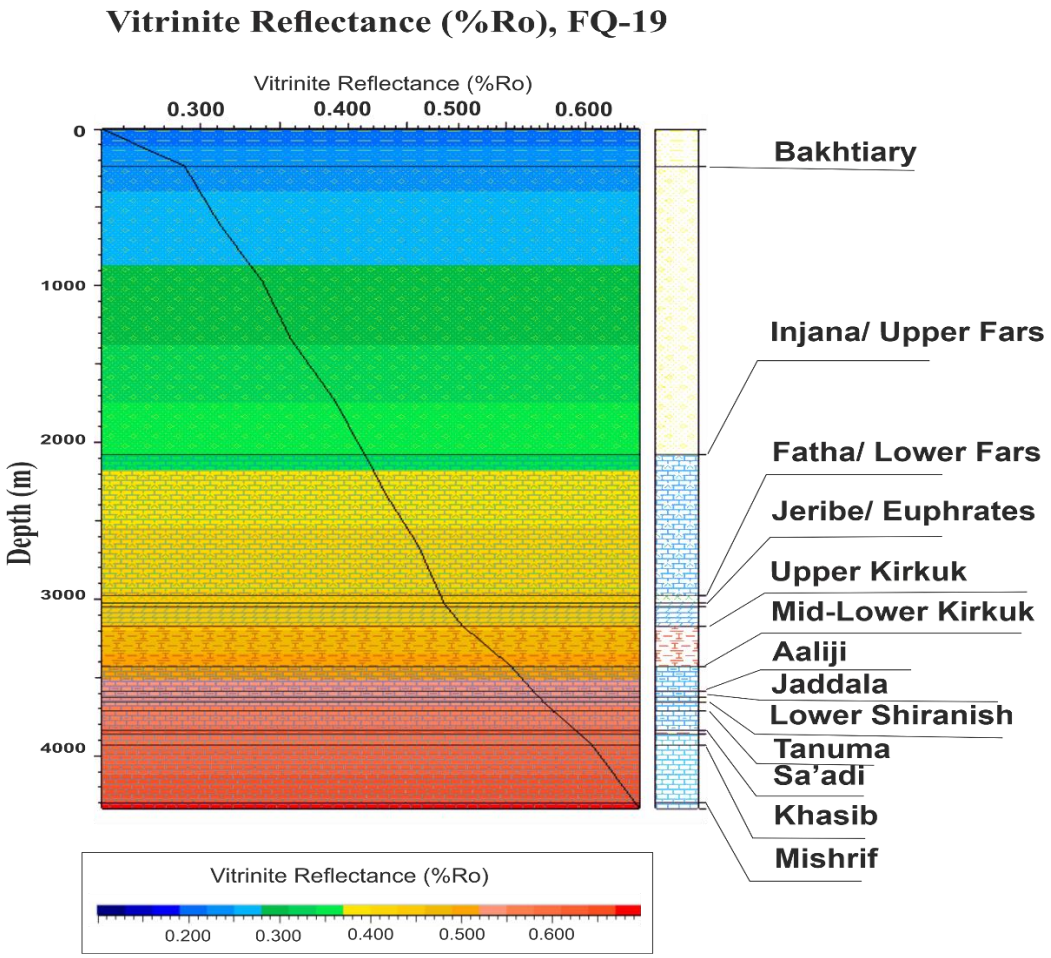

Fig. 4.7: Distribution of Vitrinite reflectance plotting with depth in studied well.

4.3.3. Petroleum Generation kinetics

A prediction of main parameters of vitrinite reflectance, organic matter concentration, and the fission rate of apatite is possible by applying the Arrhenius equation and some conversions. Arrhenius reaction is temperature dependence reactions formula (Connors, 1990):

$$K = Ae^{\frac{-E_a}{RT}} \qquad (4.8)$$

Where; k is the rate constant, A is the pre-exponential factor, Ea stands for activation energy in the same unit of R*T, R is the gas universal constant, and T is the absolute temperature in Kelvin.

These forecasting reactions are thermally sensitive, so they can be used in thermal calibration the uncertain input data like paleo heat flow.

Depending on heat flow activity and the type of migration modelling the number of kinetics ranges from 1000 to 50000 and even more in some cases. Time loops of geologic events, generation time, and migration time as programmed steps are automatically managed through the simulation process.

According to the Rock-Eval chart, the petroleum source type of the Zagros fold belt basin is type II Kerogen. Type II or sapropelic kerogen is characterized by a high H/C atomic ratio 1.2-1.5, high hydrogen indices in the Rock-Eval scale (300-600 mg HC/g TOC), and low levels of O/C atomic ratio. Liptinite is dominated in this kerogen type relative to Type III, and IV, but less than type I. Relatively to other kerogen types, this type tends to generate oil at low levels of maturity may cause by the high sulfur contents (Peters & Cassa, 1994). Usually, the mixing of marine zooplankton, phytoplankton, and bacterial remains is the main origin of type II kerogen. This type is found as originating kerogen in many source rocks for the Jurassic, Cretaceous, and Miocene periods. The transitional construction between types (II and III) that are classified as type II/III reflects a paralic environment that represents an interfingered origin of terrigenous and marine organic matter. The immature II/III type has (1- 1.2) H/C atomic ratio and HI value of (200–300 mg HC/g TOC) (Fig. 4.8) (Peters, 1986).

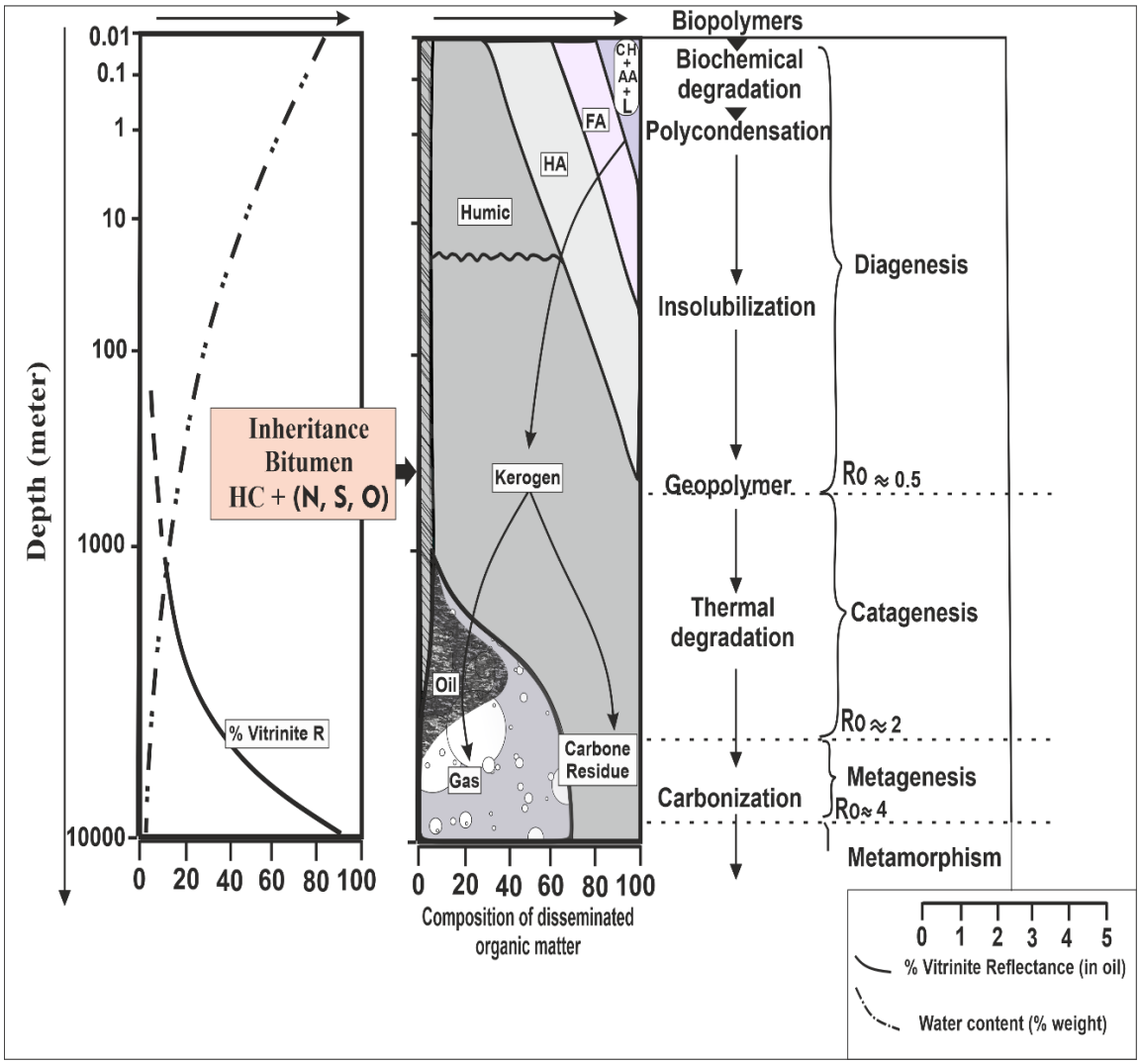

Fig. 4.8: typical (Rock-Eval) scheme of organic matter determination, inline from early deposited sediment until metamorphic zone. CH: is carbohydrates, AA: stands for amino acids, L: lipids, FA: fulvic acids, HA: humic acids, HC: hydrocarbons, N, S, 0: resin compounds (non-hydrocarbons), modified after (Selley et al., 1985).

4.4. Oil generation, migration, and accumulation

4.4.1. Generation

The Zagros orogeny due to the Arabian-Eurasian plates convergence and continent-continent collision during the Late-Eocene period, which formed a series of fold trends northwest-southeast and thrusting faults, normal and reverse. The Arabian Plate was subducted beneath the Iranian plate affected by the collision and the convergence was recently continuous (Pitman et al., 2004). The NE of the Arabian plate certifies a wide range of source rocks that are diacritic by good properties to be the main source for Cretaceous and Tertiary reservoirs. All

these sources showed to be deposited in a marine environment and have type IIS kerogen (Beydoun., 1988).

The Mesozoic stratigraphy shows many oils-prone rock layers at the northern east Zagros and the indices tend to the Shoal and intrashelf deposition environment which has an unstable range of oxic conditions of these sources registered to a time interval of middle Jurassic to middle Cretaceous that testified a continuous deposition of organic matter within alternating strata consist of shale, shaly limestone and Limestone (Murris, 1980b). The bulk of the Cretaceous and Tertiary reservoirs' oil is According to the evidence of the common occurrence of these sources' prints in the produced oil with a trace source of the lower Cretaceous (Sulay & Yamama) formations (Murris, 1980a; Al-Ameri & Zumberge, 2012; Al-Khafaji et al., 2019). Inside Iraq territory, the period of this interval is represented in the formations of, and Sargelu (Al-Ameri et al., 2009). The main source formations (Sulay and Yamama) are capped by the upper Jurassic evaporitic Gotnia formation. The main cause of sourced oil accumulation in the middle Jurassic formation belongs to the evaporitic cap of upper Jurassic (Hith & Gotnia) formations that prevented the hydrocarbons' escape. The anoxic condition of the early Cretaceous formations (Sulay and Yamama) and high organic matter contents substantiate the opinion of being sourced to the middle Cretaceous and Tertiary reservoirs (Al-Khafaji et al., 2019). These source oil formations regarding the available data of maturity may have reached the oil window at the beginning of Tertiary time prior to the Zagros orogeny events and fed out the mid-Cretaceous and Tertiary reservoirs with hydrocarbons post the Zagros orogeny (Murris, 1980b). All the shreds of evidence from biomarker analyses of Cretaceous and tertiary reservoirs suggested the marine algal origin of the oil source rocks (Beydoun., 1988).

4.4.2. Migration

The oils occur in the middle Cretaceous and Tertiary reservoirs and the chemical composition supported the argument of the Jurassic source, but the Gotnia formation seal prevented the vertical migration of oil from this source assured the post-Zagros orogeny oil migration theory supposes that migration happened due to the folding and stratum shortening which is influenced by a series of fractures and faults that affected on Gotnia Formation and permit hydrocarbons to be expelled toward the Middle Cretaceous Mishrif Formation (Fig. 4.17) (Murris, 1980a).

The migration continued horizontally and vertically via the tied pores and the fractures. The proposed vertical migration of mid-up Jurassic and upper Jurassic-lower Cretaceous oils reached and accumulated in the middle Cretaceous to Tertiary reservoirs capped by the regional evaporitic seal of Fatha (Fatha) Formation. Factually, the evaporitic layer of the Fatha Formation is confined in the lowest part of it (Beydoun., 1988) (Fig. 4.9).

4.4.3. Accumulation

As remembered previously in this chapter, the Jurassic oils migrated vertically through the fouls and fractures to the Cretaceous Mishrif Formation and the Asmari reservoir oil feeds throughout the fractures and tight pores. This movement needs a large surface area of fractures to assist the oil migration. The main cause of the fluid vertical migration is referred to as over-pressure by the burial column of the overlying strata (Pitman et al., 2004). The karsting form which is diffused in the carbonate formations supports the porosity and permeability available for fluid accumulation. The fluids gather and continuously accumulate in these permeable layers which are locally capped with non-porous and condensed carbonates. Several reservoir units in the same formation reflect the different paths of the emigrants' oil (Murris, 1980a).

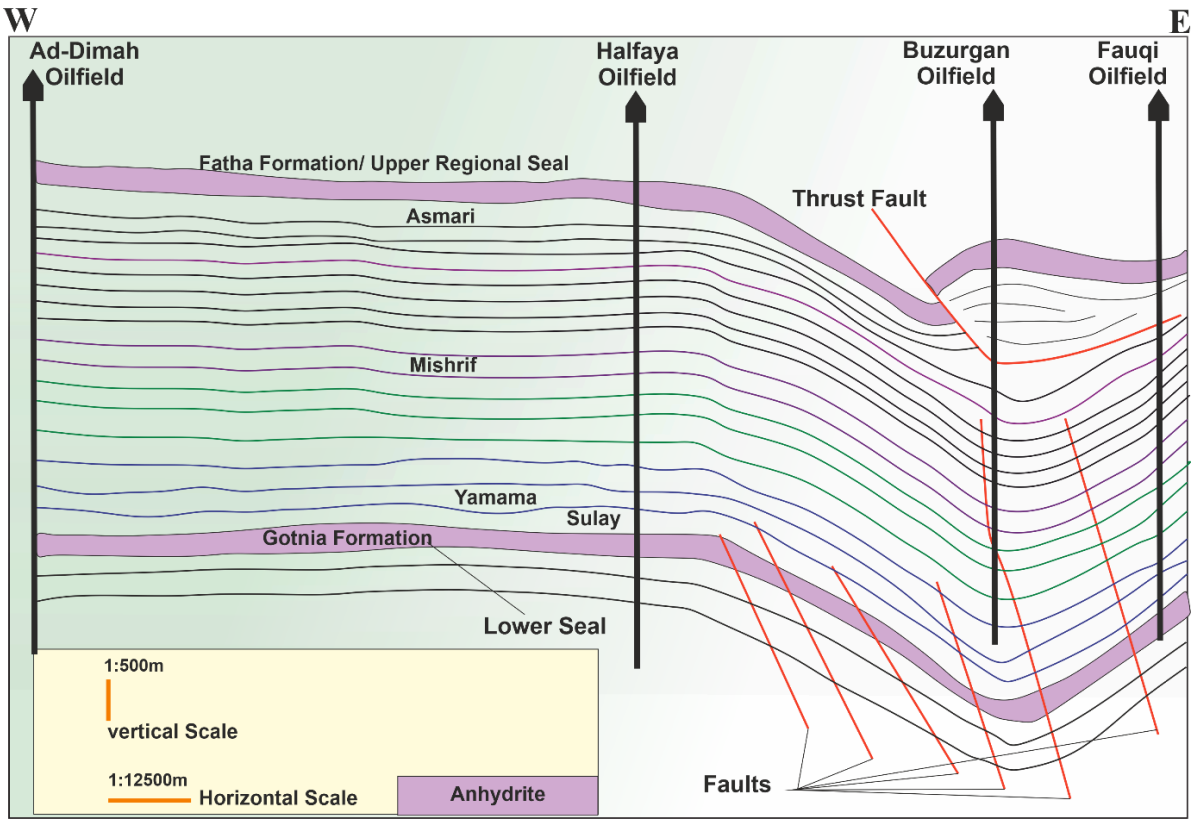

Fig. 4.9: schematic W-E cross section of (Mesopotamian-Zagros) trend, shows the main sources and the reservoirs pointed on it the post orogeny faults, after (Al-Khafaji et al., 2022).

4.5. Model Analysis

Modeling of one dimension was performed on the Fauqi oilfield depending on the PetroMod 1D option (version 2012.2). This software, as mentioned before needs a huge range of data inputs to be able to construct the desired basin modeling and these data:

4.5.1. Burial and thermal history

- Burial history

Building a model of burial history required several essential data representing lithology type and thickness of the individual layer, deposition and eroded period and thickness of erosion, paleo water depth (PWD), surface water interface temperature (SWIT), and heat flow (HF). The stratigraphic column of the studied area seemed to have gaps regarding the deposition pausing or due to erosion process in the same manner of (Guidish et al, 1985). The burial plot shows the historical geologic sequences that fit the well recordings via cores or well logs,

with five discontinuities in the region of the limited period studied in the Zagros fold belt basin. Also, a rapid subsidence period due to the collision of the Arabian Plate with the Iranian plate during the Zagros orogeny event. The rapid deposition of the Paleogene period was shown in Fig. 4.1).

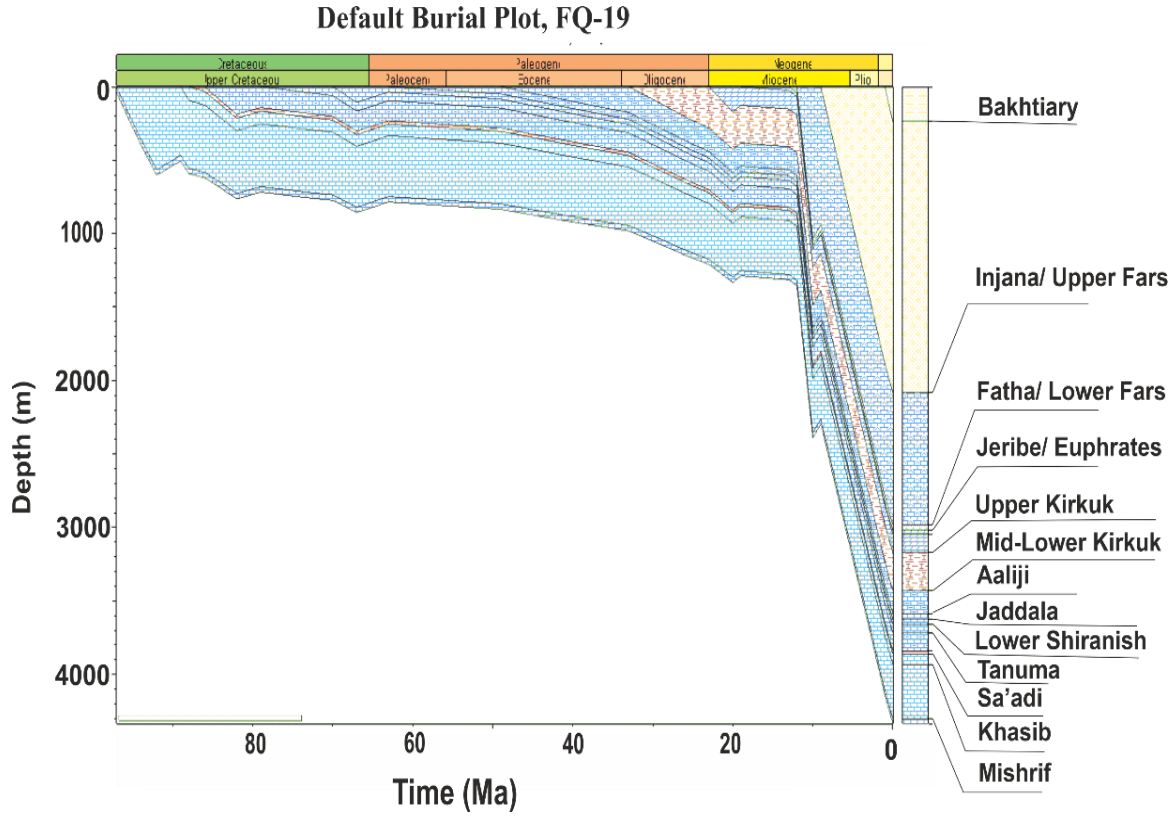

Fig. 4.10: historic burial plot of Fauqi oilfield through well FQ-19.

- ***Geothermal history***

Thermal and burial histories associated with thermal maturity together have significant importance to construct basin modeling and conclude the hydrocarbon potential for the reservoir, and the simulated results are ideal for estimating the oil migration period (Allen, 2005). The result of studied well showed that the period of Early to Mid-Paleogene was the suitable time for dominance of maximum temperature synchronized with deep burial events. A period of erosion took place at the end of the middle to upper Neogene (Pliocene) period. In conclusion, the maturity time of the source rock reached the oil window in the Cenozoic after the Synorogenic events which prepared the appropriate reservoir conditions to contain the emigrant oil (Allen, 2005).

4.5.2. Thermal Conductivity

Geothermal conductivity describes the temperature distribution identified in the rock formation (Allen, 2005). The conductivity of the temperature of the soils and rocks changes with depth according to the porosity reducing with burial increasing (Fig. 4.11).

This parameter is significant to estimate the type of rock content, where some components have high thermal conductivity like halite, quartz, and anhydrite so that the increase of thermal conductivity reflects the high presence of these minerals. In the same, the study showed the lower part of the Fatha Formation has high thermal conductivity with a low geothermal gradient in evidence of evaporite presence, while the Khasib formation has a high geothermal gradient and low thermal conductivity (Allen, 2005).

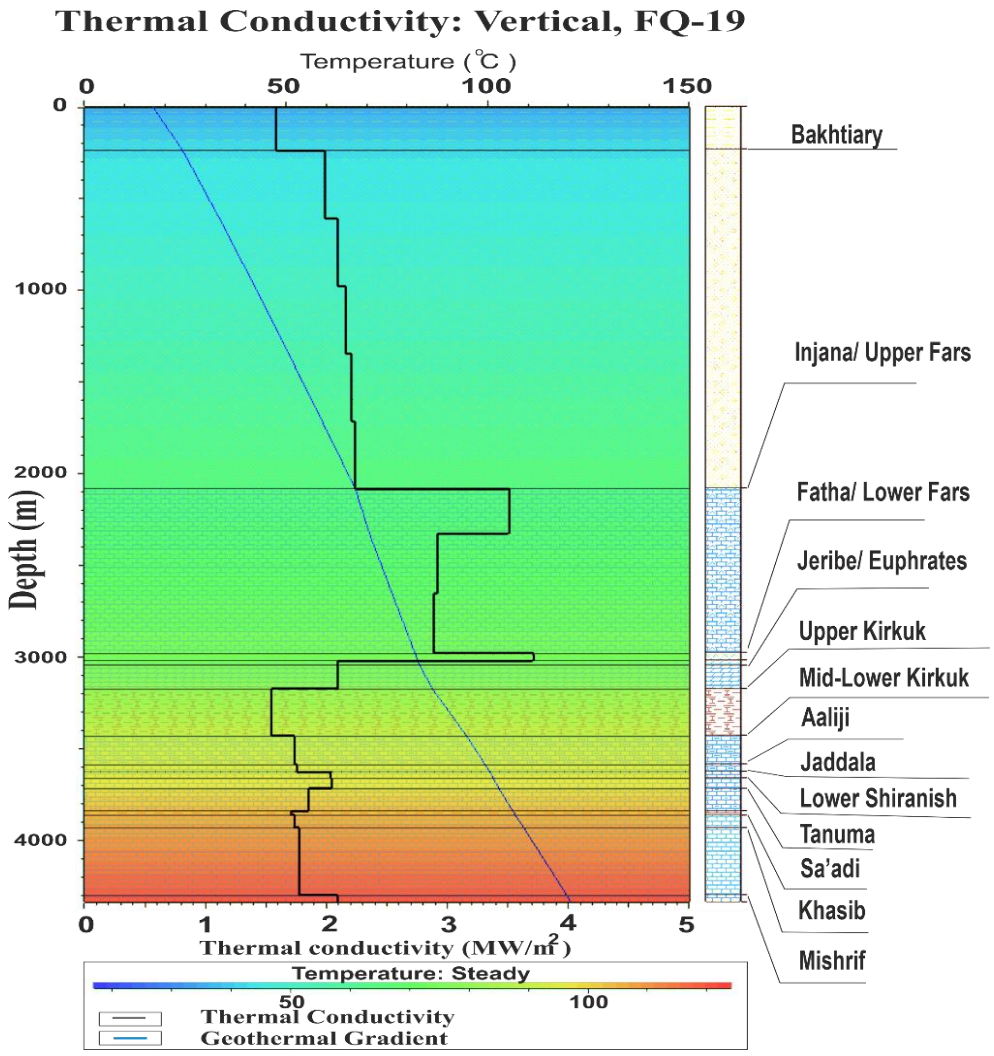

Fig. 4.11: thermal conductivity and geothermal gradient for studied well FQ-19.

4.5.3. Porosity

The porosity parameter calculates, as the best way, from the well logs data, which are Neutron, density, and sonic are usually employed for this mission. Plotting of the obtained porosity values with depth gives the compaction ratio, and the relation of porosity and depth formula (Allen, 2005):

$$\emptyset_p = \emptyset_o e^{-cZ} \qquad (4.9)$$

Where $ø_p$ is porosity at (Z) depth, $ø_o$ is the initial porosity that takes standard values depending on the lithotype (0.42 for Dolomite, 0.49 for Sandstone, 0.52 for Limestone, and 0.55 for shale), and c is stand for the coefficients of porosity/depth slope which are (0.0003 for Sandstone, 0.0004 for Dolomite, 0.0005 for Shale, and 0.0006 for Limestone).

- **Porosity evaluation**

The porosity in the hydrocarbons field aims to the pores that are available to preserve the oils and/or gas in it, and the exemplary porosity values of the various types of lithologies estimated to be (3-38% and 10-38%) for oil and gas sandstone reservoirs respectively, where this value has been variant in the carbonate reservoir and may exceed these values to reach nearly 47% in some cases (AlRuwaili, 2005). The enhancement of porosity in the carbonate's reservoir comes from the joints, fractures, and dissolution diagenesis processes as secondary porosity. So, the study shows that the maximum porosity is in the carbonate formation such as in Mishrif or Khasib formation and the fewer values in the evaporites layers like the lower part of Fatha formation (AlRuwaili, 2005) (Fig. 4.12).

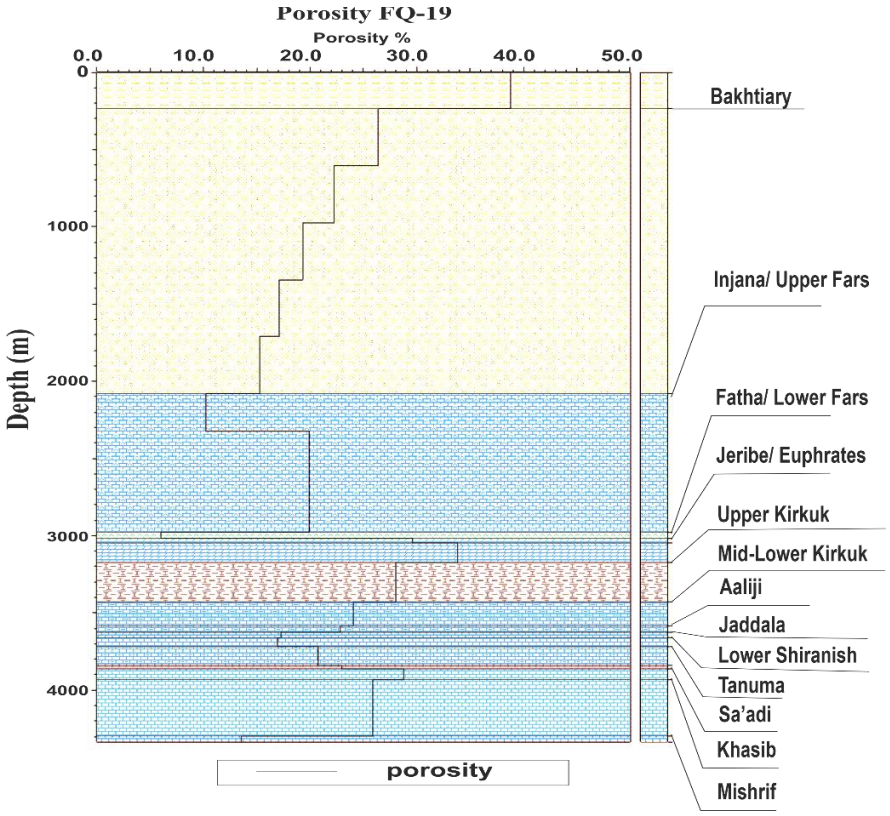

Fig. 4.12: porosity diagram after data simulation with PetroMod software.

- **Decompaction**

In order to reconstruct the original thickness on sediments T_o of the sedimentary filling grow up to the boundary of deposition pause from the cores or well logs

data (Handhal & Mahdi, 2016). In the procedure of evaluating the present porosity and thickness, using the following equation:

$$T_o = \left(\frac{1-\emptyset_p}{1-\emptyset_o}\right) * T_p \qquad (4.10)$$

Where the T_o is the initial thickness of sediment, $ø_p$ and $ø_o$ are present porosity and initial porosity respectively, and T_p is stand for the present thickness of sediment.

4.5.4. Pressure

Axiomatically, the pressure stands for the force affecting per unit area, and the unit used either in (kg/cMB11, Psi, or KPa). The pressure curve varies with change in lithology, whereas for sandstone the pressure curve is the same as the hydrostatic gradient, while the shale layer takes the pure shale curve. So, the pressure curve has increased values in the sealing layer more than in the porous layer (Ingram et al., 1997).

Overburden layers over the seal share in increasing the static pore pressure. In general, the value of pressure distribution in the formations is affected by several factors: (1) height of hydrocarbon column, (2) migration rate of fluids (hydrocarbons and water), (3) source rocks maturity, (4) vitrinite kinetics, (5) the capacity of the seal rocks, and (6) basin structure development of lithostratigraphic and affected diagenesis processes (Fig. 4.13) (Ingram et al., 1997). Pressure distribution in the study area clarified the huge variants in the pore pressure values with a significant increase during the Cretaceous period and overpressure record in the Paleogene period.

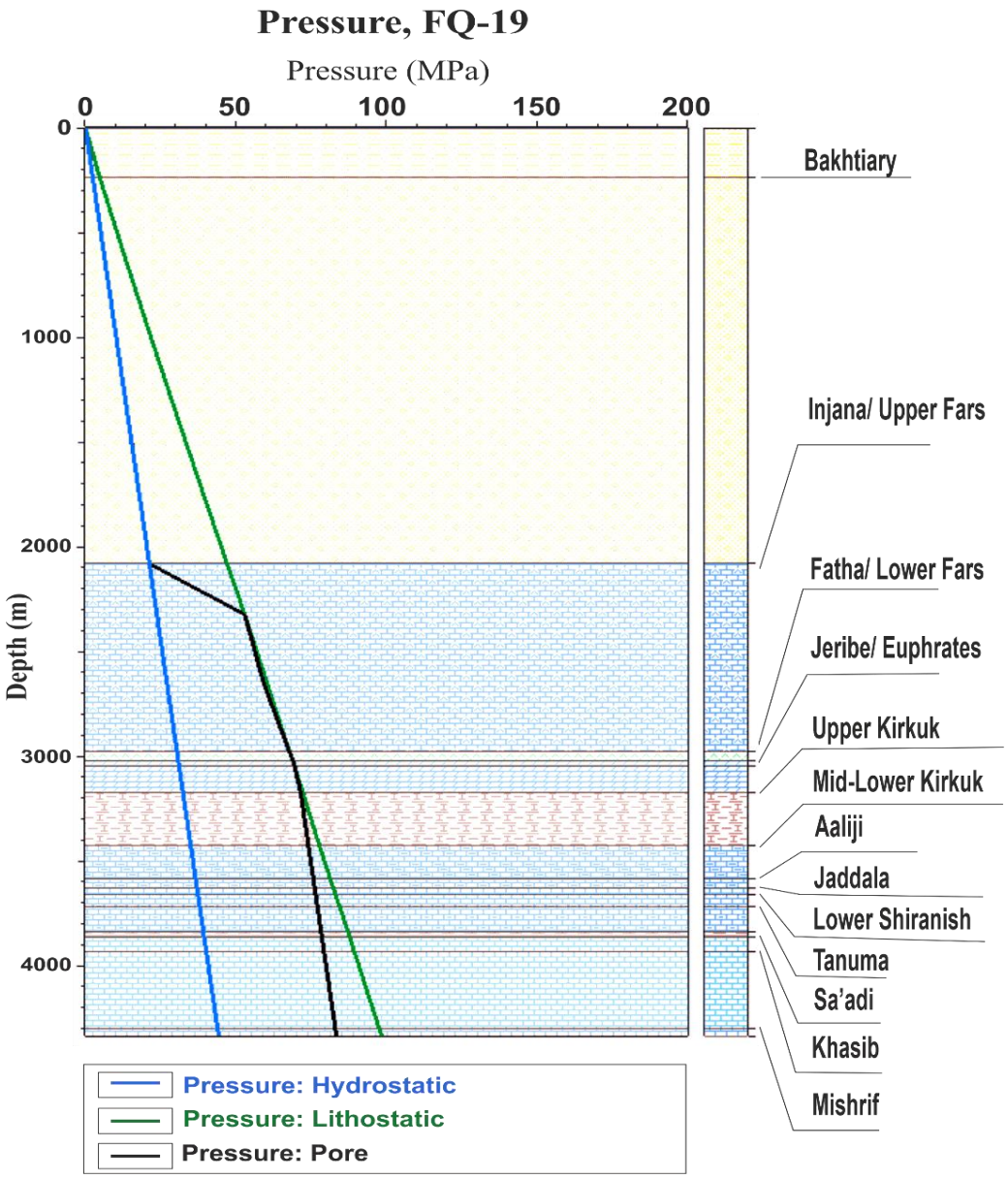

Fig. 4.13: pressure distribution showing the huge variants in pore pressure distribution.

The integral relation of pore pressure distribution and depth is clearly poor in reflection of the events evolving the basin forming and evolution as subsidence, uplift, faults, or erosion events (Fig. 4.14).

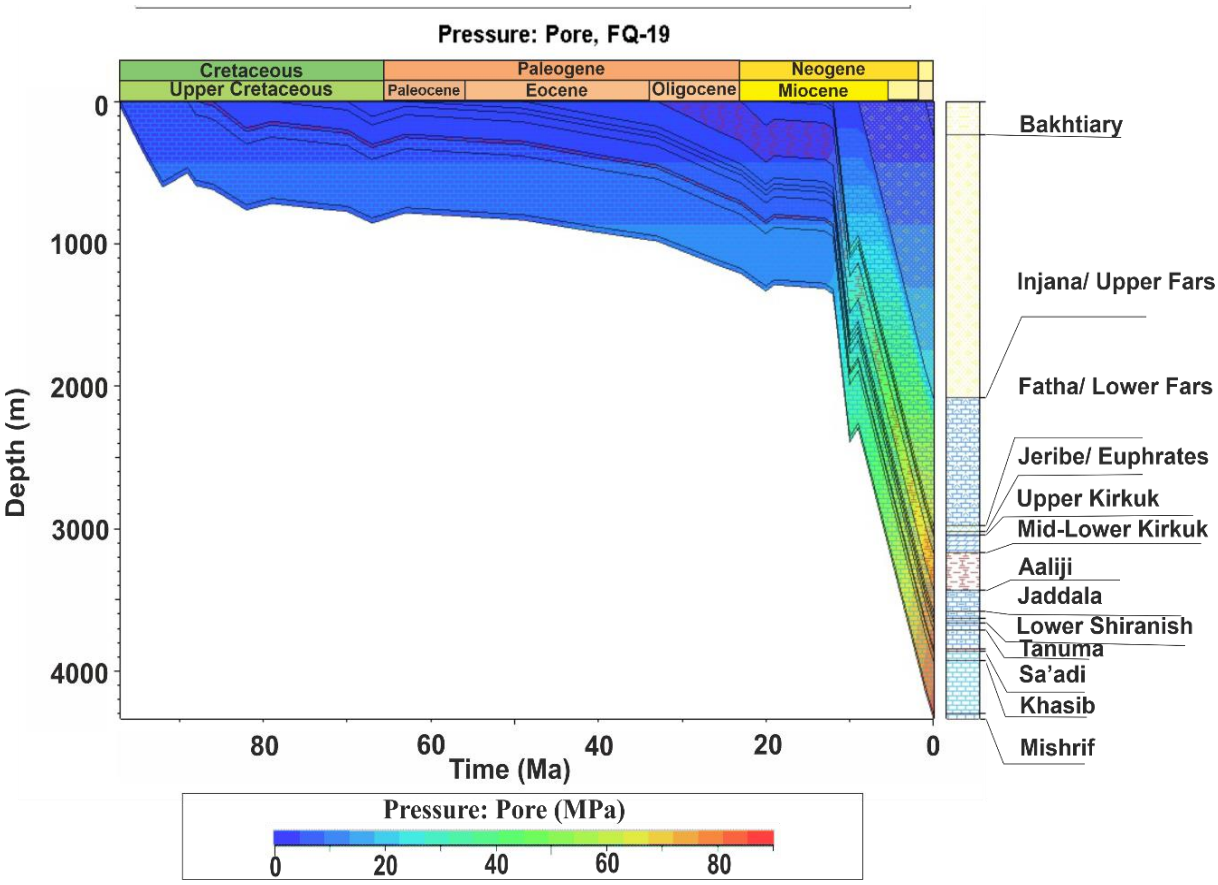

Fig. 4.14: the pore pressure distribution of studied well FQ-19.

4.5.5. Biodegradation risk assessment

One of the key risks in petroleum exploration is oil degradation. Generally, there is no sufficient data about this risk where, when or how it comes, but the studies aimed at the temperature as the main affected factor, and for that tend to assign a limit of temperatures as a critical point in a range of (70-80 °C) or even down to (65 ºC) where the bacterial activity on oil degradation increases with decreasing in the temperature despite the presence of oil reservoir with no degradation in (40 ºC) (Blanc & Connan, 1994).

On the other hand, biodegradation in the reservoir may happen also in the reservoir with a high burial depth and temperature exceeding 80 ºC depending on some factors that can be conclusive in the paleo thermal condition, the situation associated with reservoir forming, and the period if hydrocarbons been accumulated in the reservoir (Horstad et al, 1992).

The distinctive time series as (i from 1 to N) number, of thermal history and hydrocarbons accumulation rate that employed to evaluate the biodegradation diagram via the BDI equation (Pepper & Yu, 1993):

$$BDI = \sum_{i=1}^{N}[(T_i - T_C) * \Delta ti]/C \quad (4.11)$$

Where BDI stands for biodegradation indices, i=1 is the time of prefilling in the basin, i=N for the present day, T_i is the paleotemperature of the reservoir in ºC, T_C is the critical temperature related to the activity of bacteria, it is the time interval in a geologic sense, and C represents the scaling constant of basin dependent in MA, and in this study as the limited data was in the range of 1-100 Ma. The upper limit of the activity of biodegraded bacteria is respected at 60 ºC according to the nature of basin forming environment.

Generally, biodegradation is influenced by several factors in addition to the temperature which are pH, chemical components of oil, quality and quantity of organic matter, and the environment's bacterial distribution (Blanc & Connan, 1994).

The modeling of biodegradation risk assessment according to the burial plot shows the typical biodegradation at the shallower formations rather than in the parts of the deeper formations (Fig. 4.15).

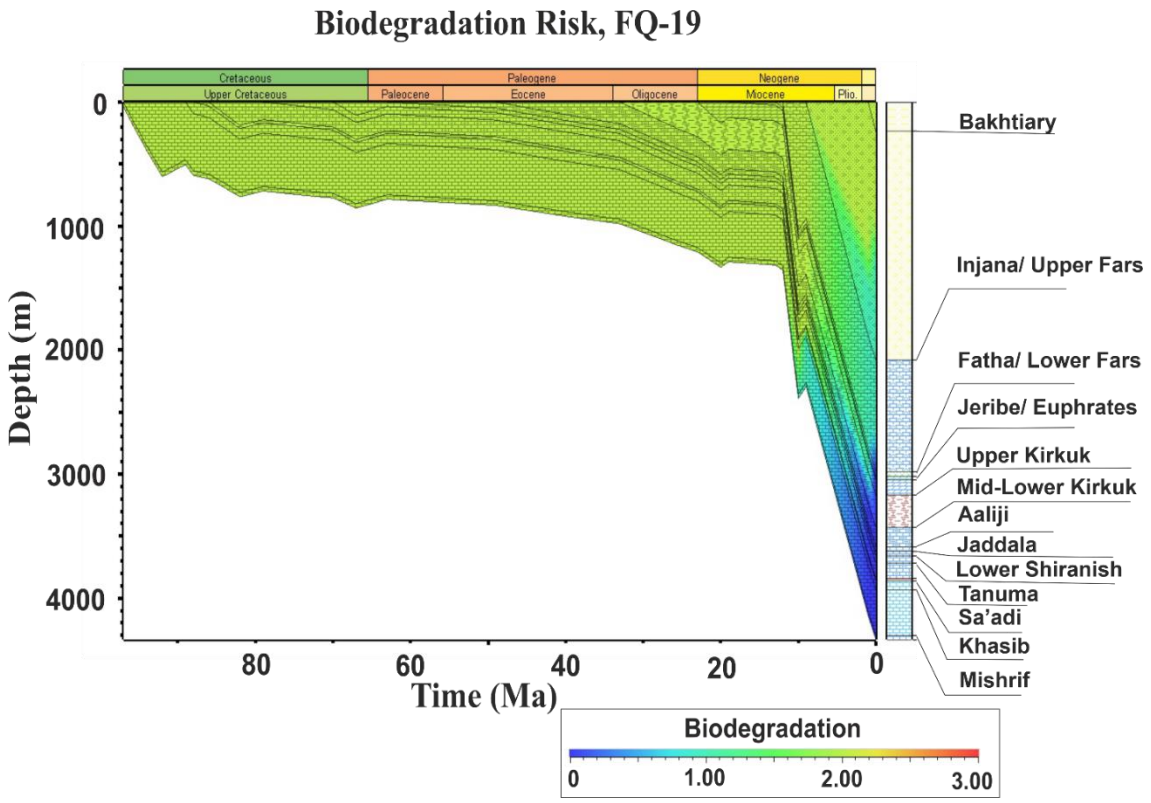

Fig. 4.15: assessment of biodegradation risk in the studied well for the Fauqi oilfield.

4.5.6. Transformation rate

The predicted kinetic parameters the controlling the transformation rate of the organic kerogens in the source rock or even in the reservoir that may reach the typical maturity degree (Beardsmore et al, 2001). In this paper of study, the model of kinetic that was used to investigate was Abu-Ali(1999) _TII-(Qusaiba) for the source rocks of Aaliji and the middle Mishrif reservoir rocks modeling that showed the variation of individual formation with the same critical point of time in about the last million years during the Pleistocene period (Fig. 4.16; Fig. 4.17).

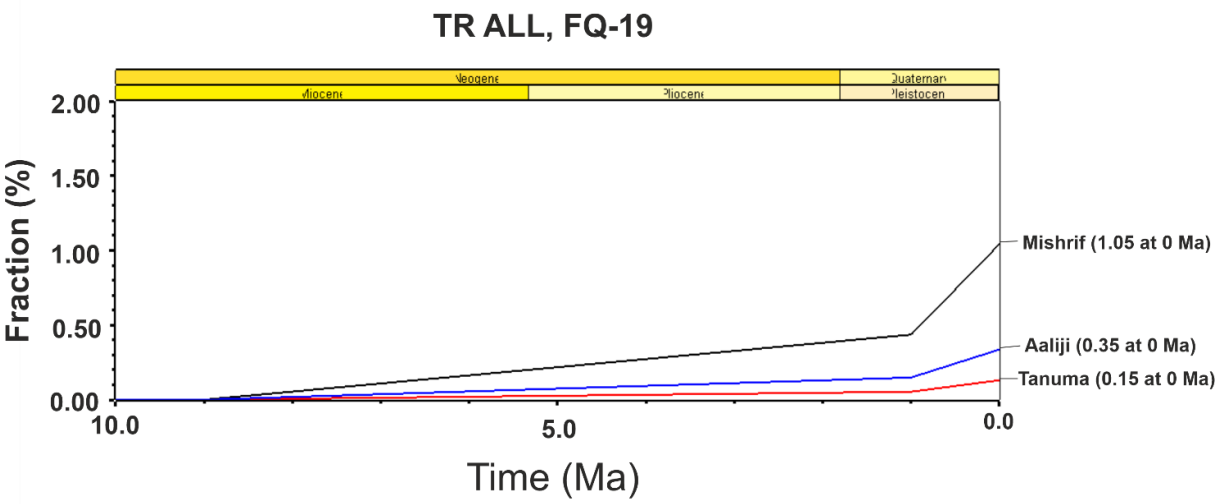

Fig. 4.16: predicted the fractional transformation ratio in the studied well.

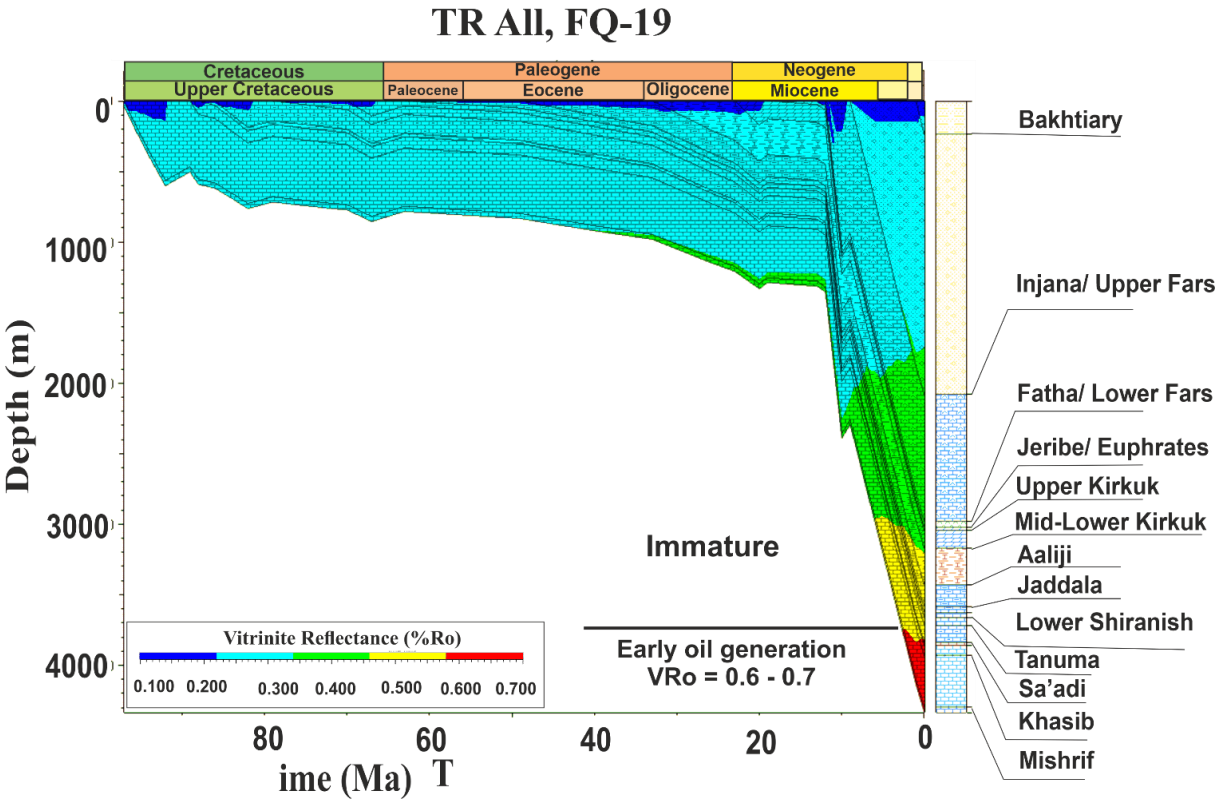

Fig. 4.17: transformation rate (TR) aiming at the maturity levels according to the vertical depth temperature distribution.

4.6. Discussion

The results of the Fauqi oilfield historical analysis showed that the slowing in subsidence continued through the Cretaceous period with distinctive uplift during the Miocene. Stratigraphic marks lend to the unity of depositions and no huge differences as evidence to belong to the same basin deposit and the structural nature was affected by tectonic events, especially during the Miocene. Thermal

conductivity has varied in relation as seen in the Khasib formation which shows a high geothermal gradient despite that the low thermal conductivity is obvious and the opposite state is seen in the Fatha formation. The range of heat flow was about 40-50 mW/MB11 which reflects maturity. Abrupt increasing decreases in the middle Cretaceous in 63 mW/MB11, and then back to the steady state the heat flow continued during the middle-upper Cretaceous to Tertiary period with a noticeable increase to 70 mW/MB11 at the beginning of the Paleogene affected by the convergence and collision of Arabian and Eurasian plates.

The porosity results obviously indicated the lower values in the evaporitic formations like the lower part of the Fatha formation and the highest porosity values in the carbonate formations that came from the secondary porosity by diagenesis processes as shown in the Khasib and Mishrif formations. The study of pressure prints lends to complicated distribution in pore pressure with overpressure marks in the Neogene period. There was last maturity evidence affected by the increasing of sediments burial vertically in the mid-Paleogene. The maturity of organic matter in the early stage can be seen in the upper Cretaceous of the organic contents in Mishrif formation. The biodegradation effects showed an ideal state by increasing bacterial biodegradation in shallow formations with the possibility of happening in the deeper formation.

Chapter Five

Chapter Five

Conclusions and Recommendations

5.1. Conclusions

- The studied area is a complicated structural region limited to the southern part of the Zagros Belt Basin in Maysan Governorate, which includes three promising oilfields: Fauqi, Abu Ghirab, and Buzurgan. Fauqi oilfield is the chosen part of the Zagros fold Belt Basin to be the area of study. The main reservoir is the Mishrif Formation
- The investigation of Shale Volume in the Mishrif Formation showed dispersed shale in the formation divided it into three rock units consisting of seven reservoir units which are MA, MB11, MB12, MB21, MB22, MC1, and MC2. The low content was in the MB21 unit and noticed the increase of the Shale Volume upward in the MA unit and downward in the MC2 unit. The overall shale content in the formation was about 20% on average.
- The primary porosity of the formation ranged from low to fair porosity, but the total porosity was good regarding the secondary porosity which is dominant in the southern part of the field. The main cause of the secondary porosity was the dissolution of rudist as diagenesis processes effect. High effective porosity was recorded in the MB21 unit. The permeability calculations consider three studied wells because of data missing from the last two wells. The best proportional register of the permeability and porosity was in the MB21 unit. Other units had no clear relation between porosity and permeability.
- The CPI plot shows the water saturation in the reservoir units. The high reflectance of water saturation is shown in the lower MC2 unit which is considered a water-bearing layer in most wells. The upper layer MB11 either shows a high-water saturation.
- The results of the six crude oils analysis were used in build some relationships to investigate the paleoenvironments at the deposition time of source rocks and estimate the paleo thermal maturity, and the age of the source rocks. The results showed reduced conditions of the carbonate marine conditions environment. Thermal maturity is in the early stage, and the age was typical of the Upper Jurassic-Lower Cretaceous source rock time deposition.

- 1D basin modeling is accomplished by PetroMod software version 12.2 to get the best understanding of the petroleum system in the studied area. The modeling perspective shows the continuous subduction state along the Cretaceous time with significant uplift during the Miocene. Thermal conductivity and geothermal gradient have variant relations. The heat flow was still steady from the Middle Cretaceous to the upper Tertiary when a rapid increase was noticed affected by the Zagros orogeny. The pressure value increased in the Mid-Paleogene period due to the huge amount of sediments deposited that shared in maturity increasing. Biodegradation was in the shallower formations due to the bacterial effect. The seismic section shows a system of folds that are complex near the studied area within the faults system. The collision of Arabian-Iranian plates caused many folds and faults that formed good traps of fluids. Two regional seals controlled on hydrocarbon reservation, the upper seal of Fatha Formation and the lower seal of Gotnia Formation. The oil window began in the Late Miocene and the peak of generation was in the Holocene. The oil migration happened from the Late Cretaceous and continued to the present day through the faults and accumulated in the preformed traps and reservoirs.

5.2. Recommendations

- Dig more wells in the north part to get effort information about this part and re-record logs from the open wells.
- Re-logging the wells with the misguiding data.
- Carefully utilize the acidizing method to de-cementation and dissolve the cemented material in the north dome to give stimulation to the oil well

References:

- Abdulaziz, A. M., Dahab, A. S. A., & Najmuddin, M. Y. (2017). Well Log Petrophysics of the Cretaceous Pay Zones in Zubair Field, Basrah, South Iraq. Open Journal of Geology, 7(10), 1552-1568.
- Al-Ameri, T. K., & Zumberge, J. (2012). Middle and upper jurassic hydrocarbon potential of the zagross fold Belt, North Iraq. Marine and Petroleum Geology, 36(1), 13-34.
- Al-Ameri, T. K., Al-Khafaji, A. J., & Zumberge, J. (2009). Petroleum system analysis of the Mishrif reservoir in the Ratawi, Zubair, North and South Rumaila oil fields, southern Iraq. GeoArabia, 14(4), 91-108.
- Al-Aradi, H. T., Alnajm, F. M., & Al-Khafaji, A. J. (2022). Reservoir Properties of the Upper Sand Member of the Zubair Formation in North Rumaila Oil Field. The Iraqi Geological Journal, 97-111.
- AlBahadily, J. K. R., & Nasser, M. E. (2017). Petrophysical properties and reservoir modeling of Mishrif formation at Amara oil field, Southeast Iraq. Iraqi Journal of Science, 1262-1272.
- Al-Baldawi, B. A. (2015). Building a 3D geological model using petrel software for Asmari reservoir, south eastern Iraq. Iraqi Journal of Science, 56(2C), 1750-1762.
- Al-Khafaji, A. J., Al-Najm, F. M., Al-Refaia, R. A., Sadooni, F. N., Al-Owaidi, M. R., & Al-Sultan, H. A. (2022). Source rock evaluation and petroleum generation of the Lower Cretaceous Yamama Formation: Its ability to contribute to generating and expelling petroleum to cretaceous reservoirs of the Mesopotamian Basin, Iraq. Journal of Petroleum Science and Engineering, 217, 110919.
- Al-Khafaji, A. J., Yonis, S. J., Ibrahim, R. N. A., Almarsomi, S., & Sadooni, F. (2021). Geochemical characterization and origin of the Cretaceous Sa'di, Khasib, Mishrif, and Nahr Umr Crude Oils in Halfaya

Oilfield, Southern Mesopotamian Basin, Iraq. Petroleum Science and Technology, 39(21-22), 993-1007.

- Al-Khafaji, A. J., Sadooni, F., & Hindi, M. H. (2019). Contribution of the Zubair source rocks to the generation and expulsion of oil to the reservoirs of the Mesopotamian Basin, Southern Iraq. Petroleum Science and Technology, 37(8), 940-949.
- Allen, M. B., Saville, C., Blanc, E. J. P., Talebian, M., & Nissen, E. (2013). Orogenic plateau growth: Expansion of the Turkish-Iranian Plateau across the Zagros fold-and-thrust belt. Tectonics, 32(2), 171-190.
- Allen, P. M., Harmel, R. D., Arnold, J., Plant, B., Yelderman, J., & King, K. (2005). Field data and flow system response in clay (vertisol) shale terrain, north central Texas, USA. Hydrological Processes: An International Journal, 19(14), 2719-2736.
- Al-Najm, F. M., Al-Khafaji, A. J., & Sadooni, F. N. (2022). The Late Cretaceous X Reservoir petrophysics properties and its Oil Geochemistry in the Nameless Oilfield, Mesopotamian Basin, South Iraq. Journal of Petroleum Research and Studies, 12(1 (Suppl.)), 54-67.
- AlRuwaili, S. B. (2005, May). Frontiers of Formation Evaluation and Petrophysics; Present and Future Technologies. In SPE Technical Symposium of Saudi Arabia Section. OnePetro.
- Alsharhan, a. S., & Nairn, a. E. M. (1988). A review of the Cretaceous formations in the Arabian Peninsula and gulf: Part II. Mid-cretaceous (Wasia group) stratigraphy and paleogeography. Journal of petroleum geology, 11(1), 89-112.
- Aqrawi, A. A. (1998). Paleozoic stratigraphy and petroleum systems of the western and southwestern deserts of Iraq. GeoArabia, 3(2), 229-248.
- Aqrawi, A. A. M., Mahdi, T. A., Sherwani, G. H., & Horbury, A. D. (2010, March). Characterisation of the Mid-Cretaceous mishrif reservoir of the

southern Mesopotamian Basin, Iraq. In American Association of Petroleum Geologists Conference and Exhibition (Vol. 7, pp. 7-10).

- Aqrawi, A. A., & Badics, B. (2015). Geochemical characterisation, volumetric assessment and shale-oil/gas potential of the Middle Jurassic–Lower Cretaceous source rocks of NE Arabian Plate. GeoArabia, 20(3), 99-140.
- Archie, G. E. (1950). Introduction to petrophysics of reservoir rocks. AAPG bulletin, 34(5), 943-961.
- Asquith, G. B., Krygowski, D., & Gibson, C. R. (2004). Basic well log analysis (Vol. 16). Tulsa: American association of petroleum geologists.
- Beardsmore, G. R., Cull, J. P., & Cull, J. P. (2001). Crustal heat flow: a guide to measurement and modelling. Cambridge university press.
- Berberian, M., & King, G. C. P. (1981). Towards a paleogeography and tectonic evolution of Iran: Reply. Canadian Journal of Earth Sciences, 18(11), 1764-1766.
- Beydoun, Z. R. (1989). The hydrocarbon prospects of the Red Sea-Gulf of Aden: a review. Journal of Petroleum Geology, 12(2), 125-144.
- Beydoun, Z. R. (1988). Petroleum habitat, northern Middle East: A review.
- Goff, J. (1990). The Middle East: Regional geology and petroleum resources: ZR Beydoun Scientific Press Ltd., PO Box 21, Beaconsfield, Bucks; 1988; ISBN 0 901 360 21 X; Price:£ 38.50.
- Blanc, E. P., Allen, M. B., Inger, S., & Hassani, H. (2003). Structural styles in the Zagros simple folded zone, Iran. Journal of the Geological Society, 160(3), 401-412.
- Blanc, P., & Connan, J. (1994). Preservation, Degradation, and Destruction of Trapped Oil: Chapter 14: Part III. Processes.
- Buday, T. (1980). The regional geology of Iraq, stratigraphy and paleotology. Som Dar Alkitab publishing house, Mosul, 445p.

- Busk, H. G. (1918). Some notes on the geology of the Persian oilfields. Institution of petroleum technologists.
- Callot, J. P., Jahani, S., & Letouzey, J. (2007). The role of pre-existing diapirs in fold and thrust belt development. In Thrust belts and foreland basins (pp. 309-325). Springer, Berlin, Heidelberg.
- Castagna, J. P., Batzle, M. L., & Eastwood, R. L. (1985). Relationships between compressional-wave and shear-wave velocities in clastic silicate rocks. geophysics, 50(4), 571-581.
- Colman-Sadd, S. P. (1978). Fold development in Zagros simply folded belt, Southwest Iran. AAPG Bulletin, 62(6), 984-1003.
- Connan, J., Restle, A., & Albrecht, P. (1980). Biodegradation of crude oil in the Aquitaine basin. Physics and Chemistry of the Earth, 12, 1-17.
- Cummins, J. J., & Robinson, W. E. (1964). Normal and Isoprenoid Hydrocarbons Isolated from Oil-Shale Bitumen. Journal of Chemical & Engineering Data, 9(2), 304-307.
- Dake, L. P. (1978). Fundamentals of Reservoir Engineering: The Netherlands.
- Darling, T. (2005). Well logging and formation evaluation. Elsevier.
- Delfiner, P., Peyret, O., & Serra, O. (1987). Automatic determination of lithology from well logs. SPE formation evaluation, 2(03), 303-310.
- Demaison, G., & Huizinga, B. J. (1991). Genetic classification of petroleum systems. AAPG bulletin, 75(10), 1626-1643.
- Demirbas, A., Alidrisi, H., & Balubaid, M. A. (2015). API gravity, sulfur content, and desulfurization of crude oil. Petroleum Science and Technology, 33(1), 93-101.
- Du, Y., Zhang, J. L., Zheng, S. F., Xin, J., Chen, J., & Li, Y. Z. (2015). The rudist buildup depositional model, reservoir architecture and development strategy of the cretaceous Sarvak formation of Southwest Iran. Petroleum, 1(1), 16-26.

- Dykstra, J. (1987). Compaction correction for burial history curves: application to Lopatin's method for source rock maturation determination. Geobyte;(United States), 2(4).
- Ehrlich, R., Kennedy, S. K., Crabtree, S. J., & Cannon, R. L. (1984). Petrographic image analysis; I, Analysis of reservoir pore complexes. Journal of Sedimentary Research, 54(4), 1365-1378.
- Elhakim, A. F. (2016). Estimation of soil permeability. Alexandria Engineering Journal, 55(3), 2631-2638.
- F.G.R. (1978). Final Geologic Report. Maysan Governorate. Maysan Oil Company.
- Explorations Oil Company (EOC), Ministry of Oil, Iraq.
- Sissakian, V. K., & Fouad, S. F. (2015). Geological map of Iraq, scale 1: 1000 000, 2012. Iraqi Bulletin of Geology and Mining, 11(1), 9-16.
- François, R. (1987). Some aspects of the geochemistry of sulphur and iodine in marine humic substances and transition metal enrichment in anoxic sediments (Doctoral dissertation, University of British Columbia).
- Geoloil Petrophysics. (n.d.). Retrieved from https://geoloil.com/
- Ghafoori, M. R., Roostaeian, M., & Sajjadian, V. A. (2009). Secondary porosity: A key parameter controlling the hydrocarbon production in heterogeneous carbonate reservoirs (case study). Petrophysics-The SPWLA Journal of Formation Evaluation and Reservoir Description, 50(01).
- Gili, E., Masse, J. P., & Skelton, P. W. (1995). Rudists as gregarious sediment-dwellers, not reef-builders, on Cretaceous carbonate platforms. Palaeogeography, palaeoclimatology, palaeoecology, 118(3-4), 245-267.
- Glover P. W. (2000). Petrophysics. University of Aberdeen, UK.
- Glover, P. W., & Luo, M. (2020). The porosity and permeability of binary grain mixtures. Transport in Porous Media, 132(1), 1-37.

- Gross, D., Sachsenhofer, R. F., Bechtel, A., Pytlak, L., Rupprecht, B., & Wegerer, E. (2015). Organic geochemistry of Mississippian shales (Bowland Shale Formation) in central Britain: Implications for depositional environment, source rock and gas shale potential. Marine and Petroleum Geology, 59, 1-21.
- Guidish, T. M., Kendall, C. S. C., Lerche, I., Toth, D. J., & Yarzab, R. F. (1985). Basin evaluation using burial history calculations: an overview. AAPG bulletin, 69(1), 92-105.
- Haddad, S. N. S., & Amin, M. A. (2007). Mid-Turonian–early Campanian sequence stratigraphy of northeast Iraq. GeoArabia, 12(2), 135-176.
- Hakimi, M. H., Abdulah, W. H., & Shalaby, M. R. (2010). Organic geochemistry, burial history and hydrocarbon generation modelling of the Upper Jurassic Madbi Formation, Masila Basin, Yemen. Journal of Petroleum Geology, 33(4), 299-318.
- Hakimi, M. H., Najaf, A. A., Abdula, R. A., & Mohialdeen, I. M. (2018). Generation and expulsion history of oil-source rock (Middle Jurassic Sargelu Formation) in the Kurdistan of north Iraq, Zagros folded belt: Implications from 1D basin modeling study. Journal of petroleum Science and engineering, 162, 852-872.
- Handhal, A. M., & Mahdi, M. M. (2016). Basin modeling analysis and organic maturation for selected wells from different oil fields, Southern Iraq. Modeling Earth Systems and Environment, 2(4), 1-14.
- Hantschel, T., & Kauerauf, A. I. (2009). Fundamentals of basin and petroleum systems modeling. Springer Science & Business Media.
- Horsfield, B., & Rullkotter, J. (1994). Diagenesis, Catagenesis, and Metagenesis of Organic Matter: Chapter 10: Part III. Processes.
- Horstad, I., Larter, S. R., & Mills, N. (1992). A quantitative model of biological petroleum degradation within the Brent Group reservoir in the

Gullfaks field, Norwegian North Sea. Organic Geochemistry, 19(1-3), 107-117.

- Huang, W. Y., & Meinschein, W. G. (1979). Sterols as ecological indicators: Geochemica et Cosmochimica Acta, v. 43.
- Hunt, J. B., & Hill, P. G. (1996). An inter-laboratory comparison of the electron probe microanalysis of glass geochemistry. Quaternary International, 34, 229-241.
- Hunt, T. S. (1861). On the theory of types in chemistry. American Journal of Science, 2(92), 256-264.
- Ingram, G. M., Urai, J. L., & Naylor, M. A. (1997). Sealing processes and top seal assessment. In Norwegian Petroleum Society Special Publications (Vol. 7, pp. 165-174). Elsevier.
- Isaksen, G. H., Patience, R., Van Graas, G., & Jenssen, A. I. (2002). Hydrocarbon system analysis in a rift basin with mixed marine and nonmarine source rocks: The South Viking Graben, North Sea. AAPG bulletin, 86(4), 557-591.
- Jahani, S., Callot, J. P., Lamotte, D. F. D., Letouzey, J., & Leturmy, P. (2007). The salt diapirs of the eastern Fars Province (Zagros, Iran): A brief outline of their past and present. In Thrust belts and foreland basins (pp. 289-308). Springer, Berlin, Heidelberg.
- Jassim, S. Z., & Goff, J. C. (2006). Geology of Iraq: DOLIN, sro, distributed by Geological Society of London.
- Johnston, N., & Beeson, C. M. (1945). Water permeability of reservoir sands. Transactions of the AIME, 160(01), 43-55.
- Kamel, M. H., & Mabrouk, W. M. (2002). An equation for estimating water saturation in clean formations utilizing resistivity and sonic logs: theory and application. Journal of Petroleum Science and Engineering, 36(3-4), 159-168.

- Kamel, M. H., & Mabrouk, W. M. (2003). Estimation of shale volume using a combination of the three porosity logs. Journal of Petroleum Science and Engineering, 40(3-4), 145-157.
- Kendall, J., Vergés, J., Koshnaw, R., & Louterbach, M. (2020). Petroleum tectonic comparison of fold and thrust belts: the Zagros of Iraq and Iran, the Pyrenees of Spain, the Sevier of Western USA and the Beni Sub-Andean of Bolivia. Geological Society, London, Special Publications, 490(1), 79-103.
- Kent, W. N. (2010). Structures of the Kirkuk Embayment, northern Iraq: foreland structures or Zagros Fold Belt structures?. GeoArabia, 15(4), 147-188.
- Koop, W. J., & Stoneley, R. (1982). Subsidence history of the Middle East Zagros basin, Permian to recent. Philosophical Transactions of the Royal Society of London. Series A, Mathematical and Physical Sciences, 305(1489), 149-168.
- Lawa, F. A., Koyi, H., & Ibrahim, A. (2013). Tectono-stratigraphic evolution of the NW segment OF the Zagros fold-thrust belt, Kurdistan, NE Iraq. Journal of Petroleum Geology, 36(1), 75-96.
- Lawson, M., Formolo, M. J., Summa, L., & Eiler, J. M. (2018). Geochemical applications in petroleum systems analysis: new constraints and the power of integration. Geological Society, London, Special Publications, 468(1), 1-21.
- Le Garzic, E., Vergés, J., Sapin, F., Saura, E., Meresse, F., & Ringenbach, J. C. (2019). Evolution of the NW Zagros Fold-and-Thrust Belt in Kurdistan Region of Iraq from balanced and restored crustal-scale sections and forward modeling. Journal of Structural Geology, 124, 51-69.
- Liu, X., Wen, Z., Wang, Z., Song, C., & He, Z. (2018). Structural characteristics and main controlling factors on petroleum accumulation in

Zagros Basin, Middle East. Journal of Natural Gas Geoscience, 3(5), 273-281.

- Magoon, L. B., & Dow, W. G. (1994). The petroleum system: chapter 1: Part I. Introduction.
- Mahdi, T. A., & Aqrawi, A. A. M. (2014). Sequence stratigraphic analysis of the mid-cretaceous Mishrif formation, southern Mesopotamian basin, Iraq. Journal of petroleum geology, 37(3), 287-312.
- Maysan Oil Company (MOC), Ministry of Oil, Iraq.
- McCullough, C., Valencia, J. J., Levi, C. G., & Mehrabian, R. (1989). Phase equilibria and solidification in Ti-Al alloys. Acta Metallurgica, 37(5), 1321-1336.
- Misra, A. A., Sinha, N., & Mukherjee, S. (2015). Repeat ridge jumps and microcontinent separation: insights from NE Arabian Sea. Marine and Petroleum Geology, 59, 406-428.
- Moldowan, J. M., & Jacobson, S. R. (2000). Chemical signals for early evolution of major taxa: biosignatures and taxon-specific biomarkers. International Geology Review, 42(9), 805-812.
- Murris R. J. (1980a). Hydrocarbon habitat of the Middle East .
- Murris, R. J. (1980b). Middle East: stratigraphic evolution and oil habitat. AAPG Bulletin, 64(5), 597-618.
- Nandakumar, V., & Jayanthi, J. L. (2021). Hydrocarbon Fluid Inclusions in Petroliferous Basins. Elsevier.
- Ou, C., Chen, W., Li, C., & Zhou, W. (2016). Structural geometrical analysis and simulation of decollement growth folds in piedmont Fauqi Anticline of Zagros Mountains, Iraq. Science China Earth Sciences, 59(9), 1885-1898.
- Owen, R. M. S., & Nasr, S. N. (1958). Stratigraphy of the Kuwait-Basra Area: Middle East.

- Pepper, A. S., & Yu, Z. (1993). Influence of an inclined salt sheet on petroleum emplacement in the Pompano field area, offshore Gulf of Mexico basin.
- Peters, K. E., & Cassa, M. R. (1994). Applied source rock geochemistry: Chapter 5: Part II. Essential elements.
- Peters, K. E., Walters, C. C., & Moldowan, J. M. (2007). The biomarker guide: Volume 2, Biomarkers and isotopes in petroleum systems and earth history. Cambridge University Press.
- Peters, K. E. (1986). Guidelines for evaluating petroleum source rock using programmed pyrolysis. AAPG bulletin, 70(3), 318-329.
- Pickett, G. R. (1966). A review of current techniques for determination of water saturation from logs. Journal of petroleum Technology, 18(11), 1425-1433.
- Pickett, G. R. (1973). Pattern recognition as a means of formation evaluation. The Log Analyst, 14(04).
- Pitman, J. K., Steinshouer, D., & Lewan, M. D. (2004). Petroleum generation and migration in the Mesopotamian Basin and Zagros Fold Belt of Iraq: results from a basin-modeling study. *GeoArabia*, *9*(4), 41-72.
- Poelchau, H. S., Baker, D. R., Hantschel, T., Horsfield, B., & Wygrala, B. (1997). Basin simulation and the design of the conceptual basin model. In Petroleum and basin evolution (pp. 3-70). Springer, Berlin, Heidelberg.
- Pratt, W. E. (1944). The earth's petroleum resources. The Journal of Business of the University of Chicago, 17(3), 129-145.
- Pushnov, A. S. (2006). Calculation of average bed porosity. Chemical and Petroleum Engineering, 42(1), 14-17.
- Reulet, J. (1970). Sedimentological study of the Mishrif Reservoir. Department of Exploration, ELF–Iraq.
- Sadooni, F. N. (1995). Petroleum prospects of Upper Triassic carbonates in northern Iraq. Journal of Petroleum Geology, 18(2), 171-190.

- Saura, S., Vogt, P., Velázquez, J., Hernando, A., & Tejera, R. (2011). Key structural forest connectors can be identified by combining landscape spatial pattern and network analyses. Forest Ecology and Management, 262(2), 150-160.
- Schlumberger Ltd. (1984). Log interpretation charts .
- Selley, R. C., & Sonnenberg, S. A. (1985). Methods of Exploration, Elements of Petroleum Geology.
- Selley, R. C. (1998). Elements of petroleum geology. Gulf Professional Publishing.
- Sepehr, M., Cosgrove, J., & Moieni, M. (2006). The impact of cover rock rheology on the style of folding in the Zagros fold-thrust belt. Tectonophysics, 427(1-4), 265-281.
- Sharland, P. R., Boote, D., Casey, D. M., Davies, R. B., & Simmons, M. D. (2003, May). North Africa and Arabian Plate First and Second Order Sequence Stratigraphy. In AAPG Annual Meeting 2003.
- Sharland, P. R., Casey, D. M., Davies, R. B., Simmons, M. D., & Sutcliffe, O. E. (2004). Arabian plate sequence stratigraphy–revisions to SP2. GeoArabia, 9(1), 199-214.
- Smith, G. C., & Cook, A. C. (1980). Coalification paths of exinite, vitrinite and inertite. Fuel, 59(9), 641-646.
- Sofer, Z. (1984). Stable carbon isotope compositions of crude oils: application to source depositional environments and petroleum alteration. AAPG bulletin, 68(1), 31-49.
- Summons, R. E., Jahnke, L. L., Hope, J. M., & Logan, G. A. (1999). 2-Methylhopanoids as biomarkers for cyanobacterial oxygenic photosynthesis. Nature, 400(6744), 554-557.
- Sweeney, J. J., & Burnham, A. K. (1990). Evaluation of a simple model of vitrinite reflectance based on chemical kinetics. AAPG bulletin, 74(10), 1559-1570.

- Tao, S., Wang, C., Du, J., Liu, L., & Chen, Z. (2015). Geochemical application of tricyclic and tetracyclic terpanes biomarkers in crude oils of NW China. Marine and Petroleum Geology, 67, 460-467.
- Timur, A. (1968, June). An investigation of permeability, porosity, and residual water saturation relationships. In SPWLA 9th annual logging symposium. OnePetro.
- Tissot, B. P., & Welte, D. H. (1984). From kerogen to petroleum. In Petroleum formation and occurrence (pp. 160-198). Springer, Berlin, Heidelberg.
- Tixier, M. P., Alger, R. P., & Doh, C. A. (1959). Sonic logging. Transactions of the AIME, 216(01), 106-114.
- Ungerer, P. (1990). State of the art of research in kinetic modelling of oil formation and expulsion. Organic Geochemistry, 16(1-3), 1-25.
- van Golf-Racht, T. D. (1982). Fundamentals of fractured reservoir engineering. Elsevier.
- Vergés, J., Saura, E., Casciello, E., Fernandez, M., Villaseñor, A., Jimenez-Munt, I., & García-Castellanos, D. (2011). Crustal-scale cross-sections across the NW Zagros belt: implications for the Arabian margin reconstruction. Geological Magazine, 148(5-6), 739-761.
- Vomocil, J. A. (1965). Porosity. Methods of soil analysis: Part 1 physical and mineralogical properties, including statistics of measurement and sampling, 9, 299-314.
- Wahl, J. S., Tittman, J., & Johnstone, C. W. (1964). The dual spacing formation density log. Journal of Petroleum Technology, 16(12), 1411-1416.
- Waples, D. W. (1994). Maturity Modeling: Thermal Indicators, Hydrocarbon Generation, and Oil Cracking: Chapter 17: Part IV. Identification and Characterization.

- Welte, D. H., Hantschel, T., & Wygrala, B. (1997). Petroleum Systems and the Role of Multi-Dimensional Basin Modeling.
- Wheaton, R. (2016). Fundamentals of applied reservoir engineering: appraisal, economics and optimization. Gulf Professional Publishing.
- Wylie, H. G. (1958). Factors That Affect Host Finding by Nasonia vitripennis (Walk.) (Hymenoptera: Pteromalidae) 1, 2. The Canadian Entomologist, 90(10), 597-608.
- Zerrouki, A. A., Aifa, T., & Baddari, K. (2014). Prediction of natural fracture porosity from well log data by means of fuzzy ranking and an artificial neural network in Hassi Messaoud oil field, Algeria. Journal of Petroleum Science and Engineering, 115, 78-89.
- Zolfegharifar, S. Y., Mohammadi, S., Mirasi, S., & Hashemi Jokar, M. (2018). A study of the earthquakes occurrence distribution in probabilistic seismic hazard analyses method (Case study: Zagros fault, Iran). Geotechnical Geology, 14(1), 187-192.
- Zumberge, J. E. (1987). Prediction of source rock characteristics based on terpane biomarkers in crude oils: A multivariate statistical approach. Geochimica et Cosmochimica Acta, 51(6), 1625-1637.

المستخلص

تركز هذه الدراسة على النظام البترولي للمنطقة المختارة الواقعة في منطقة معقدة من سلسلة الطيات والصدوع التي تشكلت خلال تكون جبال زاكروس في محافظة ميسان جنوب شرق العراق. يعتبر حقل الفكة هو المنطقة المستهدفة والتي تحتوي على مكمنين نفطيين هما تكوين المشرف ومجموعة الأسمري.

تم حساب الخصائص المكمنية وتقدير العمر والبيئة الترسيبية للصخور المصدرية المحتملة وعمل نموذج للنظام النفطي. وقد اقتصرت البيانات التي تم الحصول عليها على تكوين مشرف، لذا فإن جميع التفسيرات البتروفيزيائية تعود إلى تكوين المشرف (Cenomanian-Late Maastrichtian) عبر بيانات خمسة آبار اعتمادًا على بيانات المجسات، صور المجسات، مقطع زلزالي، والزيوت الخام. توزعت أربعة آبار في الطية الجنوبية لجبل فكة وهي FQ-4 و FQ-6 و FQ-19 و FQ-20 مع بئر واحد فقط في الطية الشمالية، FQ-14. تم جمع بيانات الإدخال لملفات las، وسجلات الصور، والخارطة الكنتورية للآبار الخمسة من شركة النفط الوطنية (NOC).

أظهرت النتائج أن المكمن الرئيسي هو تكوين المشرف وهو مكون من سبع وحدات مكمنية تم تمييزها في التكوين من خلال التغاير الحاد في حجم الشيل، التشبع المائي والمسامية الفعالة. هذه الوحدات هي MA، MB11، MB12، MB21 ، MB22، MC1، و MC2. الوحدة الرئيسية في المكمن هي MB21 والتي تتميز بمسامية فعالة جيدة ناتجة عن القيمة العالية للمسامية الثانوية بسبب عمليات التكسير والاذابة التي اثرت في التكوين، محتوى مائي منخفض لأقل من ٢٠٪ ، وتشبع الهيدروكربوني عالي. تشير تحليلات عينات النفط الخام إلى إن عمر صخور المصدر هو الجوراسي الاعلى-الطباشيري الاسفل والمصادر المتوقعة هي تكوينات السلي واليمامة للكريتاسي المبكر واحتمالية سارجيلو ونجمة من الجوراسي الأوسط والاعلى. كما أظهرت دراسة المادة العضوية بداية النضج الحراري لصخور المصدر وان المادة العضوية هي كيروجن من النوع الثاني Type IIs. يُظهر نموذج التدفق الحراري قيمة ثابتة تتراوح بين ٤٥-٥٠ ميغاواط / م ٢ من الطباشيري الأوسط إلى نهاية العصر الثلاثي حيث تظهر زيادة ملحوظة في فترة النيوجين تصل حوالي ٧٣ ميغاواط / م ٢ تعكس تأثير الفترة البانية للجبال والتي كونت جبال زاغروس. حدد النموذج احادي البعد تأثير تاريخ الدفن على زيادة النضج والوصول إلى نافذة النفط خلال العصر الثلاثي بناءً على تاريخ التدفق الحراري. بدأ توليد النفط في أوائل العصر الطباشيري، وبدأت ذروة الطرد في أواخر العصر الميوسين، بينما كانت قمة النضوج لتكوين النفط في الهولوسين. بدأت هجرة النفط اعتباراً من أواخر العصر الطباشيري واستمرت حتى الوقت الحاضر، اخذت طريقها عبر الصدوع التي تأثرت بها المنطقة، وتراكمت في المكامن والمصائد النفطية التي تشكلت قبل توليد النفط كنتيجة للتشوهات المصاحبة لتكوين جبال زاكروس.

وزارة التعليـــم العـالي والبحث العلمي
جامعـــة بابـــــــل
كليـــة العلـــــــوم
قسم علم الارض التطبيقي

جيولوجيا النفط جنوب حوض حزام طيات زاغروس، محافظة ميسان، العراق

رسالة مقدمة الى كلية العلوم في جامعة بابل
كجزء من متطلبات نيل شهادة الماجستير في علم الارض

إعداد
مهدي علوان عزيز حميدي
بكالوريوس جيولوجي، جامعة بغداد، ١٩٩٣م

إشراف
الأستاذ الدكتور عامر جاسم الخفاجي الدكتور قصي حسين عبيد

٢٠٢٢م